Technical Report Documentation Page

1. Report No.	2. Government Accession No.	3. Recipients Catalog No.
FHWA/TX-92+1127-2		

4. Title and Subtitle	5. Report Date
SHEAR STRENGTH OF PRETENSIONED CONCRETE GIRDERS IN NEGATIVE MOMENT REGIONS	February 1990
	6. Performing Organization Code

7. Author(s)	8. Performing Organization Report No.
Anthony C. Powers, Michael E. Kreger, and John E. Breen	Research Report 1127-2

9. Performing Organization Name and Address	10. Work Unit No. (TRAIS)
Center for Transportation Research The University of Texas at Austin Austin, Texas 78712-1075	11. Contract or Grant No. Research Study 3-5-87-1127
	13. Type of Report and Period Covered Interim
12. Sponsoring Agency Name and Address Texas Department of Transportation Transportation Planning Division P. O. Box 5051 Austin, Texas 78763-5051	14. Sponsoring Agency Code

15. Supplementary Notes
Study conducted in cooperation with the U. S. Department of Transportation, Federal Highway Administration
Research Study Title: "Reinforcement Detail Design in Structural Concrete"

16. Abstract

This report presents the results of an experimental study performed to evaluate the suitability of current AASHTO/ACI design provisions for shear as applied to thin-web pretensioned I-girders subject to shear and negative-moment bending. Eight tests were performed on four pretensioned beams with varying tendon profiles and amounts of shear reinforcement. Behavior was measured and observed to collect information on cracking loads, inclination and size of diagonal cracks, failure modes and loads, steel strains, and end slip of prestressing strands. Observed behavior was compared to predicted behavior based on the 1983 AASHTO Specifications for Highway Bridges and the 1983 ACI Building Code.

In addition, the application of strut-and-tie models to thin-web, pretensioned I-beams was examined. Four variations of a basic strut-and-tie model were evaluated. Based on observed web-crushing failures, a strut-width definition for non-parallel diagonal struts was proposed in conjunction with a concrete efficiency factor definition for thin webs.

17. Key Words	18. Distribution Statement
design provisions, shear, thin-web pretensioned I-girders, negative-moment bending, beams, tendon profiles, reinforcement, cracking loads, strains, end slip, strands, struts, concrete	No restrictions. This document is available to the public through the National Technical Information Service, Springfield, Virginia 22161.

19 Security Classif. (of this report)	20. Security Classif. (of this page)	21. No. of Pages	22. Price
Unclassified	Unclassified	140	

SHEAR STRENGTH OF PRETENSIONED CONCRETE GIRDERS IN NEGATIVE MOMENT REGIONS

by

Anthony C. Powers, Michael E. Kreger, and John E. Breen

Research Report No. 1127-2

Research Project 3-5-87-1127
"REINFORCEMENT DETAIL DESIGN IN STRUCTURAL CONCRETE"

Conducted for

Texas Department of Transportation

In Cooperation with the
U.S. Department of Transportation
Federal Highway Administration

by

CENTER FOR TRANSPORTATION RESEARCH
BUREAU OF ENGINEERING RESEARCH
THE UNIVERSITY OF TEXAS AT AUSTIN

FEBRUARY 1990

The contents of this report reflect the views of the authors who are responsible for the facts and accuracy of the data presented herein. The contents do not necessarily reflect the official views or policies of the Federal Highway Administration. This report does not constitute a standard, specification, or regulation.

PREFACE

This report is the second in a series which summarizes the results of a study of shear strength in negative moment regions of prestressed girders, in addition to a more general study of reinforcement details in structural concrete. This report includes a description of test results for eight shear tests, and evaluates current shear strength provisions in light of these test results. A strut-and-tie approach for modeling the response of the test specimens is also investigated.

The work is part of research project 3-5-87/9-1127 entitled "Reinforcement Detail Design in Structural Concrete." The research was conducted by the Phil M. Ferguson Structural Engineering Laboratory as part of the overall research programs of the Center for Transportation Research of The University of Texas at Austin. The work was sponsored jointly by the Texas Department of Transportation and the Federal Highway Administration under an agreement with The University of Texas at Austin and the Texas Department of Transportation.

Liaison with the Texas Department of Transportation was maintained through the contact representative, Ms. M.L. Rawls. Mr. Peter Chang was the contact representative for the Federal Highway Administration.

This portion of the overall study was directed by Michael E. Kreger, Assistant Professor of Civil Engineering. Co-investigators for the overall program also included James O. Jirsa, who holds the Janet S. Cockrell Centennial Chair in Engineering, and John E. Breen, who holds the Nasser I. Al-Rashid Chair in Civil Engineering. The development of the testing apparatus and supervision of the tests was performed by Anthony C. Powers, Assistant Research Engineer.

SUMMARY

This report presents the results of an experimental study performed to evaluate the suitability of current AASHTO/ACI design provisions for shear as applied to thin-web pretensioned I-girders subject to shear and negative-moment bending. Eight tests were performed on four pretensioned beams with varying tendon profiles and amounts of shear reinforcement. Behavior was measured and observed to collect information on cracking loads, inclination and size of diagonal cracks, failure modes and loads, steel strains, and end slip of prestressing strands. Observed behavior was compared to predicted behavior based on the *1983 AASHTO Specifications for Highway Bridges* and the *1983 ACI Building Code.*

In addition, the application of strut-and-tie models to thin-web, pretensioned I-beams was examined. Four variations of a basic strut-and-tie model were evaluated. Based on observed web-crushing failures, a strut-width definition for non-parallel diagonal struts was proposed in conjunction with a concrete efficiency factor definition for thin webs.

IMPLEMENTATION

This report provides a detailed background for current design recommendations for shear in prestressed concrete girders. Results of the experimental program described in this report confirm that current shear design provisions can be safely used for design of thin-web prestressed girders in regions with negative moment. Recommendations for use of current provisions for design of such regions are presented. In addition, strut-and-tie models for the test beams were used to aid in refining a strut-width definition for non-parallel diagonal struts and a concrete efficiency factor for thin webs. Results from this portion of the study will be useful for developing general design guidelines for use with strut-and-tie models for reinforcement detailing in structural concrete.

TABLE OF CONTENTS

LIST OF FIGURES

LIST OF TABLES

CHAPTER 1
INTRODUCTION

1.1 Background

The use of precast, pretensioned concrete construction for highway bridges has increased in recent years due to economy of standardization, ease and speed of construction, and low transportation costs. In Texas, pretensioned I-beams are a mainstay for the range of spans most commonly encountered in stream crossings and highway grade separations (approximately 70 to 120 ft). The upper limit primarily reflects the problems involved in transporting beams of that length.

In an effort to overcome this limitation, the Texas Department of Transportation (TxDOT) has in recent years employed pretensioned concrete beams in what is referred to as "semi-continuous" construction. In this scheme, shown in Figure 1.1, the center span of a three span bridge can be extended beyond the limits of simple-span pretensioned I-beams by cantilevering the side-span beams a short distance over the interior supports and employing a simply-supported "drop-in" span between the dapped ends of the cantilevers. This results in a large negative moment accompanied by high shear forces at the interior supports, in contrast to the simple-span shear forces and moments typically encountered in pretensioned beam construction. Beams utilized in this situation contain pretensioned or post-tensioned tendons in the top flange in the negative-moment region, in addition to the straight strands in the bottom flange for positive bending, which are draped to the bottom flange in the positive moment region and near the end of the beam. Consequently, in the interior support region the beam contains strands in both flanges.

Application of the empirical design equations for shear in the *American Association of State Highway and Transportation Officials Specifications for Highway Bridges* (AASHTO)[1]

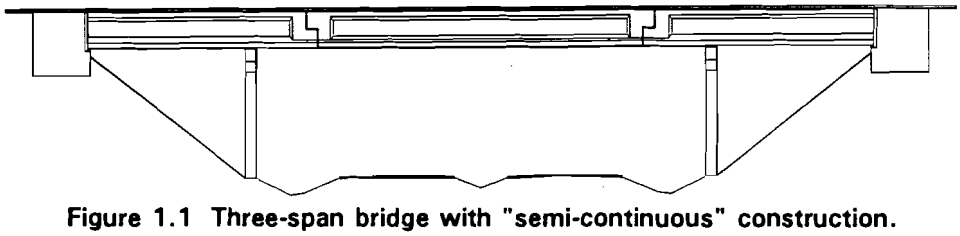

Figure 1.1 Three-span bridge with "semi-continuous" construction.

presents difficulties in interpreting the specification for this type of beam. Specifically, AASHTO allows the use of 80 percent of the total section height, h, in lieu of the smaller actual distance from the extreme compression fiber to the centroid of the prestressing force, d, in Equations 9-27 and 9-29 (Equations 2.7 and 2.5 in this study). In question is the safety and suitability of these equations to situations where the actual centroid of the strands is near mid-height of a section carrying appreciable moment and shear.

On a more general level, the AASHTO Specifications for shear have been criticized for their relative complexity and empiricism. The plasticity-based strut-and-tie model has recently received increasing support in the literature as a more rational alternative to the currently used methods. Its primary advantage is that it can be applied to unusual design problems because it is based on a simple behavioral model for reinforced/prestressed concrete. For this reason, the strut-and-tie model will be investigated as an alternative to the AASHTO method for the shear design of semi-continuous pretensioned I-beams.

1.2 Objectives and Scope

This investigation is part of a larger study funded by the Texas Department of Transportation to develop design guidelines for detailing of structural concrete. The greatest portion of the larger study has been devoted to the general development of the strut-and-tie model.

The primary goal of the research described herein was to determine the applicability of the current AASHTO shear provisions to negative-moment regions of pretensioned concrete beams as discussed in Section 1.1. A secondary objective was to examine the application of strut-and-tie (truss) models for design of shear reinforcement in prestressed concrete members.

To fulfill these goals, eight tests were performed on four high-strength pretensioned concrete beams. The principal variables were the profile of the prestressed reinforcement and the amount of transverse reinforcement. These variables were investigated in order to determine the accuracy and safety of the AASHTO Specifications for shear design as applied to beams with different combinations of prestressed reinforcement profile and

amount of transverse reinforcement. Results were compared to AASHTO design predictions and to predictions from strut-and-tie models.

The research reported herein consisted of three major parts. First, a review of the literature pertaining to the shear behavior of prestressed concrete beams was undertaken. This review, presented in Chapter 2, concentrated on the development of the AASHTO/ACI shear provisions for prestressed concrete and the application of the strut-and-tie model to prestressed concrete. Second was the experimental program described in Chapter 3, the results of which are presented in Chapter 4. Finally, test results are analyzed in Chapter 5, in light of the AASHTO and strut-and-tie model predictions. Conclusions are summarized in Chapter 6.

CHAPTER 2
SHEAR IN PRESTRESSED BEAMS

2.1 Introduction

A great deal of research effort has been expended during the past century investigating the shear behavior of reinforced concrete. As a product of this research, numerous models of varying complexity, rationale, and accuracy have been proposed. Of these, only two will be discussed in this chapter: 1) the modified 45° truss model currently employed in the AASHTO *Specifications for the Design of Highway Bridges*[1] and the American Concrete Institute *Building Code Requirements for Reinforced Concrete*,[4] and 2) the strut-and-tie model. Emphasis will be placed on the application of these two models to prestressed beams, particularly those with draped tendons subject to negative-moment bending. First, a brief review of the mechanisms of shear resistance, modes of shear failure, and the effects of various design variables will be presented.

The basic provisions for shear in prestressed concrete members are identical in the AASHTO Bridge Specifications and the ACI Building Code and will hereafter be referred to as the *Specifications*. Differences will be noted where appropriate.

2.2 Shear Behavior of Prestressed Concrete Beams

2.2.1 Mechanisms of Shear Resistance. There are five basic mechanisms identified[2] for shear transfer in reinforced and prestressed concrete members: 1) elastic shear stresses in uncracked concrete, 2) interface shear transfer (also known as aggregate interlock), 3) dowel action, 4) arching, and 5) shear reinforcement. Of these, only elastic stresses in the uncracked concrete and shear reinforcement are considered explicitly in the *Specifications* and strut-and-tie model, although several authors have proposed methods of considering arching action in the strut-and-tie model.[34, 25]

2.2.1.1 Shear Stresses in Uncracked Concrete. The combination of shear, axial, and bending stresses on a member results in principal tensile and compressive stresses in the

concrete. If these principal stresses exceed either the tensile or compressive strength of the concrete, failure will occur. The *Specifications* design equations for shear are based on the limiting concrete tensile strength as related to the modulus of rupture. This assumes no additional concrete strength beyond cracking.

2.2.1.2 Interface Shear Transfer. This mechanism has been called by many names: aggregate interlock, surface roughness shear transfer, shear friction, and tangential shear transfer.[2] All are less than perfectly accurate, but all describe the same transfer of shear across crack surfaces. This transfer can be in the form of friction along the face of the crack (resistance to displacement along the crack surface), compression across the crack, or some combination of the two. Compression is carried across the crack when redistribution of forces after cracking results in an orientation of principal stresses different from that which existed at first cracking. When this occurs, the concrete experiences a reduction in compressive strength related to the magnitude of the transverse tensile stresses.

2.2.1.3 Dowel Action. Where reinforcement crosses a shear crack, the resistance to displacement along the crack provided by the reinforcement is referred to as dowel action. While preventing movement along the crack, dowel action introduces tensile stresses in the concrete around the bar which can cause splitting along the bar. After splitting, the effectiveness of the dowel action is reduced and depends on the stiffness of the concrete directly below the dowel.

2.2.1.4 Arching Action. Deep beams, particularly post-tensioned deep beams, can derive a large portion of their "shear" strength from arch action. Although arch action is not a true shear transfer mechanism (vertical loads are carried in the arch by compression in the concrete rib), it carries a portion of the vertical load between load point and support, reducing the portion to be carried by other shear mechanisms. When an arch mechanism develops in a beam, the concrete between the load point and the nearest support acts as the compression rib of a tied arch, with the longitudinal tension reinforcement providing the tie. (A strut-and-tie model employing a direct strut between loads and reactions represents the same mechanism). Arch action is partially due to the influence of vertical compressive stresses from concentrated loads and reactions which are most significant in beams with short shear-spans. Horizontal compressive stresses imposed by prestressing can also contribute to the development of arch action.

2.2.1.5 Shear Reinforcement. The role of shear reinforcement (typically vertical stirrups or bent-up longitudinal bars) is generally assumed to be that of vertical ties in the truss model (strut-and-tie model) which act only in tension, resisting the vertical component of force in the compression struts. Both the *Specifications* and the strut-and-tie model rely on this assumption. However, this assumed function of the shear reinforcement ignores the contribution it can make to interface shear transfer, arch action, and dowel action. This is generally accomplished by restraining movement along or perpendicular to crack surfaces.

2.2.2 Modes of Shear Failure. Thin-webbed I-beams are susceptible to numerous failure modes including flexure, diagonal tension, web crushing, shear-compression, and shear-tension. Diagonal tension and web crushing are of greatest interest in this study. All failure modes are in some way related to, or caused by, inclined cracking due to diagonal tensile stresses.

Two distinct types of inclined crack have been identified: web-shear and flexure-shear. The first type is found almost exclusively in thin webs of highly prestressed I-beams and is caused by principal tensile stresses in the web. The second type, which is more common and develops after flexural cracking, is the result of an inclined crack propagating from a crack that initiated due to flexural stresses. These cracking modes will be discussed more completely in Section 2.3 during discussion of the development of the *Specifications* equations for shear.

2.2.3 Effects of Design Variables. The amount and location of prestressed and non-prestressed longitudinal reinforcement, amount of shear reinforcement, concrete strength, and type of cross section are some of the variables affecting shear behavior. The factors most pertinent to this study are addressed in this section.

2.2.3.1 Prestressing.

Location of Prestressing Strands. The *Specifications* allow the use of $0.8h$ in lieu of the actual distance from the extreme compression fiber to the centroid of the prestressed reinforcement when calculating the shear capacity of prestressed members. In the *1963 ACI Code*, use of $0.8h$ in lieu of d was only allowed in the equation for V_{cw} (Equation 2.5).[5] The *1971 ACI Commentary*[6] states that 80% of the height of the section can be used as the effective depth "because the centroid of the prestressing tendons may vary in prestressed

beams." Presumably, this refers to the fact that, in cases where the centroid of the prestressing tendons is less than $0.8h$ from the extreme compression fiber, the centroid of the force in the prestressed reinforcement at ultimate will be farther from the extreme compression fiber than the centroid of the tendons due to the strain distribution across the section. This provision typically will only be applicable in beams with draped tendons since tendons are generally placed as far from the centroid of the section as possible to provide maximum flexural strength. In the case of beams with draped tendons (assuming that not all of the tendons are draped), less force will be carried by the draped tendons under applied loads than by their straight counterparts as the result of smaller effective depths and lower effective prestress in draped strands due to friction losses associated with the draping hardware. Both effects add to the conservatism of the *Specifications'* assumption.

Draped Reinforcement. MacGregor et al.[34] performed tests on 19 pretensioned I-beams with draped prestressed reinforcement. From these tests they concluded that draping of prestressed reinforcement had opposite effects on the web-shear and flexure-shear cracking strengths. This reflects the difference in cracking mechanisms for the two types of inclined cracking. However, in all cases the observed failure loads were greater than predicted.

The web-shear cracking load is theoretically increased by the presence of draped tendons because the upward component of the prestress force effectively reduces the applied shear, thus reducing the principal tensile stresses in the web. However, if the draped reinforcement enters the web in the shear-span, stress concentrations due to shear transfer at the junction of the web and flange, combined with the reduction in web area caused by the strands, can result in critical principal stresses at this location. In one of the tests by Hawkins et al.[34] diagonal cracks initiated at the location where strands entered the web at a load that was only 81% of the predicted cracking load.

In contrast to the web-shear cracking behavior of prestressed beams with draped tendons, the flexure-shear behavior is not enhanced by the presence of the draped reinforcement. In fact, test results [34] indicated that both the flexure-shear cracking load and the ultimate load (when flexure-shear was the controlling mode) were reduced by draping the prestressed reinforcement. This effect can be explained by the substantial reduction in the flexural cracking load required to produce the initiating flexural crack necessary to propagate a flexure-shear crack. The lower eccentricity of the prestress force reduces the

cracking moment and allows the flexural crack to open wider as a result of the smaller amount of longitudinal steel near the extreme tension fiber. The Joint ASCE-ACI Committee 426[2] cited Leonhardt's prediction of decreasing flexure-shear capacity with increased draping of prestress based on a larger region of the tension flange being cracked in flexure at a given load than in a comparable beam with straight strands.

Finally, the presence of draped tendons introduces a plane of weakness, in addition to the one at the junction of the web and flange, on which a splitting failure can occur. This is due to the fact that a draped strand in uncracked concrete is likely to experience lower strain than a straight one due to its proximity to the neutral axis. Consequently, the strain differential between the strand in uncracked and cracked concrete is greater for a draped strand than for a straight one, increasing the shear flow along the crack and increasing the probability of splitting failure along the strand.

Level of Prestress. The level of prestress present in a beam, as expressed by the prestressed reinforcement index, ρ_w, is an important factor affecting the failure mode. Highly prestressed beams are likely to experience web-shear cracking and web crushing failure since prestressing delays the occurrence of flexural cracking. In contrast, lightly prestressed beams are more likely to develop flexure-shear cracks and experience a flexural or flexure-shear failure. In general, the prestress force increases the moment capacity, effectively decreasing the flexural compression stress in the web, and thus increasing the shear capacity.[19]

2.2.3.2 Negative Bending/Continuous Construction. Based on tests of two-span continuous prestressed beams at the University of Illinois, Hawkins et al.[24] suggested that the design procedures developed for simply-supported beams (Equations 2.1, 2.2, 2.5 and 2.7) were also appropriate for continuous beams. They noted that the basic mechanisms of failure in shear were similar to those observed for simply-supported beams. It has been suggested that, in the region of contraflexure in a continuous beam, a direct strut between the load point and support (for a top-loaded beam) delays the incidence of shear cracks in the shear-span,[2] but does not necessarily improve the ultimate behavior.

Concern has been raised by Rodrigues and Darwin[41] about the *top bar effect* in reinforced concrete beams subject to negative bending. They suggested the lower bond strength of top-cast bars in regions of negative bending as an explanation for observed

flexural and flexure-shear cracks that were wider in negative bending regions than in positive bending regions. Haddadin, Hong, and Mattock[21] also reported similar observations. Ferguson[20] suggested that continuous beams may have reduced shear strength due to flexure-shear cracks which result in an effectively reduced shear span and, hence, a reduced concrete contribution to the shear capacity. Prestressing may effectively diminish these effects by delaying the appearance of flexural cracks and reducing their width after they do form.

2.2.3.3 Non-Prestressed Flexural Reinforcement. An increase in mild reinforcement ratio will help control crack widths, thus maintaining the interface shear mechanism, and will provide added dowel action.[15] The effect of additional mild reinforcement is not as great as that due to additional prestressed reinforcement because the mild reinforcement does not significantly increase the cracking moment.[19]

2.2.3.4 Shear Reinforcement. Transverse shear reinforcement enhances the shear strength of a beam by directly carrying part of the shear force; restricting the diagonal crack opening width, thereby maintaining the interface shear transfer mechanism; and by restraining the longitudinal reinforcement so it can more effectively act as a dowel.[2] In addition, web reinforcement can resist a limited force through dowel action, and can provide confinement to the compression zone.

MacGregor et al.[33] observed that the inclusion of even a small amount of shear reinforcement improved both the strength and ductility of prestressed beams failing in shear. In addition, they noted that beams with draped tendons required more shear reinforcement to prevent shear failures than did beams with straight tendons because the flexural cracking load is reduced with draping. In beams with draped strands that are also effective for positive bending, the top-bar effect can reduce the bond strength of the draped strands requiring additional shear reinforcement to prevent bond failure.

2.2.3.5 Concrete Strength. The increasingly frequent use of high strength concrete (f'_c up to 12,000 psi) has led to questions about the *Specifications* equations for shear strength, because these equations are based on tests of beams with concrete strengths of 6000 psi or less. Tests by Elzanaty et al.[19] and Hartmann[22] indicated that the *Specifications* equations were indeed conservative for a wide range of shear reinforcement ratios and concrete strengths up to 12,000 psi. However, Elzanaty et al. noted that while the ratio of

test to predicted web-shear cracking loads increased with increasing concrete strength, values for flexure-shear cracking decreased. Carino and Lew[10] showed that the split-cylinder strength is more proportional to $f_c'^{(0.75)}$ than it is to $\sqrt{f_c'}$. In addition, the biaxial strength properties of concrete indicate that, for a given prestress force, the reduction in the ratio of compressive stress to f_c' for increasing f_c' results in a smaller reduction in tensile strength of the concrete than with a lower f_c'.[19] The combination of these two factors explain the conservatism of the *Specifications* for web-shear cracking in high-strength concrete prestressed beams.

Elzanaty et al.[19] explain the reduction in factor of safety for flexure-shear cracking as follows: after flexural cracking, an additional increment of shear is required to transform the flexural crack into an inclined crack. The *Specifications* assumes this increment to be a constant $0.6\sqrt{f_c'}\ b'd$. The complex shear behavior after cracking is dependant on three mechanisms: 1) aggregate interlock, 2) dowel action, and 3) shear stress in the uncracked concrete. The rate of development from a flexural crack to an inclined crack is dependant on the intensity of stress at the crack tip. As Elzanaty et al.[19] observed, the crack surfaces in high-strength concrete tend to be relatively smooth (it is common to have cracks propagate through the aggregate in high-strength concrete) rendering the aggregate interlock mechanism less effective. The remaining uncracked concrete is then required to carry a larger portion of the shear force, increasing the magnitude of the stresses at the crack tip.

2.2.3.6 Top Loading. Beams loaded on their top flange and supported at their bottom flange are referred to as *directly loaded*. For beams with short effective shear-spans (a/d < 2.5) direct loading results in increased shear capacity due to compressive stresses along a line between the load point and support.[2] In terms of the strut-and-tie model, this can be thought of as a *direct strut* between the load point and support. In *indirectly loaded* beams – beams loaded near the bottom flange – this direct strut or arch action cannot form, so these beams do not have the increased capacity of *directly loaded* beams. However, tests have shown[45] that for longer effective shear-spans (a/d > 2.5 to 3) there was no reduction in shear capacity due to indirect loading.

2.3 AASHTO/ACI Design Method

2.3.1 General. According to the *Specifications,* members shall be designed such that

$$V_u \leq \phi (V_c + V_s) \tag{2.1}$$

where V_u = the factored shear force at the section under consideration,
V_c = nominal shear strength provided by concrete (the lesser of V_{cw} and V_{ci}),
V_s = nominal shear strength provided by shear reinforcement,
ϕ = strength reduction factor equal to 0.9 for shear.

Thus, according to the *Specifications*, the nominal shear resistance of a member is the sum of a concrete contribution and a steel contribution.

2.3.2 Steel Contribution. The steel contribution is based on the 45° truss analogy proposed by W. Ritter in 1899 that was later revised by E. Morsch. This assumes that a 45° crack occurs in the web (defining a diagonal truss member) which is crossed by transverse reinforcement having a capacity V_s. The horizontal projection of the crack is approximately d, the effective depth of the section, and the shear force carried by the stirrups in this distance is

$$V_s = \frac{A_v f_y d}{s} \tag{2.2}$$

where A_v = area of shear reinforcement over a distance, s,
f_y = specified yield strength of shear reinforcement,
d = distance from the extreme compression fiber to the centroid of tension reinforcement, but need not be taken less than $0.8h$ for prestressed members,
h = overall depth of the member,
s = spacing of shear reinforcement in the direction parallel to longitudinal reinforcement.

2.3.3 Diagonal Cracking. Diagonal cracks in prestressed beams are typically at shallower angles than in non-prestressed beams, corresponding to the shallower angle of the

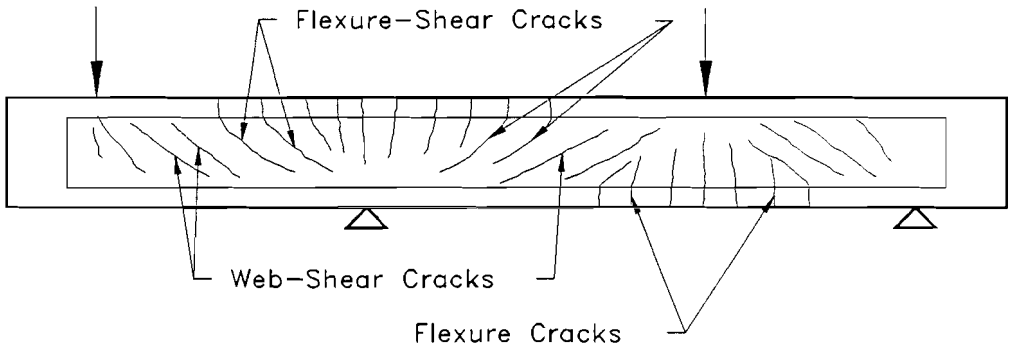

Figure 2.1 Types of cracking in reinforced and prestressed concrete beams.

principal stresses caused by the prestress force. Elzanaty et al.[19] reported observed diagonal crack angles of 15 to 30° in 34 tests of high-strength prestressed I-beams and T-beams. Shallower crack angles result in a longer horizontal projection of the diagonal crack, so more stirrups than provided by the 45° assumption are intersected by a crack and are therefore effective in resisting shear. Thus, the 45° crack angle assumption built into the V_s provision is conservative in assuming the participation of only the stirrups within a distance d along the beam.

Two types of diagonal crack are considered in determining the nominal shear strength, V_c, provided by the concrete: web-shear (V_{cw}) and flexure-shear (V_{ci}). Examples of both types of inclined cracks are shown in Figure 2.1. The *Specifications* consider each type with a separate equation. The lowest resistance offered by the two equations controls the design.

2.3.3.1 Web-Shear. The web-shear equation is based on elastic theory and the application of Mohr's circle to determine the principal stresses at the centroid of the beam cross section. There are no bending stresses at the centroid, so the principal stresses are determined from the applied shear and prestressing forces only. From Mohr's circle for stress (Figure 2.2), the shear stress associated with principal tensile stresses equal to the tensile strength of the concrete can be determined. The resulting equation for the web-shear cracking, V_{cw}, is as follows:

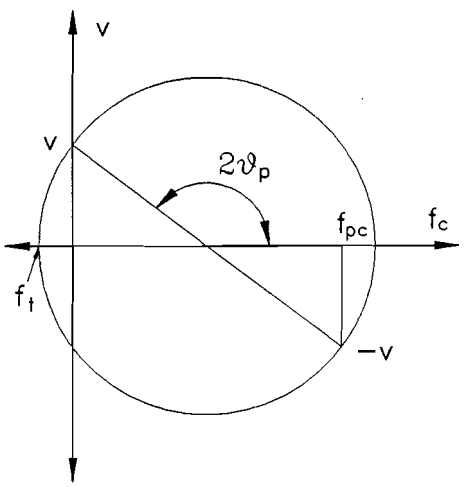

Figure 2.2 Mohr's circle representation of stress at centroid of prestressed concrete beams.

$$V_{cw} = f_r \sqrt{1 + \frac{f_{pc}}{f_r}}\, b'd \qquad (2.3)$$

where f_r = modulus of rupture of concrete given by Equation 2.4,
f_{pc} = compressive stress due to prestress at the centroid of the section,
b' = width of web,
d = effective depth.

Research by MacGregor et al.[34] indicated that the actual tensile strength was between 60 and 100% of the modulus of rupture, where the modulus of rupture was defined as

$$f_r = \frac{3000}{4 + \frac{12{,}000}{f_c'}} \qquad (2.4)$$

They proposed using only 50 to 66% of this value for design. A value of approximately 50% of f_r was adopted in the *Specifications* in the simplified form $f_r = 3.5\sqrt{f_c'}$. In addition, Equation 2.3 was simplified by Mattock (to a linear relationship which is a close but conservative estimate of the curve represented by Equation 2.3). The term V_p was added to reflect the reduction in principal tensile stress caused by the vertical component of the prestress force in members with inclined tendons. The resulting equation (AASHTO Equation 9-29 and ACI Equation 11-13) is

$$V_{cw} = (3.5\sqrt{f_c'} + 0.3\, f_{pc})\, b'd + V_p \qquad (2.5)$$

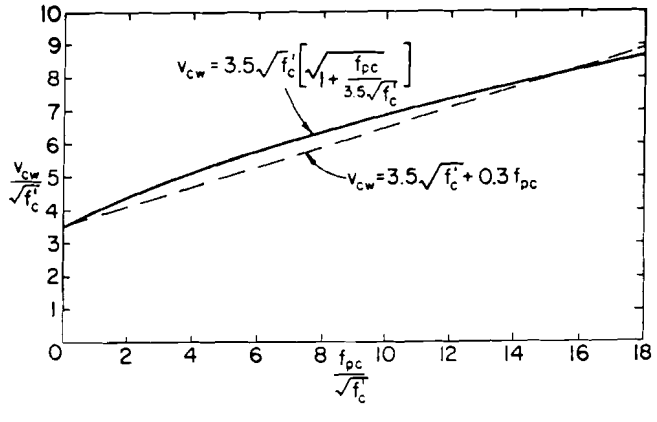

Figure 2.3 Equations for prediction of web shear cracking (Eq.2.3 with $f_r = \sqrt{f_c'}$ and Eq.2.5 with $V_p = 0$).[5]

Unfortunately, in its present form, the equation has little physical significance. But, as can be seen in Figure 2.3, Equation 2.5 matches the more complex relationship very well.

Web-shear cracks for beams with small *a/d* ratios should originate at the centroid of the cross section, with the

centroid being the location of maximum principal tensile stresses. As *a/d* ratios increase in simply supported beams, the influence of the tensile bending stresses tends to move the location of the highest principal tensile stress toward the tension flange. However, at the same time, the increasing *a/d* ratio influences the properties of the beam such that flexural cracking in the tension flange occurs before web-shear cracking, diminishing the significance of the principal stresses in the web. As a result, MacGregor et al.[34] assumed that the web-shear cracking load could be determined by considering only the principal stresses at the centroid.

Based on tests of two-span continuous prestressed beams, Hawkins et al.,[25] observed that the same was not true of continuous beams. In some of the continuous beams tested, web-shear cracking loads were as much as 20% lower than the values calculated at the centroid, indicating that the critical location for maximum principal tensile stresses was closer to the tension flange in areas near the maximum moment section.

2.3.3.2 Flexure-Shear. The current *Specifications'* equation for flexure-shear cracking is a modification of a relation proposed by Sozen and Hawkins[43] in 1962 based on tests of simply-supported beams at the University of Illinois.[34, 44, 30, 23] The shear to produce a flexure-shear crack was defined as

$$V_{ci} = 0.6\sqrt{f_c'}\, b'd + \frac{M_{cr}}{\frac{M_{max}}{V_i} - \frac{d}{2}} + V_d \qquad (2.6)$$

where M_{cr} = flexural cracking moment due to externally applied loads,
= $(I/y_t)(6\sqrt{f_c'} + f_{pe} - f_d)$,
M_{max} = maximum factored moment due to externally applied loads,
V_i = factored shear force due to externally applied loads occurring simultaneously with M_{max},
I = moment of inertia of gross section resisting externally applied factored loads,
y_t = distance from centroidal axis of gross section to extreme fiber in tension.

This equation, the derivation of which can be found in Reference,[5] is made up of three parts. The term $M_{cr}/(M_{max}/V_i - d/2)$ represents the shear force required to cause a flexural crack at a distance $d/2$ (in the direction of decreasing moment) away from the section under consideration. The dead load shear, V_d, is considered separately because it is typically a distributed load, while live loads can be applied with any distribution. In addition, in composite construction the effect of dead load is applied to the prestressed section alone, while the live load effect is computed on the composite section. Finally, the term $0.6\sqrt{f_c'}\ b'd$ represents the additional shear required to turn the initiating flexural crack into a diagonal crack. This portion of the equation is a purely empirical relationship which provides a very good match with test data and "appears to be a function of the cross section and the strength of the concrete."[5] Figure 2.4 is a plot of Equation 2.6 showing it to be a good lower bound for the test data presented.

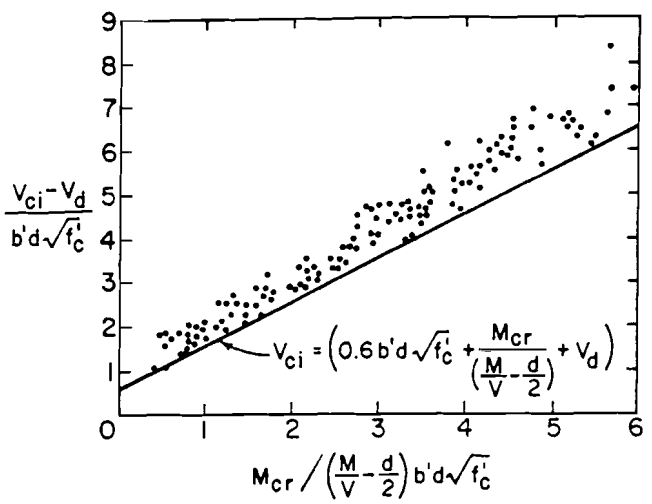

Figure 2.4 Plot showing correlation of Equation 2.6 with test data.[5]

Equation 2.6 was simplified to its current form (Equation 2.7) and made more conservative, based on a paper by MacGregor and Hanson[32] who proposed dropping the $d/2$ from the second term. This change results in a more conservative equation because in its revised form the flexural cracking load is computed at the section under consideration instead of at a distance $d/2$ away from that section, where the moment is lower.

$$V_{ci} = 0.6\sqrt{f_c'}\ b'd + \frac{M_{cr}\,V_i}{M_{max}} + V_d \qquad (2.7)$$

2.3.4 Limitations of AASHTO/ACI Method. The *Specifications*' method for shear design has proven to be generally satisfactory for typical reinforced and prestressed concrete beams. However, for atypical situations it can be confusing and difficult to apply. This is primarily due to the fact that it lacks a consistent theoretical basis, as can be inferred from the following observations:

1) The V_{cw} equation (Equation 2.5) is based on an analysis of principal stresses, while one of three terms in the V_{ci} equation (Equation 2.7) is purely empirical.
2) Equation 2.5 was simplified to a linear empirical relationship, obscuring its theoretical basis.
3) The concrete contribution term (V_c) in Equation 2.1 ignores any post-cracking strength.
4) The *Specifications* method ignores the contribution of aggregate interlock, dowel action, and arch action.
5) The *Specifications* divorces flexure and shear in the design process, ignoring their interdependence.
6) The *Specifications* fails to recognize the similarity in behavior between prestressed and non-prestressed reinforcement at ultimate.

2.4 Strut-and-Tie Model

2.4.1 General. Schlaich et al.,[42] Marti[35, 36] and others have outlined the theoretical background and general guidelines for use of the strut-and-tie model. In addition, a thorough review of the basic concepts and application of the strut-and-tie model was presented by Anderson.[7] The treatment of the strut-and-tie model provided by these authors will not be repeated except where directly applicable to this study.

In this chapter, consideration will be given to the application of the strut-and-tie model to prestressed beams. The specific difficulties associated with application of the strut-and-tie model to the beams tested in this program will be treated in Chapter 5.

2.4.2 Background and Assumptions. The strut-and-tie model has been proposed as a design concept capable of providing a consistent and valid level of safety for all parts of any structural concrete system.[42] The strut-and-tie model, a lower bound (static) plasticity solution, is a refinement and generalization of the classical 45° truss analogy. Its application consists of modeling the structure as a series of compression struts, tension ties, and nodes dimensioned to provide a possible equilibrium system of forces within the structure at ultimate load. As proposed by Schlaich,[42] the struts, ties, and nodes should generally follow the lines of elastic principal tensile and compressive stresses in the structure.

The following assumptions as summarized by Anderson[7] are central to the application of the strut-and-tie model:

1) Failure is characterized by the formation of a mechanism resulting from yielding of one or more ties.
2) Struts and ties carry only axial forces.
3) All external loads are applied directly to the nodes. Care should be taken in the case of distributed loads to ensure that the structure can locally accommodate the assumed replacement of distributed loads with concentrated loads.
4) Crushing of the concrete struts is prevented prior to yielding of the ties.
5) Reinforcement is adequately detailed to prevent local bond and anchorage failure.

2.4.3 Strut-and-Tie Model For Prestressed Beams. Although much has been written about the application of the strut-and-tie model to reinforced concrete, very little guidance is available to extend the application to prestressed concrete. Schlaich et al.[42] indicated that one of the advantages of the strut-and-tie model is that it is equally applicable to structural concrete with prestressed or non-prestressed reinforcement. They caution, however, that this is only true at ultimate load. We are reminded that at service loads the effect of prestressing distinguishes the behavior of prestressed concrete from concrete with only mild reinforcement.

According to Schlaich et al.,[42] prestressed concrete can be treated in exactly the same manner as concrete without prestressing. For example, in modeling a pretensioned beam with straight tendons, the tendons would be considered passive tension reinforcement acting in combination with any non-prestressed longitudinal reinforcement to make up the tension chord of a parallel-chord truss. The prestress force would then be considered as an additional axial load applied to the ends of the beam at the centroid of the tendons. Prestressing steel can only function as reinforcement if it is bonded. In unbonded post-tensioned beams the prestressing steel cannot be considered as reinforcement; it can only act as a tie in a tied-arch system.

2.4.3.1 Prestress as an External Load. Schlaich et al.[42] proposed that the prestress force at the time of release be considered as a permanent, unchanging load applied to the member. Losses of prestress after release (the current terminology for the changes in stress in the prestressing steel over time) should also be attributed to the loads that cause them.

These include creep, shrinkage and elastic shortening of the concrete, and relaxation of the tendons.

There is one major difference between the prestressing steel and any non-prestressed tension reinforcement present in a prestressed beam. The total force capacity of the prestressing steel available to carry loads other than the prestress force is the capacity of the tendon (the maximum capacity of a tendon would typically be between the yield and ultimate loads for that tendon as determined by the appropriate code) less the prestress force. This can be expressed in equation form as follows:

$$T_{ps,\,avail} = T_{ps\,max} - F_{ps} \tag{2.8}$$

where $T_{ps,\,avail}$ is the available capacity of the tendon in excess of the prestress force, F_{ps}, and $T_{ps,\,max}$ is the maximum capacity of the tendon. If the tension chord of the truss also contains non-prestressed reinforcement, then the total chord capacity can be expressed as

$$T = T_{ps,\,avail} + T_s \tag{2.9}$$

where T is the total capacity of the tension chord for loads other than the prestress force, and T_s is the yield capacity ($A_s f_y$) of the non-prestressed longitudinal reinforcement. This slightly confusing formulation is necessary because the prestress force is applied by the tendons. Hence, the tendons must be loaded by the amount of the prestress force prior to the application of any other loads. Thurliman[46] noted that typically the level of prestress corresponds approximately to the difference in the yield stresses of the prestressing and ordinary longitudinal reinforcement. Therefore, he suggests that after decompression of the concrete, the strains in both steels increase together and both reach yield simultaneously.

2.4.3.2 Transfer of Prestress. In the method proposed by Schlaich et al.[42] and intended basically for post-tensioned concrete, the prestress force is applied to the beam as a point load at the end of the beam at the centroid of the prestressing steel, inclined to match the inclination of the tendons at the end of the beam. This method is not completely applicable to pretensioned concrete since it does not explicitly account for the transfer length of the strand, commonly assumed to be $50d_b$[1, 4, 28] where d_b is the diameter of the prestressing strand. Bergmeister[8] proposed a simple strut-and-tie model (Figure 2.5) for the

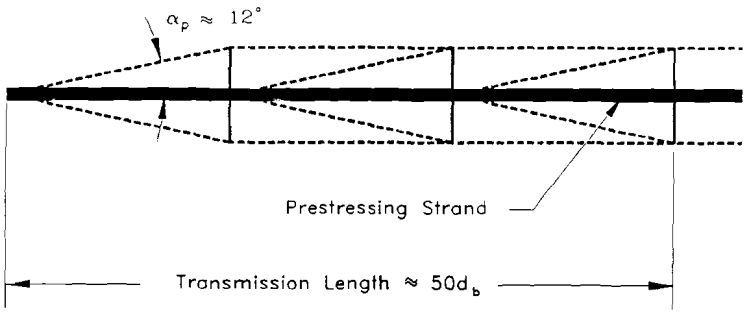

Figure 2.5 *Strut-and-tie model for transfer of prestress to concrete (adapted from Ref. 8).*

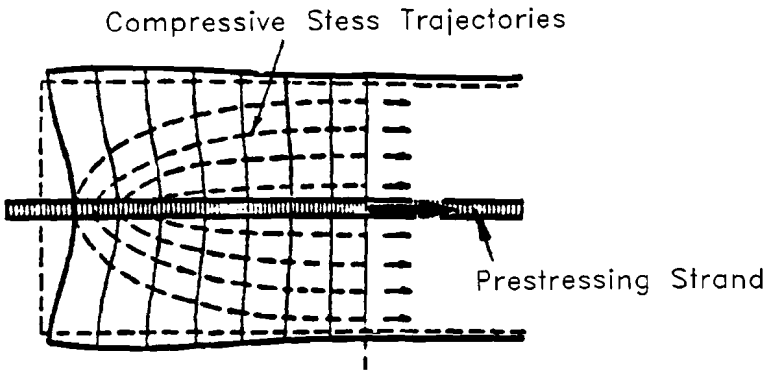

Figure 2.6 Bond stress distribution at end of pretensioned strand.[27]

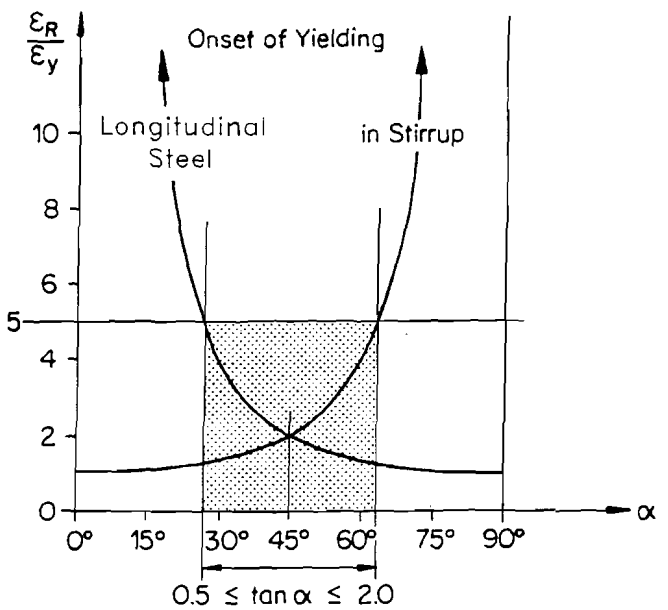

Figure 2.7 Relationship between mean crack strain and strains in reinforcement for different strut angles α.[46]

transfer of bond stress to the concrete based on the bond stress distribution described by Leonhardt[27] (Figure 2.6).

2.4.3.3 Draped Tendons. This author found no clear treatment in the literature of the application of the strut-and-tie model to pretensioned beams with draped tendons. In principle, there is no difference between beams with straight or draped tendons. However, the case of draped tendons is complicated by the need to consider the vertical component of the prestress force. Additionally, in the case of bonded, draped tendons the tension chord must reflect the tendon profile. A possible solution for the beams tested in this program will be presented in Chapter 5.

2.4.3.4 Strut Angles. The relative amount of longitudinal and transverse reinforcement required for a given strut-and-tie or truss model are dependant on the inclination of the compression struts α. Small inclinations result in large longitudinal reinforcement

quantities and small amounts of transverse reinforcement. The reverse is true for large inclinations. This relationship is expressed graphically in Figure 2.7 in terms of the ratio of mean crack strain, ϵ_r (as defined in Figure 2.8), to yield strain, ϵ_y, of the steel. Ideally, the chosen strut angle will closely coincide with the angle of the principal compressive stresses at ultimate so that the struts are defined by the direction of the diagonal cracks. Strut angles which deviate greatly from the angle of principal compressive stress at failure require a high degree of redistribution of forces in the member. Redistribution results in large strains in the reinforcement and high stresses in the struts. Consequently, proponents of the strut-and-tie model and its variations have proposed a variety of limits on the strut angle.[14, 37, 46] These generally restrict the strut angle to a range of 30 to 60° as is required in the CEB Code.[16] However, prestressing results in a flatter angle of principal compressive stresses making values lower than 30° reasonable. The Canadian Code[18] allows values of α between 15 and 75.° These values are reasonable if proper detailing is provided.

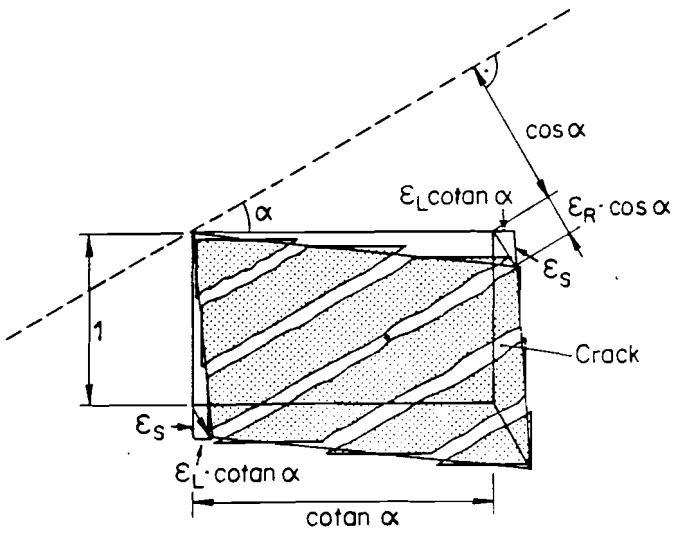

Figure 2.8 Definition of mean crack strain ϵ_r.[46]

2.4.3.5 Struts. Evaluation of the stresses in struts as a check against compression failure of the concrete has typically been done in a manner similar to that proposed by Thurliman[46] based on Figure 2.9

$$f_d = \frac{V}{b'z\cos\alpha\sin\alpha} \qquad (2.10)$$

where V is the applied shear force at the section under consideration, b' is the width of the web, z is the distance between truss chords, and α is the strut angle. In lightly reinforced beams with short

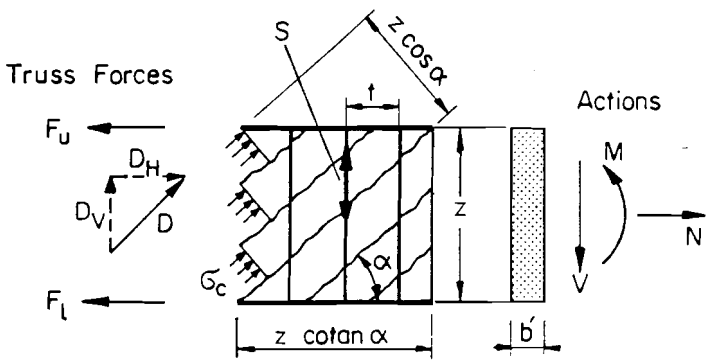

Figure 2.9 Evaluation of compressive stresses in struts.[46]

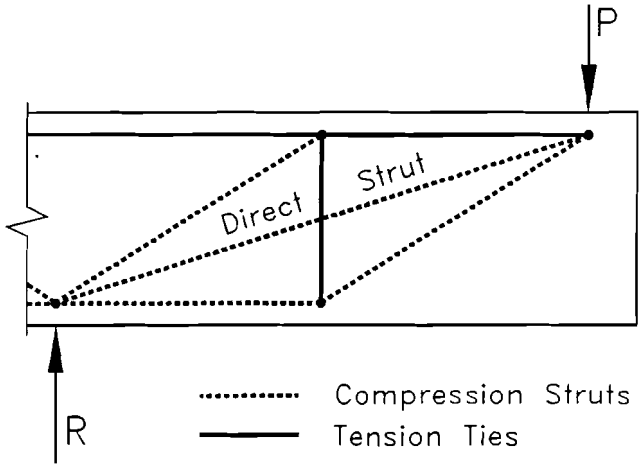

Figure 2.10 Strut-and-tie model with direct strut between applied load and support.

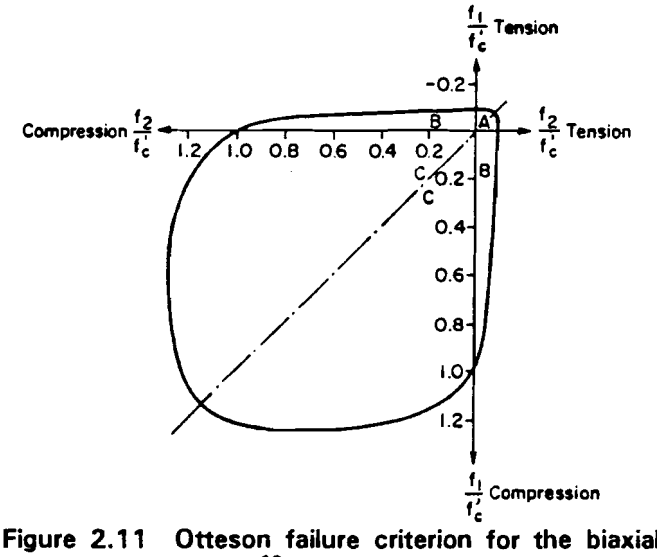

Figure 2.11 Otteson failure criterion for the biaxial strength of concrete.[19]

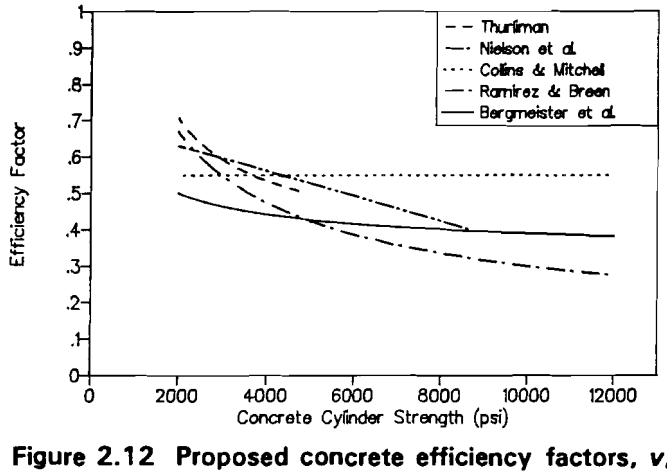

Figure 2.12 Proposed concrete efficiency factors, *v*, for compression struts.

effective shear-spans, a direct strut between the load point and support, similar to that shown in Figure 2.10, can form in addition to the struts anchoring vertical ties in the shear-span. Cook and Mitchell,[17] and Kaufman and Ramirez[26] developed truss models using a direct strut to account for the "concrete contribution" (the additional shear above that which can be carried by the stirrups). Checking the concrete compressive stress by Equation 2.9 is no longer valid in this case. A method for checking concrete stresses in cases such as this will be outlined in Chapter 5.

2.4.3.6 Efficiency Factors.

Concrete subjected to transverse tensile stress will fail in compression at a load less than f'_c. This is apparent in Figure 2.11. Diagonal crack angles at failure in reinforced and prestressed concrete beams are typically shallower than initially observed at first cracking. This effect is due to the redistribution of forces within the member after cracking. As a result, the compression struts at failure are crossed by the initial web-shear cracks as well as by the transverse tensile reinforcement. Both factors contribute to a reduced effective concrete compressive strength. Constant efficiency factors, ν,[12] factors based on states of strain,[13, 17, 42, 47] and factors based on concrete strength[8, 18, 39]

have been proposed to account for this reduction. Efficiency factors proposed in five separate studies are plotted in Figure 2.12.

2.4.4 Limitations of Strut-and-Tie Model. Conceptually, the application of the strut-and-tie model to the design of prestressed concrete is quite simple. In practice, certain aspects of this application are not so simple, or have not been adequately addressed in the literature:

1) A method of modeling the mechanism of force transfer between prestressing steel and concrete in pretensioned members (i.e. the introduction of the prestress force into the struts and ties of the model) has not been clearly defined.
2) Definition of the geometry of nodal regions with prestressed reinforcement as ties, and limiting design stresses for these regions have not been addressed, although research on this topic is currently under way at The University of Texas at Austin. Node definition for junctions of multiple struts and ties is also unclear.
3) The definition and use of efficiency factors in evaluating the effective strength of struts remains as an empirical "weak link" in the strut-and-tie model.
4) The strut-and-tie model ignores the mechanisms of interface shear transfer and dowel action, as do conventional AASHTO Specifications and ACI Code provisions.

CHAPTER 3
EXPERIMENTAL PROGRAM

3.1 Introduction

The primary goal of the experimental portion of this program was verification of the applicability of current AASHTO[1] shear provisions for negative moment regions of cantilevered, prestressed concrete beams. In particular, confirmation was sought for the use of 80% of the total section height, h, in lieu of the actual distance from the extreme compression fiber to the centroid of the prestressing force, d, in AASHTO equations 9-27 and 9-29. A secondary objective was to examine the application of strut-and-tie (truss) models to detailing of prestressed concrete.

3.2 General Information

Eight shear tests were performed on four beams using the loading arrangement shown in Figure 3.1. The testing program for each end of a test beam typically consisted of two cycles of static loading. Tests 1A-1-0.6 and 2A-8-0.6 included a third load cycle due to the failure of a support bearing in Test 1A-1-0.6 and a premature bond failure at a reaction location in Test 2A-8-0.6. Load was applied monotonically in each test to a cantilever having a shear span-to-depth ratio, a/d, of 3.1. All beams had the same cross-section and length.

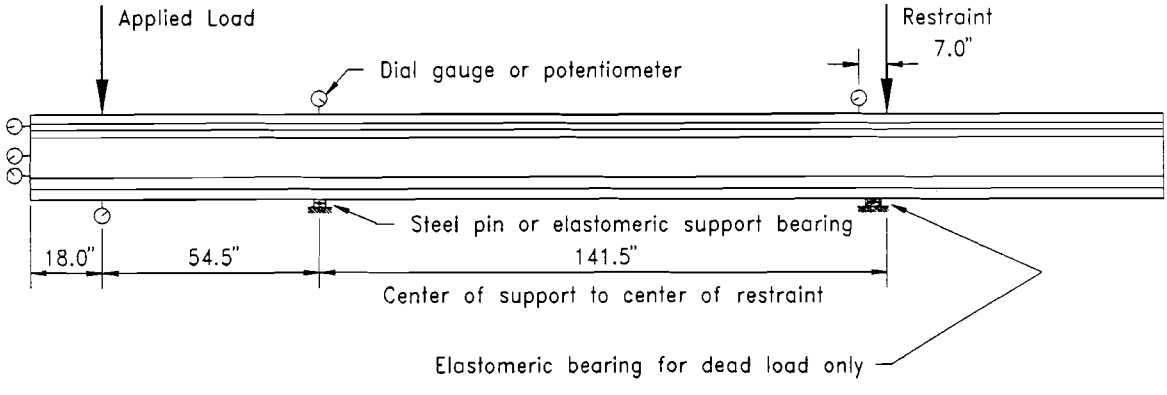

Figure 3.1 Loading arrangement showing deflection and strand slip measurement locations.

The primary test variables were: 1) the profile of the prestressed reinforcement, and 2) the amount of shear reinforcement. Specifically, four of the beam ends had draped strands and four had a straight strand profile. The center of gravity of the prestressed reinforcement in beam ends with straight strands was located at either 0.6*h* or 0.8*h*, where *h* was the total height of the section with a monolithically cast deck slab. The center of gravity of prestressed reinforcement in beam ends with draped strands was 0.8*h* in the vicinity of the support nearest the applied load location and decreased to 0.6*h* in the vicinity of the applied load. A precise description of strand profiles for each specimen is presented in Section 3.3. Transverse reinforcement in test regions of beams was proportioned to provide a nominal shear strength, V_s, of either $1\sqrt{f_c'}$ b'd, $4\sqrt{f_c'}$ b'd, $8\sqrt{f_c'}$ b'd, or $12\sqrt{f_c'}$ b'd, based on a nominal concrete compressive strength, f_c', of 8000 psi. The limits for V_s were chosen because $1\sqrt{f_c'}$ b'd is a practical lower limit for shear reinforcement and $8\sqrt{f_c'}$ b'd is the greatest amount allowed by the AASHTO Bridge Specifications (Section 9.20.3.1).

3.3 Description of Test Specimens

3.3.1 General. Test specimens were constructed using the long-line precasting method, with two beams per cast. Beams from the first cast are labeled *1A* and *1B*. Beams from the second cast are labeled *2A* and *2B*. Because both ends of each beam were tested, the individual tests will be distinguished by a name that includes the cast number, beam designation (*A* or *B*), amount of shear reinforcement, and strand profile. For example, Test 1B-8-D refers to the test of Beam *B* from the first cast, at the end that has $V_s = 8\sqrt{f_c'}$ b'd and a draped tendon profile; and Test 2A-8-0.6 refers to the test of Beam *A* from the second cast, at the end that has $V_s = 8\sqrt{f_c'}$ b'd and a straight tendon profile with centroid of the prestressed reinforcement located 0.6*h* above the bottom of the beam.

All beams were constructed using the cross section shown in Figure 3.2. The section, based on a one-third scale Texas Type IV girder, was modified to increase the height/width ratio of the web to a value of 5.0 so that the effect of web-slenderness on shear behavior could be observed. All beams were 23'-7" long, and had a monolithically cast deck slab. Both ends of each beam had a region 18" long between the load point and the end of the beam for anchorage and development of the prestressed reinforcement.

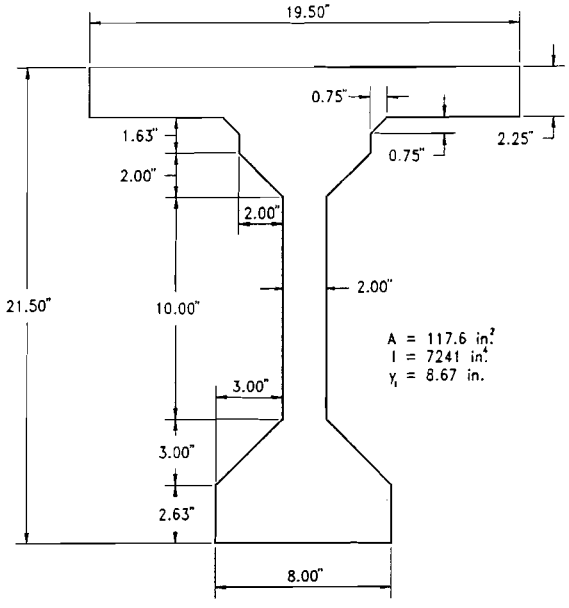

Figure 3.2 Typical cross section and section properties.

Prestressed reinforcement consisted of nine 3/8" diameter, 7-wire, 270 ksi, low-relaxation strands placed on a 1-1/4" grid in each beam. In each beam, four strands were straight and five were draped.

Flexural reinforcement (both prestressed and non-prestressed) was designed to satisfy stress limits at release and ultimate strength. Due to the small eccentricity of the prestress force, no tensile bending stresses were present in the beams at release. A composite I-beam designed for negative-moment bending necessarily has a neutral axis high in the section, thus precluding a large eccentricity. It was therefore necessary to over-reinforce the beams for flexure by adding non-prestressed flexural reinforcement in both tension and compression regions to ensure shear failures. This reinforcement helped provide a minimum factor of safety of 1.3 against flexural failure at ultimate that could not be provided with the prestressed reinforcement alone. It was therefore necessary to perform the flexural design using the strain compatibility method.[37]

Non-prestressed flexural reinforcement was used in the bottom flange and the deck slab in all specimens. Bottom-flange compression reinforcement consisted of two #3 and two #4 deformed bars, except in Beam 2A in which there were four #4 bars. The amount of tension reinforcement in the slab varied, consisting of either eight #4, or four #4 and four #5 deformed bars.

Shear design was done according to the *AASHTO Specifications for Highway Bridges*.[1] The concrete contribution to the shear strength, V_{ci} or V_{cw}, was calculated using a nominal concrete strength f'_c = 8000 psi and an assumed initial prestress force. In all cases, except Beam 2A-12-D, web cracking, V_{cw}, in the cantilever controlled the design. For Beam 2A-12-D flexure-shear cracking, V_{ci}, on the interior side of the cantilever support controlled.

Table 3.1 Design Summary for All Beams.

Specimen No.	Design V_s / $b'd\sqrt{f'_c}$	Actual V_s / $b'd\sqrt{f'_c}$	Draped Strand Profile	d
1A-1-0.6	1	0.97	N	0.6*h*
1A-1-D	1	0.99	Y	--
1B-1-0.8	1	0.96	N	0.8*h*
1B-8-D	8	7.75	Y	--
2A-8-0.6	8	7.24	N	0.6*h*
2A-12-D	12	11.05	Y	--
2B-8-0.8	8	7.47	N	0.8*h*
2B-4-D	4	3.92	Y	--

Table 3.1 summarizes the design data for all test beams, and shows both the design level of shear reinforcement based on a nominal concrete strength of 8000 psi, and based on the measured concrete strength at the time of testing. The column entitled "Draped" indicates whether the strands are straight or draped in the cantilever test region. If they are draped, the value of d in the last column varies between 0.8*h* over the support and 0.6*h* at the end of the girder.

Additional transverse reinforcement was added for two feet at each end of the beams for confinement of strands in anchor regions and to prevent local failure under the applied test loads. This reinforcement, consisting of additional stirrups, modified stirrups, and straight bars is shown in Figures 3.3 and 3.4. End detail reinforcement was designed according to the PCI method.[28]

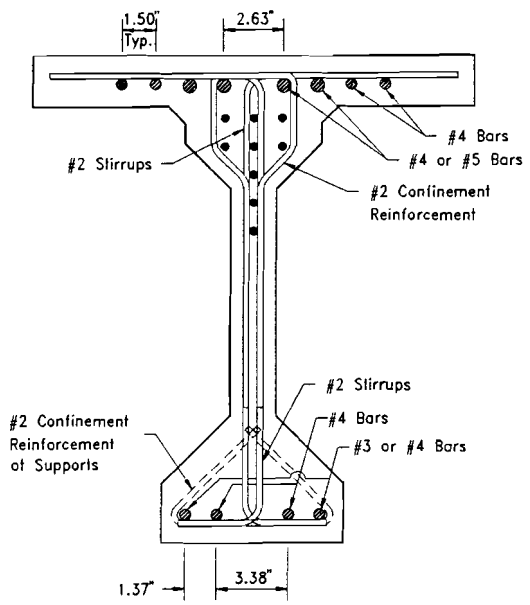

Figure 3.3 Section showing end detail steel.

Additional confinement reinforcement was also added in the bottom flange at the support points to prevent local splitting failure. It consisted of seven #2 hoops over a length of 9 in. at each support.

Reinforcement details for each test beam are presented in Figures 3.5 through 3.16.

3.3.2 Beam 1A. Figure 3.5 shows the strand profile and stirrup locations for Beam *1A*. End *A*, corresponding to Test 1A-1-0.6, had only straight strands, with the tendon centroid located at 0.6*h* as shown in Figure 3.6a. The cross section in Figure 3.6a also illustrates the layout of non-

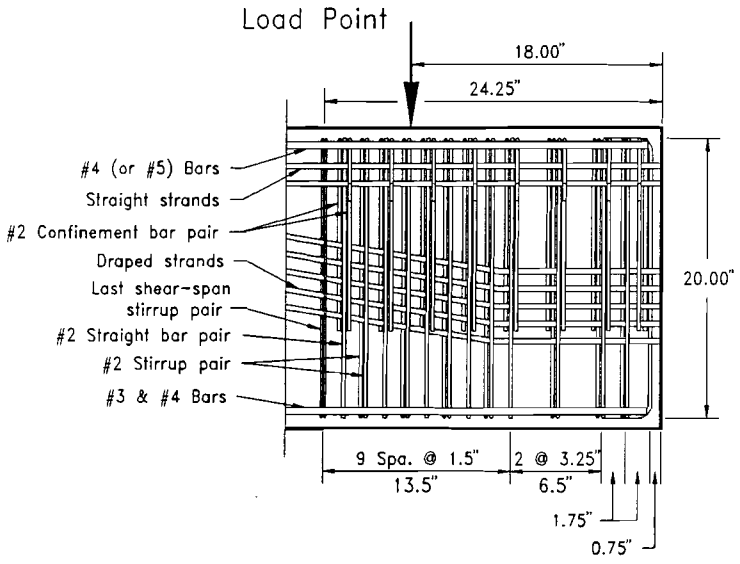

Figure 3.4 Elevation of end detail steel.

prestressed longitudinal reinforcement and stirrups. End *B*, corresponding to Test 1A-1-D, had draped strands as shown in Figures 3.5 and 3.6b.

Both ends had the same amount of shear reinforcement in the cantilever regions ($V_s = 1\sqrt{f_c'}\, b'd$, based on a nominal concrete compressive strength of 8000 psi). In order to satisfy maximum spacing

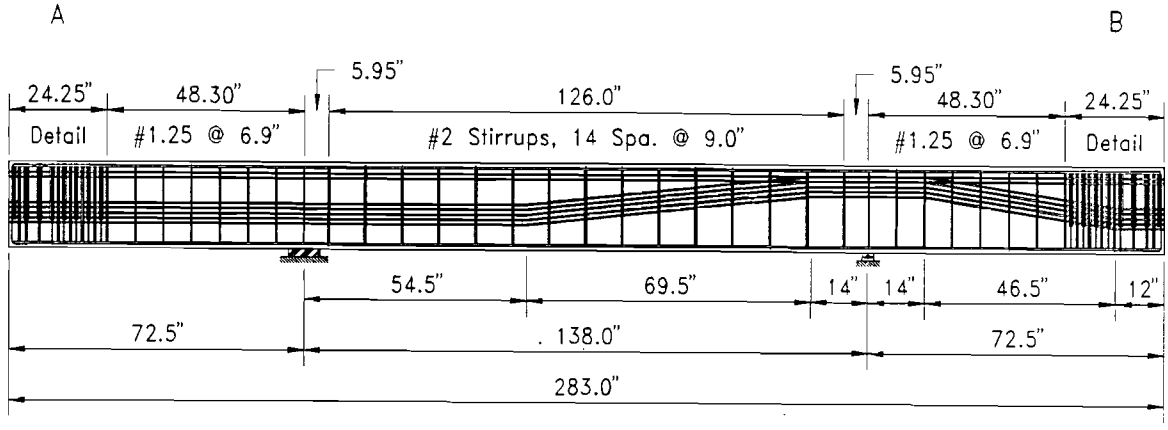

Figure 3.5 Beam 1A dimensions, stirrup locations, and tendon drape points.

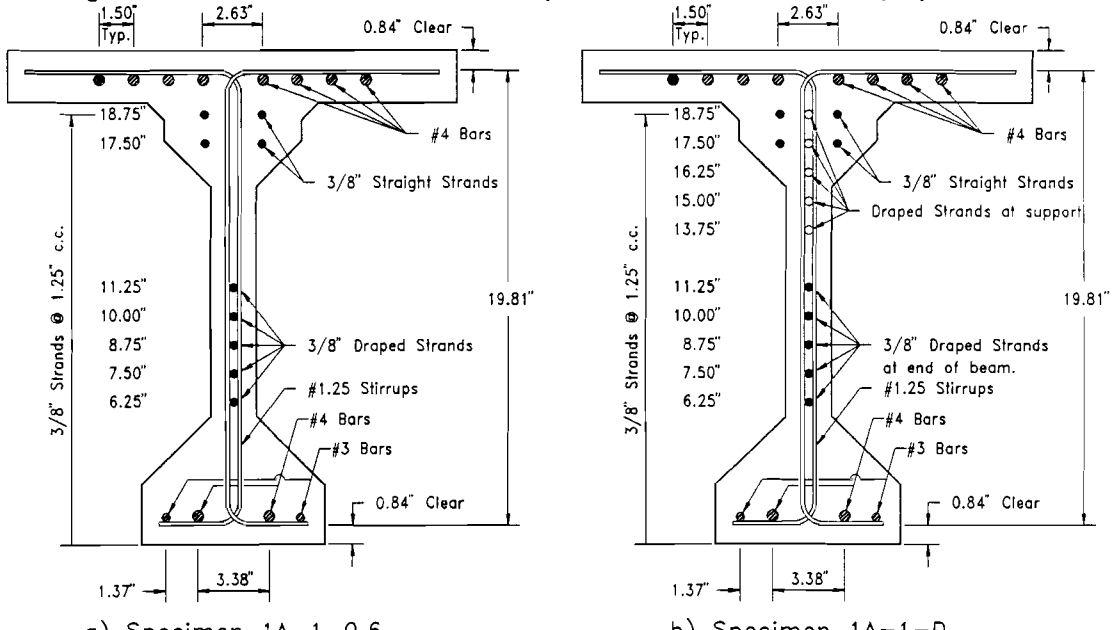

Figure 3.6 Reinforcement for Beam 1A.

limits, #1-1/4 deformed bars with a yield strength, f_y, of 35 ksi were used. The interior region was more heavily reinforced to prevent a shear failure in an undesired location. Deformed #2 (6 mm) bars with a yield strength of 75 ksi were used.

3.3.3 Beam 1B. Figure 3.7 shows the strand profile and stirrup locations for Beam *1B*. End *A*, corresponding to Test 1B-1-0.8, had straight strands, with the tendon centroid located at 0.8*h* as shown in Figure 3.8a. The figure also illustrates the non-prestressed longitudinal reinforcement and stirrups. End *B*, corresponding to Test 1B-8-D, had draped strands as shown in Figures 3.7 and 3.8b.

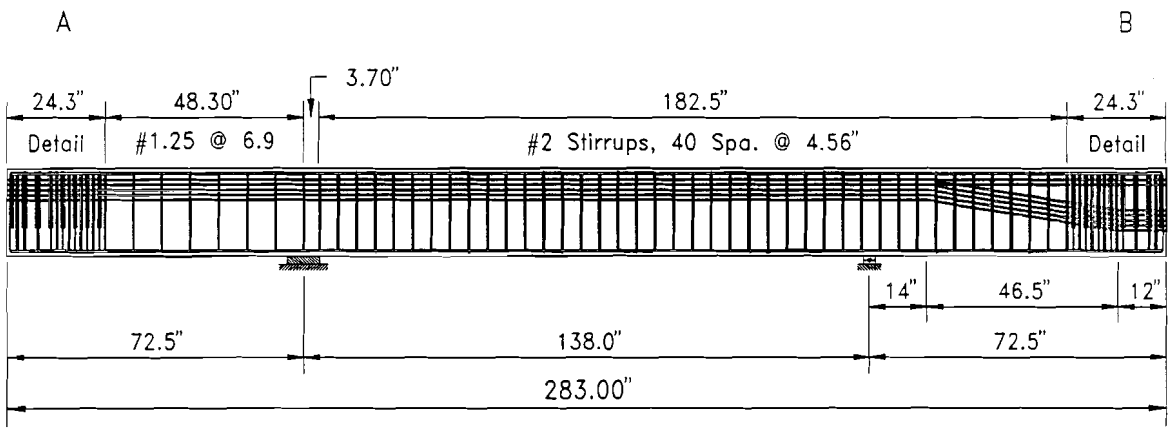

Figure 3.7 Beam 1B dimensions, stirrup locations, and tendon drape points.

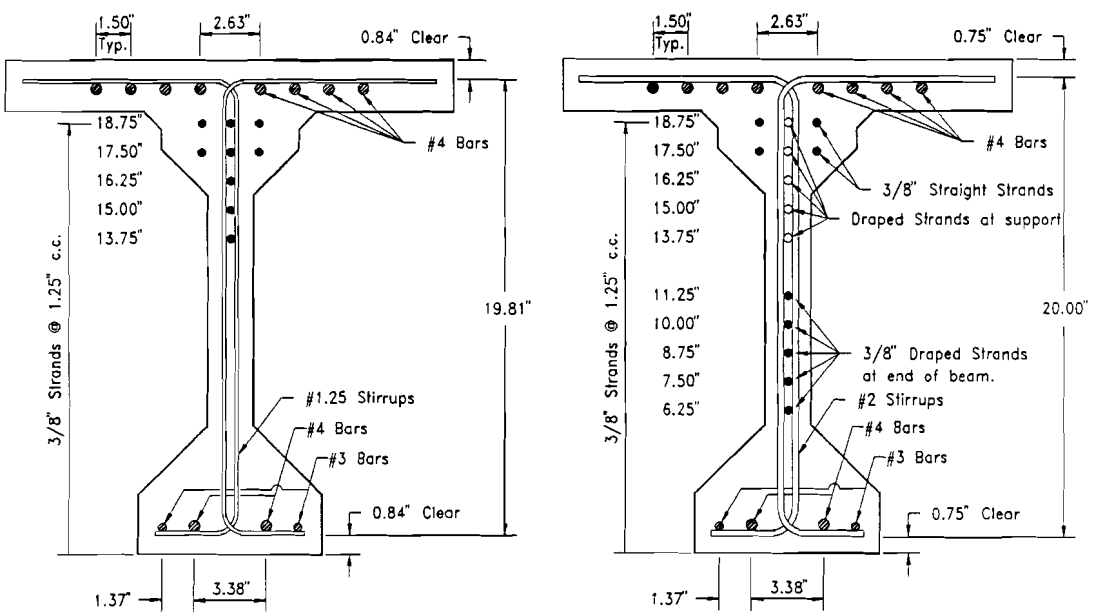

Figure 3.8 Reinforcement for Beam 1B.

End *A* had the minimum amount of web reinforcement examined in this study placed in the cantilever region ($V_s = 1\sqrt{f_c'}\ b'd$). In order to satisfy maximum spacing requirements, #1-1/4 deformed bars with a yield strength of 34.9 ksi were used. The interior region from the support to, and including, the cantilever region of end *B* had the maximum amount of web reinforcement permitted by pertinent design specifications and codes ($V_s = 8\sqrt{f_c'}\ b'd$ using #2 (6 mm) deformed bars).

3.3.4 Beam 2A. Figure 3.9 shows the strand profile and stirrup locations for Beam *2A*. End *A*, corresponding to Test 2A-8-0.6, had straight strands, with the tendon centroid located at 0.6*h*. This specimen had the same non-prestressed longitudinal reinforcement as the other specimens, except that the central four #4 bars in the deck slab were replaced in this specimen by four #5 bars as shown in Figure 3.10a. End *B*, corresponding to Test 2A-12-D, had draped strands as shown in Figures 3.9 and 3.10b.

End *A* incorporated the maximum permissible web reinforcement in the cantilever region ($V_s = 8\sqrt{f_c'}\ b'd$). The interior region from the support to the center of the beam had even more web reinforcement ($V_s = 12\sqrt{f_c'}\ b'd$) to prevent failure in this region while testing end *B*. This was necessary because Test 2A-12-D (end *B*) was designed to fail in the *flexure-shear* mode between the support and midspan where the amount of web reinforcement was $V_s = 1\sqrt{f_c'}\ b'd$. The cantilever region of end *B* was also heavily reinforced ($V_s = 12\sqrt{f_c'}\ b'd$), again with the intent of forcing the failure to the interior side of the support.

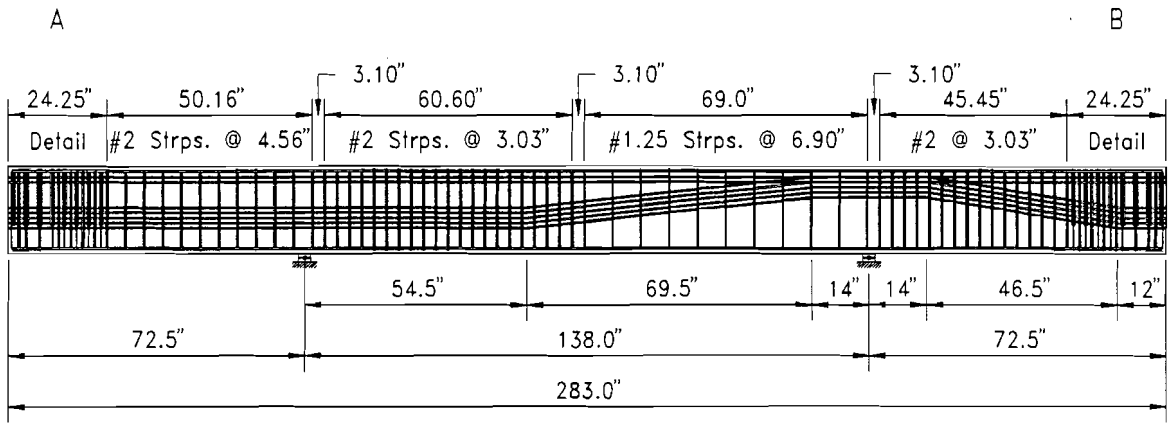

Figure 3.9 Beam 2A dimensions, stirrup locations, and tendon drape points.

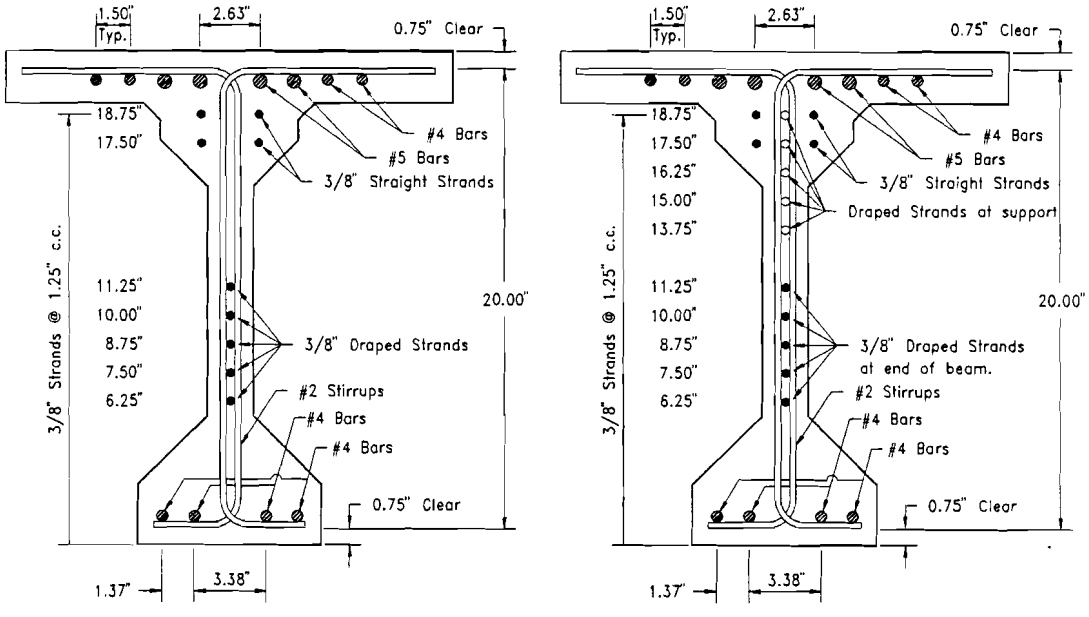

Figure 3.10 Reinforcement for Beam 2A.

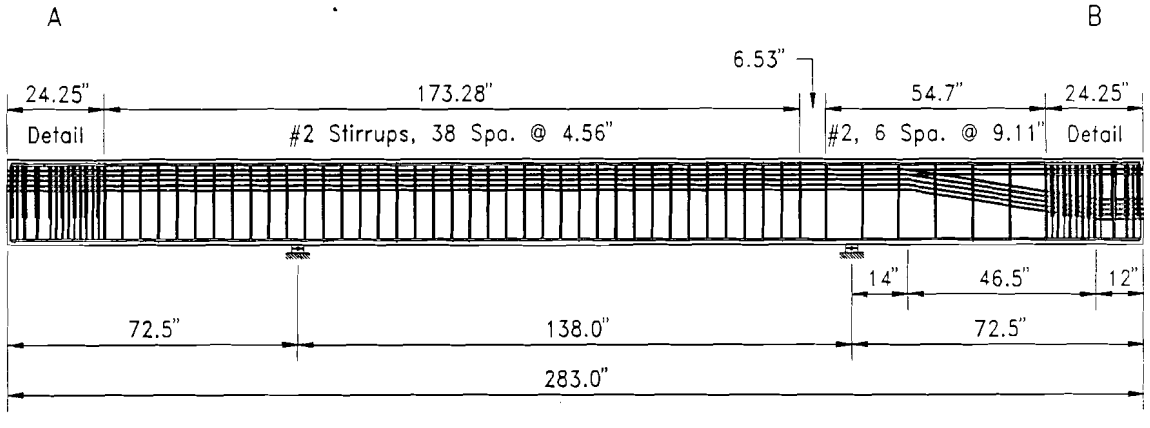

Figure 3.11 Beam 2B dimensions, stirrup locations, and tendon drape points.

Deformed #2 bars were used where the quantity values of web reinforcement was intended to be $V_s = 8\sqrt{f_c'}\ b'd$ or $V_s = 12\sqrt{f_c'}\ b'd$. Deformed #1-1/4 bars were used for the interior side of the support at end *B* where the amount of web reinforcement provided was $V_s = 1\sqrt{f_c'}\ b'd$.

3.3.5 Beam 2B. Figure 3.11 shows the strand profile and stirrup locations for Beam *2B*. End *A*, corresponding to Test 2B-8-0.8, had straight strands, with the tendon centroid

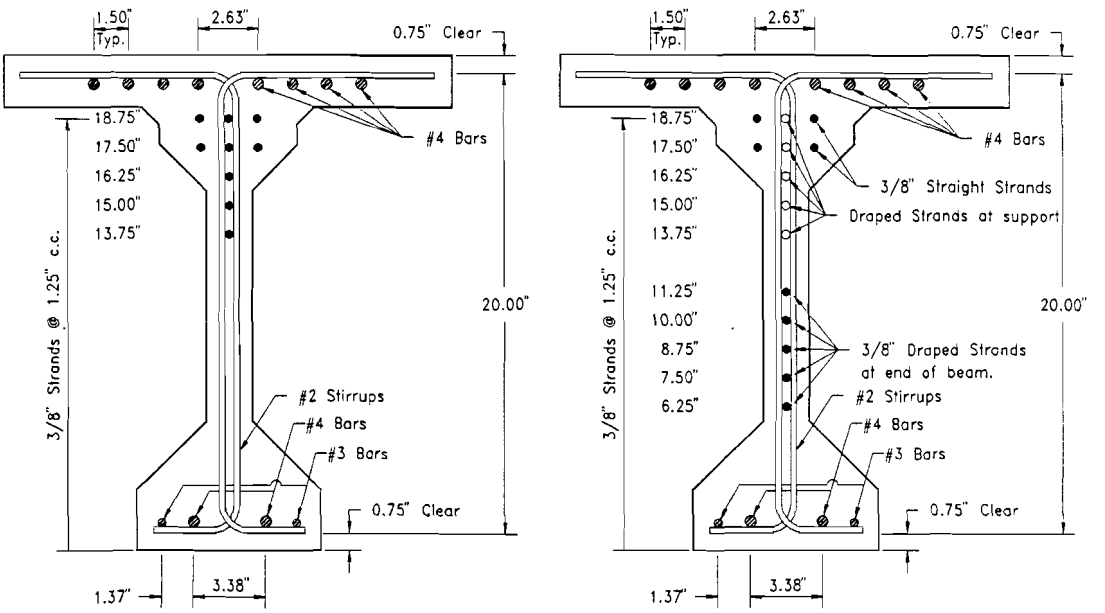

Figure 3.12 Reinforcement for Beam 2B.

located at 0.8*h*. End *B*, corresponding to Test 2B-4-D, had draped strands as shown in Figures 3.11 and 3.12b. The cross section illustrated in Figure 3.12b also shows the location of non-prestressed longitudinal reinforcement and stirrups.

End *A* contained the maximum amount of transverse reinforcement ($V_s = 8\sqrt{f_c'}\ b'd$) in the cantilever region and up to the support at end *B*. The cantilever at end *B* contained half as much reinforcement $V_s = 4\sqrt{f_c'}\ b'd$. Deformed #2 (6 mm) bars were used for all shear reinforcement in this beam.

3.4 Materials

3.4.1 Concrete. The concrete mix for all specimens was designed to provide a 28-day compressive strength of 8000 psi. Concrete was obtained from a local ready mix plant. The mix design employed 3/8" pea gravel for coarse aggregate because of congestion of prestressed and mild reinforcement in the 2" web. Fly ash replaced 30% of the cement, by weight, in the mix. Details of the mix design can be found in Table 3.2.

Table 3.2 Concrete Mix Design.

Cement	525 lb./cu. yd.
Fly Ash	225 lb./cu. yd.
3/8" Pea Gravel	1,580 lb./cu. yd.
Sand	1,303 lb./cu. yd.
Water	270 lb./cu. yd.
Water Reducer	22.5 oz./cu. yd.
Superplasticizer (added on site)	112 oz./cu. yd.

Table 3.3 Concrete Strength at Time of Testing.

Specimen No.	Concrete Strength f'_c (psi)
1A-1-0.6	10,020
1A-1-D	9,650
1B-1-0.8	10,250
1B-8-D	10,150
2A-8-0.6	11,640
2A-12-D	11,330
2B-8-0.8	10,930
2B-4-D	9,970

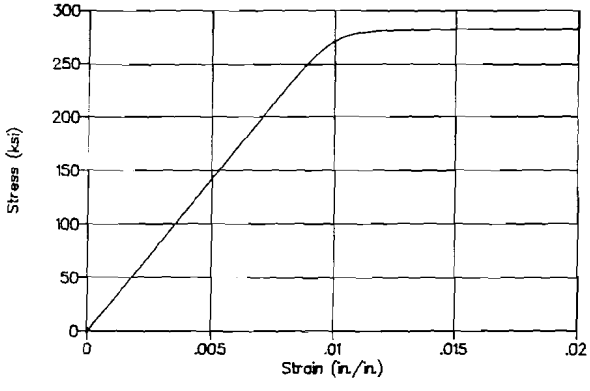

Figure 3.13 Stress-strain curve for 3/8", 270 ksi, low-relaxation prestressing strand.

Thirty-eight 6 x 12" concrete cylinders were made using plastic molds, during the first cast, and forty-five were made during the second cast. Cylinders were stored with the test specimens and tested at release of prestress, at 7, 14, and 28 days, and on each day on which beams were tested. In addition, split cylinder tests were performed on each test day. Test specimens were covered with plastic and were moist cured for two to four days.

Actual compressive strengths at the time of testing ranged from f'_c = 9650 psi for Test 1A-1-D to f'_c = 11,640 psi for Test 2A-8-0.6, and are shown in Table 3.3

3.4.2 Prestressing Steel. A 3/8" diameter, Grade 270 ksi, seven wire, low relaxation prestressing strand donated by the Florida Wire and Cable Company was used in all specimens. The load-strain behavior provided in the mill report is shown in Figure 3.13. The modulus of elasticity from the mill report was 28,400 ksi. Tensile tests were conducted in the laboratory with strain gauges mounted on two of the seven wires. Data from these tests indicated an apparent modulus of elasticity of 28,700 psi (a difference of 1.1%). The latter modulus was used to interpret strand strain data.

Strand was stored in the laboratory for approximately three years before being used. The surface of the strand was lightly pitted as a result of corrosion.

3.4.3 Non-Prestressed Reinforcement. Deformed reinforcing bars were used for both shear and non-prestressed flexural reinforcement in all specimens. Because of the relatively small size of the test specimens (approximately 1/3 scale) and the relatively small amount of shear reinforcement used in some of the specimens, extremely small reinforcing bars were required. Because #3 bars are the smallest size typically available in the United States, #1-1/4 and #2 (6 mm) bars were obtained from Mexico and Sweden, respectively.

As received from the manufacturer, the #1-1/4 bars had a high yield point and very limited ductility, making them unsuitable for use in the test specimens. To improve the properties of these bars, the steel was annealed at a local heat-treating plant. After treatment, the yield stress was 35 ksi based on a net area of 0.0192 in^2. The stress-strain characteristics before and after treatment are shown in Figure 3.14.

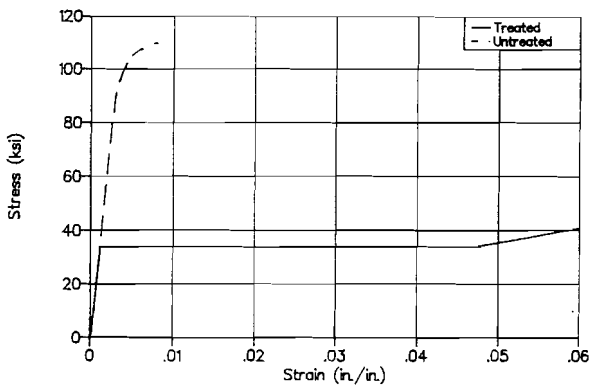

Figure 3.14 Typical stress-strain curve for #1-1/4 Mexican bars.

The #2 deformed bars had much more suitable properties than the #1-1/4 bars, and were used without heat-treatment. They had a yield stress of 75 ksi based on a net area of 0.0475 in^2. Stress-strain behavior for these bars is shown in Figure 3.15.

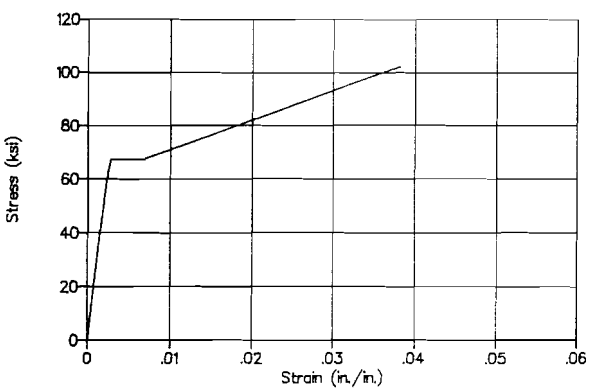

Figure 3.15 Typical stress-strain curve for #2, #3, #4, and #5 bars.

Grade 60 #3, #4, and #5 bars were used for auxiliary flexural reinforcement. The #3, #4, and #5 bars all had stress-strain behavior very similar to that shown in Figure 3.15. Number 3 bars were used

for compression reinforcement in the bottom flange of all test beams. They had a yield stress of 67 ksi. Number 4 bars, with a yield stress of 65 ksi, were used for tension reinforcement in the deck slab and compression reinforcement in the bottom flange of all beams. Number 5 bars were used in the deck slab of Beam 2*A* only to provide additional flexural strength. These bars also had a yield stress of 65 ksi.

3.5 Fabrication

3.5.1 Introduction. All test specimens were fabricated in a pretensioning bed at the Ferguson Structural Engineering Laboratory (FSEL). The long-line method of prestressing was used to cast two beams simultaneously.

3.5.2 Formwork. Wooden forms built by Castrodale[11] were used to fabricate all beams. As originally built, these forms provided an approximately 1/3 scale model of a standard Texas 54" Type IV section. They were modified by Hartmann[22] to allow the deck slab to be cast monolithically with the beam. For this experimental program it was necessary to further modify the forms to provide a section with a depth/width ratio for the web of 5.0. This was accomplished by adding beveled plywood strips in the area that was previously the lower portion of the top flange, thus making the web deeper and the top flange shallower.

3.5.3 Pretensioning Procedure. Because the beams in this test program were designed for negative-moment bending, they incorporated draped strands in inverted configurations compared to those encountered in typical pretensioned girders. Draping hardware was connected to the base slab at hold-down points, and to steel frames at hold-up points. The frames and draping hardware were fabricated in the laboratory. Figure 3.16 shows the hardware used at a typical drape point.

The prestressing operation was accomplished in two stages. The first stage involved using a monostrand hydraulic ram at the dead end of the prestressing bed to pull each strand to an initial tension stress of 50 ksi ($0.185f_{pu}$). This was done to ensure uniform initial tension in all strands. This also provided safe working conditions, as well as taut strands, for tying the reinforcement cage. Tensioning was controlled by a pressure transducer and strain gauges on the strands, and was checked using strand elongation measurements.

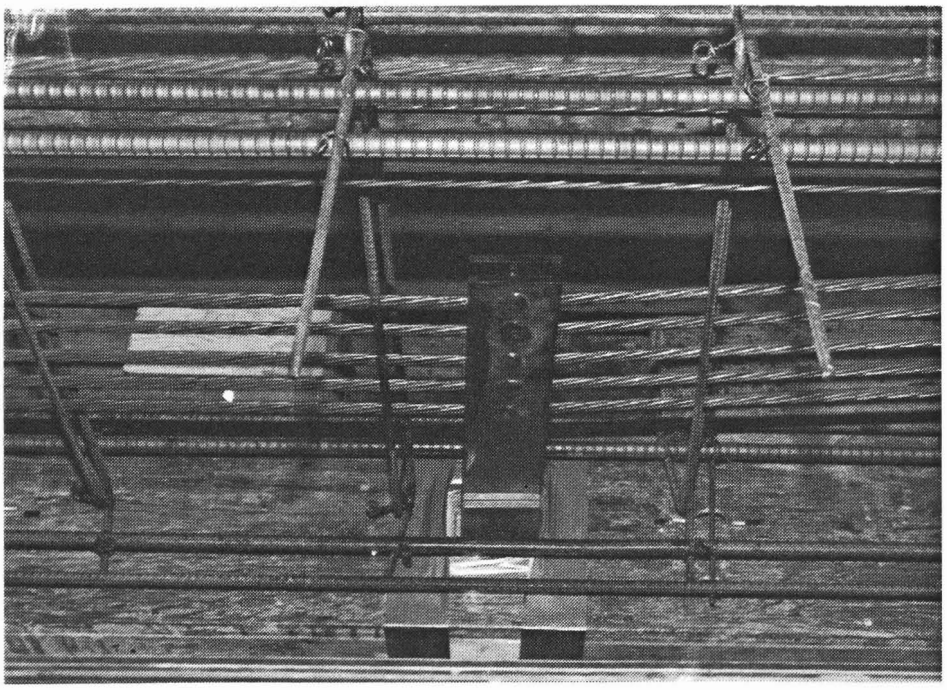

Figure 3.16 Draping hardware.

In the second stage, all strands were tensioned together to an average stress of 216 ksi ($0.80f_{pu}$) using the 1000 kip hydraulic ram at the live end of the prestressing bed. After tensioning, the position of the steel plate used to pull the strands at the live end was secured with lock nuts, then the pressure in the ram was released. In this operation, tensioning was controlled primarily by strain gauges on two strands, and checked using elongation measurements (i.e. movement of the live-end anchor plate). Ram pressure was not used because of the large, unquantifiable friction losses inherent in the prestressing bed.

Anchor hardware (chucks and wedges) was donated by the Great Southwest Marketing Company. Due to the close spacing of the strands and the size of the prestressing chucks, a two-level anchoring system employing chairs fabricated in the laboratory was necessary.

Transfer of prestress to the girders was also accomplished in two stages. First, the nuts securing the draping hardware were loosened, beginning with the hold-up points and finishing with the hold-down points. Next, the ram was again loaded until the locking nuts were loose, after which time the pressure was released slowly, providing a gradual transfer of prestress. After transfer, the strands were cut and ground flush with the end of the beam.

3.5.4 Girder Fabrication. Stirrups and detail reinforcement were bent and strain gauges affixed in the laboratory. Strands were cut to length and threaded into place in the pretensioning bed. After strain gauges were attached to the strands and wired to strain indicator boxes, initial tension was applied to the strands.

The reinforcement cage was then assembled using the strands as temporary supports. The four outer bars in the deck slab were left out until after the forms were erected so they could be supported by the deck forms. Temporary ties between the strand and reinforcing cage were cut before final tensioning to avoid movement of the cage.

Forms were erected and concrete was cast as soon as possible following final tensioning of strands (one day later for the first cast and three days later for the second cast) to avoid loss of prestress before casting. Strains in strands were checked before casting, and in both cases there were no significant losses.

3.5.5 Casting Procedure. Beams were cast two at a time and in two lifts using an overhead crane and bucket. Superplasticiser was added to the truck upon arrival to increase the slump from 3 or 3-1/2" to approximately 9-1/2" to facilitate placement. Strands in the web prevented internal vibration except in the top flange and deck slab, necessitating the use of external vibration. Consolidation was generally very good in spite of the congestion of longitudinal and transverse steel. The deck was screeded, but smooth finishing was made difficult by the high cement content of the mix.

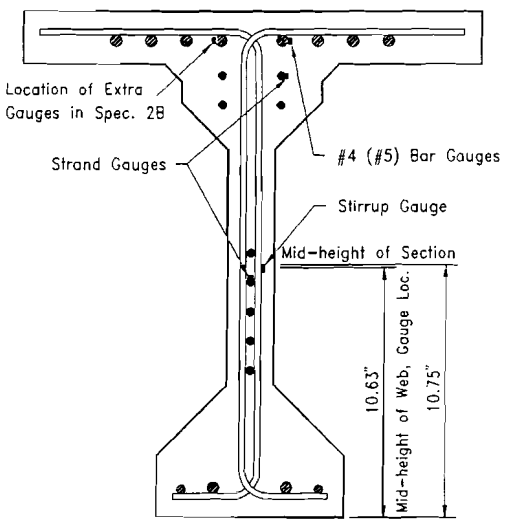

Figure 3.17 Strain gauge locations.

Concrete was moist cured under wet burlap and plastic for two to four days, at which time forms and cylinders were stripped. Prestress was transferred to the girders four days after each cast.

3.6 Instrumentation

3.6.1 Internal Strain Gauges. Electronic resistance strain gauges were mounted on both transverse and longitudinal reinforcement. Figures 3.17 to 3.22 show strain gauge locations for all specimens. Stirrup-mounted strain gauges were located at mid-height and on alternating sides of the web. Longitudinal bars in the deck slab had strain gauges mounted in the support regions. All gauges were applied, waterproofed, and protected according to standard laboratory guidelines.

Strand-mounted gauges were affixed to one wire in the strand, and were oriented along the axis of that wire. An apparent modulus of elasticity of 28,700 ksi was used to convert measured strains to equivalent stresses. All strand gauges remained connected to strain indicator boxes from before initial tensioning until they were connected to a Hewlett-Packard data acquisition system prior to testing. Readings were taken at time of connection, initial tensioning, final tensioning, prior to casting, and before connection to the data acquisition system for each test.

3.6.2 Girder Deflections. Girder deflections were measured electronically using linear potentiometers and mechanically using dial gauges. In the first group of four tests, only one linear potentiometer placed under the load point was used. In the second group of four tests, a second potentiometer was used at the hold-down location. Dial gauges were placed as shown in Figure 3.1 under the load point, over the support, and at the hold-down position. These were placed as closely as possible to the girder centerline at each location.

Two dial gauges were also used to measure roll at the support. They were placed horizontally on the face of the deck slab and bottom flange as shown in Figure 3.23.

3.6.3 Strand Slip Detection. Dial gauges were used to measure slip of strands relative to the end of the beam. These were supported horizontally by a light steel frame epoxied to the faces of the deck and bottom flange as shown in Figure 3.24.

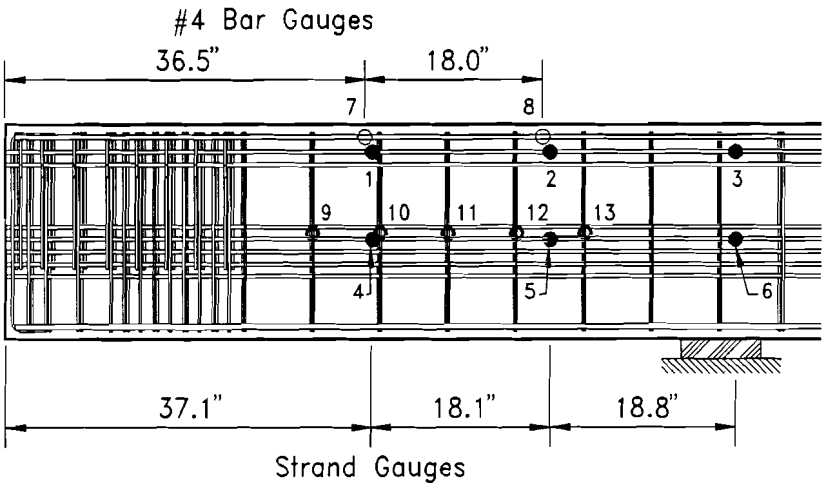

a) Specimen 1A−1−0.6

● Strain Gauges on Strand
○ Strain Gauges on #4 Bars
o Strain Gauges on Stirrups

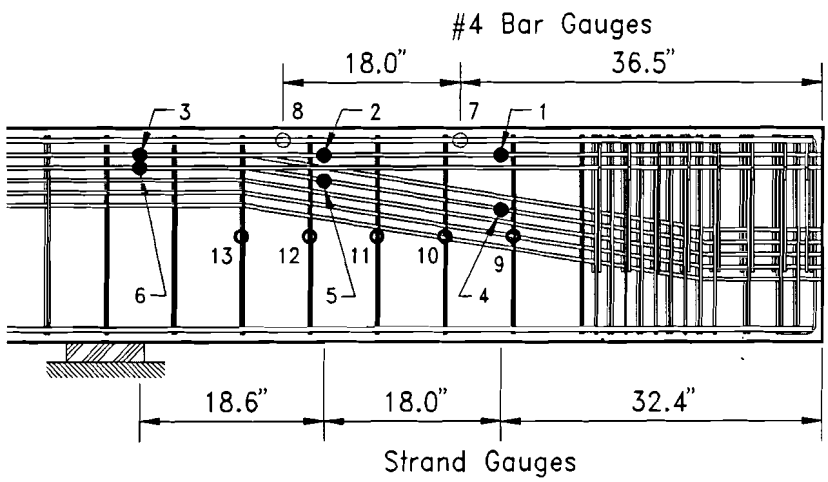

b) Specimen 1A−1−D

Figure 3.18 Strain gauge locations in Beam 1A.

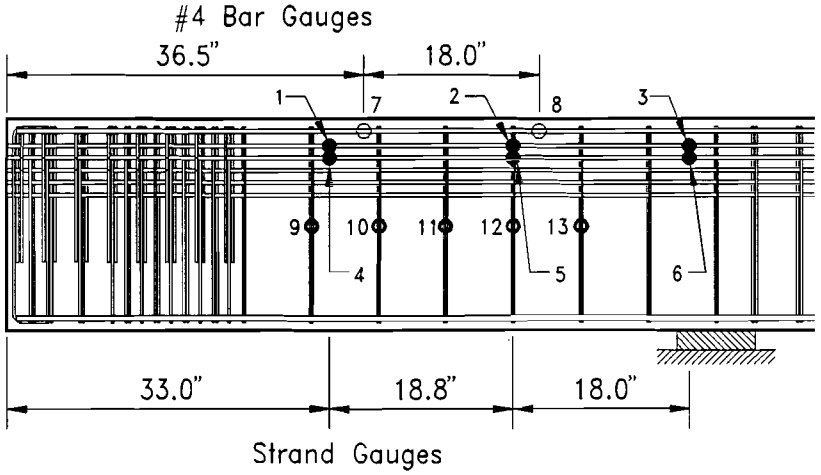

a) Specimen 1B−1−0.8

● Strain Gauges on Strands
○ Strain Gauges on #4 Bars
o Strain Gauges on Stirrups

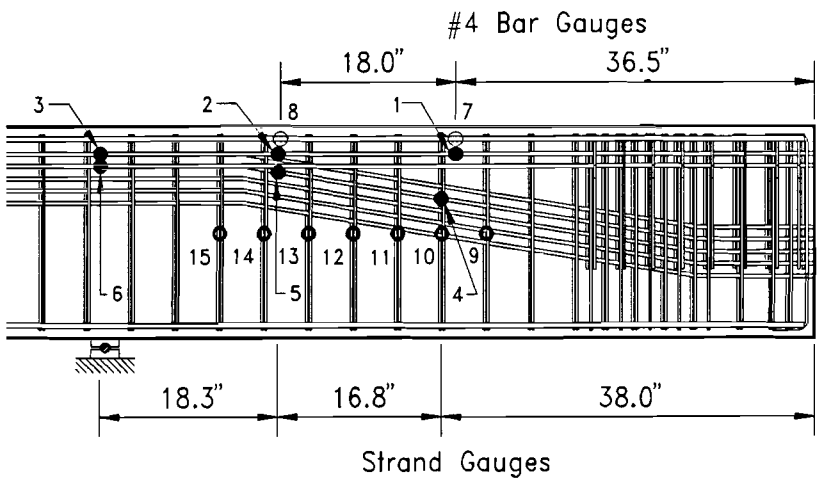

b) Specimen 1B−8−D

Figure 3.19 Strain gauge locations in Beam 1B.

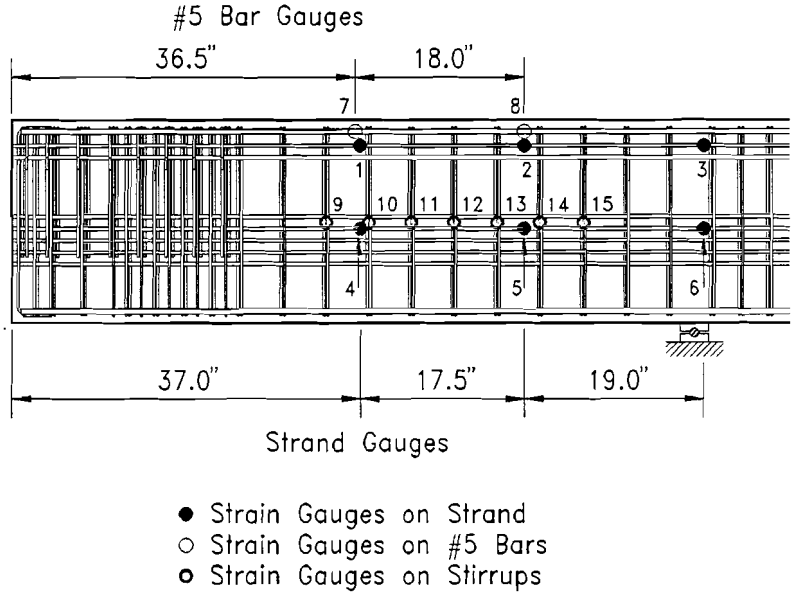

Figure 3.20 Strain gauge locations in Specimen 2A-8-0.6.

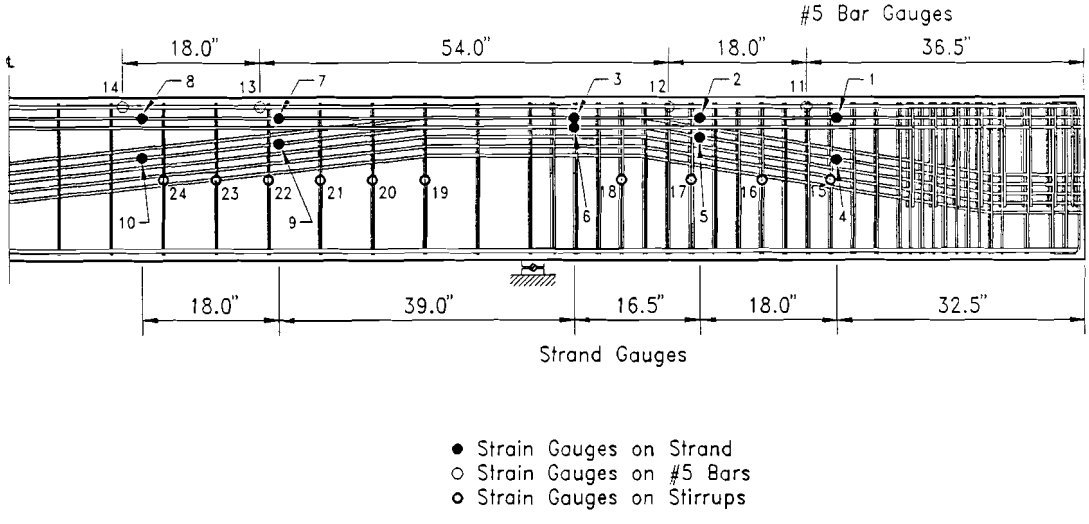

Figure 3.21 Strain gauge locations in Specimen 2A-12-D.

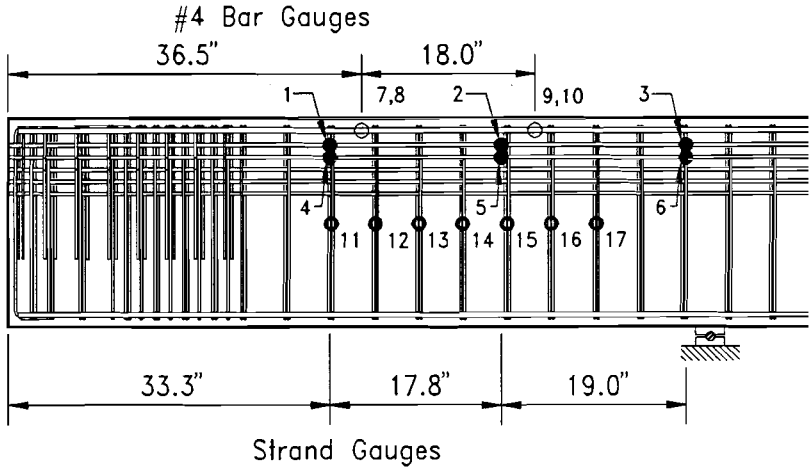

a) Specimen 2B−8−0.8

- ● Strain Gauges on Strands
- ○ Strain Gauges on #4 Bars
- ⊙ Strain Gauges on Stirrups

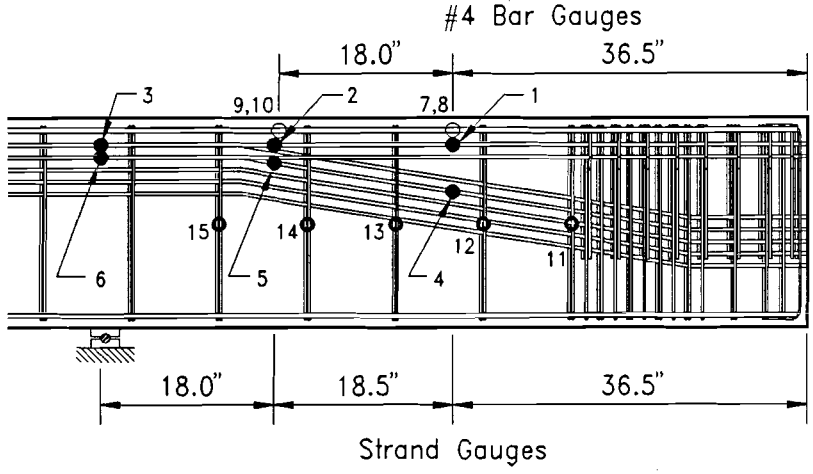

b) Specimen 2B−4−D

Figure 3.22 Strain gauge locations in Beam 2B.

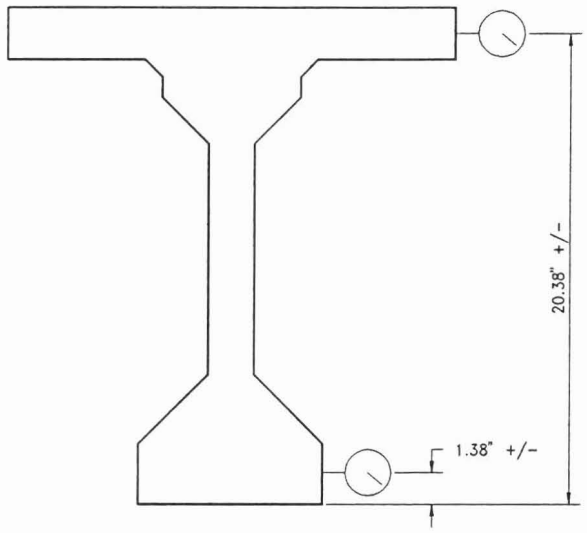

Figure 3.23 Dial gauges to measure roll of section.

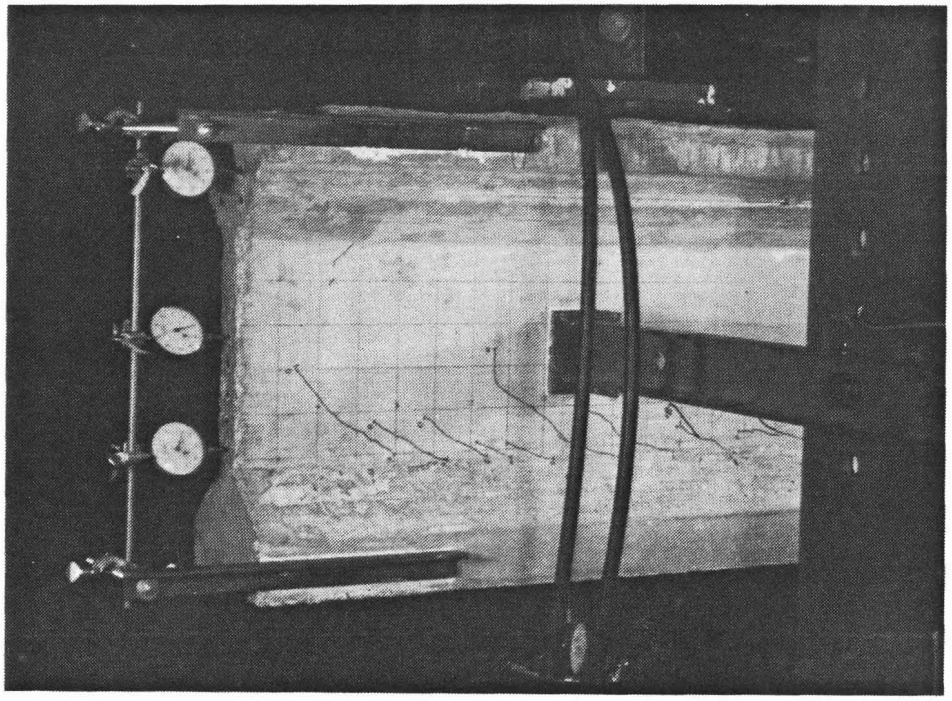

Figure 3.24 Dial gauges to monitor strand slip.

3.7 Test Setup and Loading System

3.7.1 General. All shear tests were performed on the elevated testing slab at FSEL. Figure 3.25 shows the general test setup. A single point load was applied to the top flange of the test specimen by a hydraulic ram hinged at top and bottom. A 7/8" neoprene pad was placed between the top flange and the 8-7/8 x 9-1/4" loading head. Hydrostone was used where necessary to level the top of the slab. In all tests, the load was applied 54-1/2" from the support (18" from the end of the beam). The back span was approximately 141", except for test 2A-8-0.6 in which the back span measured 82". Lateral restraint at the load point was provided by channels connected to the loading frame. The channels were made to bear on the web through teflon sheets.

3.7.2 Bearings. All test beams were supported by two bearings spaced 138" apart. However, due to the loading scheme used, the support farthest from the load point was only active under dead load. The reaction under live load at this point was provided by a hold-down beam tied to the floor with high-strength threaded rods. This reaction will hereafter be referred to as the "hold-down," and any use of the term "support" will refer to the vertical reaction located near the load point.

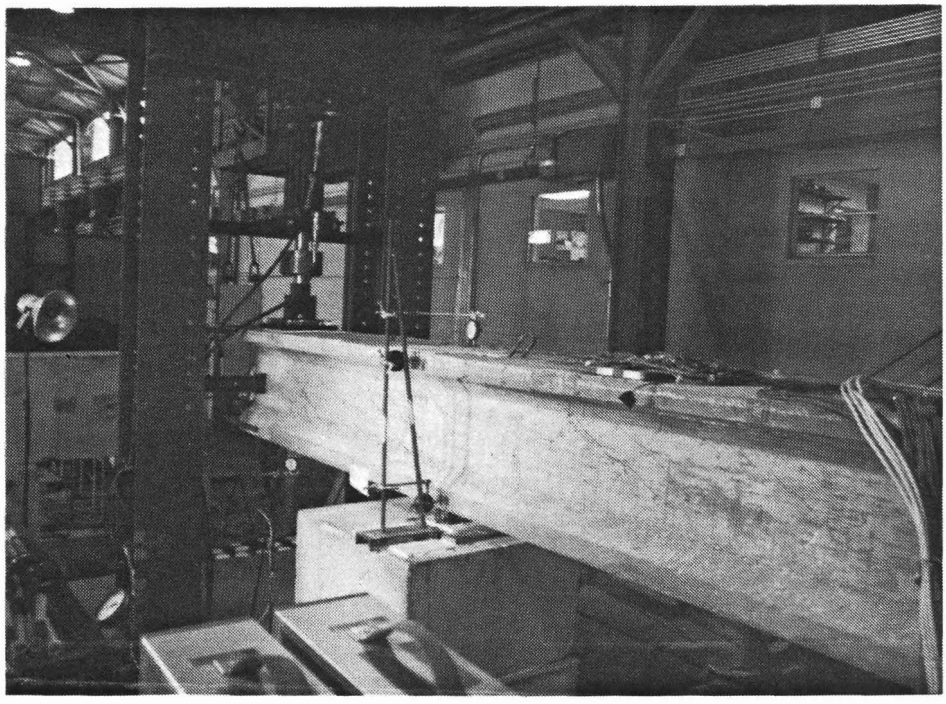

Figure 3.25 Overall test setup.

A 3/4 x 8 x 16" neoprene pad was used to transfer reaction forces from the hold-down beam to the top of slab. The hold-down provided only vertical restraint to the beam since the top ends of the threaded rods were not prevented from translating along the longitudinal axis of the beam.

Beams were supported by either an elastomeric bearing or a steel-pin bearing. For the first test (1A-1-D) a 1-1/16 x 8 x 8" unreinforced elastomeric bearing was used. This performed adequately, but bulged substantially beyond the side face of the bottom flange. Since higher loads were required for later tests, 2 x 3 x 7" neoprene pads laminated with nine 14 gauge steel shims were used for Test 1A-1-0.6. These failed prematurely by rolling as evidenced by Figure 3.26. The test was completed after replacing the failed pad with a steel-pin bearing which was also used for later tests. This bearing is shown in Figure 3.27. It consisted of a 1" diameter steel pin placed between two grooved 3 x 8 x 1" steel plates. This proved to be satisfactory for all remaining tests. Hydrostone was used between the top plate and the beam to ensure uniform bearing.

3.7.3 Applied Load Measurement. Load was measured by a load cell placed between the ram and loading head, and by a pressure gauge and two pressure transducers in the hydraulic line between a hand pump and the ram. One transducer was connected to the data acquisition system. The other was connected to a strain indicator box, and was used to monitor application of the load. The dial gauge was used only as a backup for the other devices.

3.8 Test Procedure

Each specimen was loaded monotonically in one to four kip increments until first inclined cracking occurred. The specimen was then unloaded and reloaded to failure. At each load step all dial gauges were read manually, and all strain gauges, potentiometers, load cell and pressure transducer were scanned by the data acquisition system. Also, at each load step after first cracking, cracks were marked on the beam using a large felt-tip marker, and crack sizes were measured visually. A plot of load versus load point deflection was monitored throughout each test.

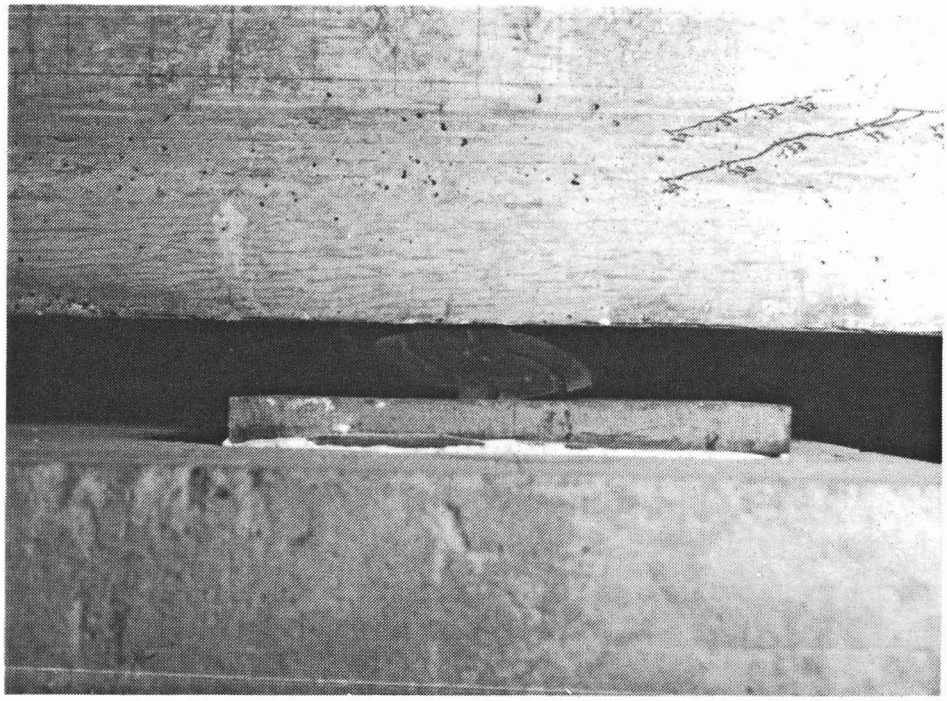

Figure 3.26 Failed elastomeric bearing during Test 1A-1-0.6.

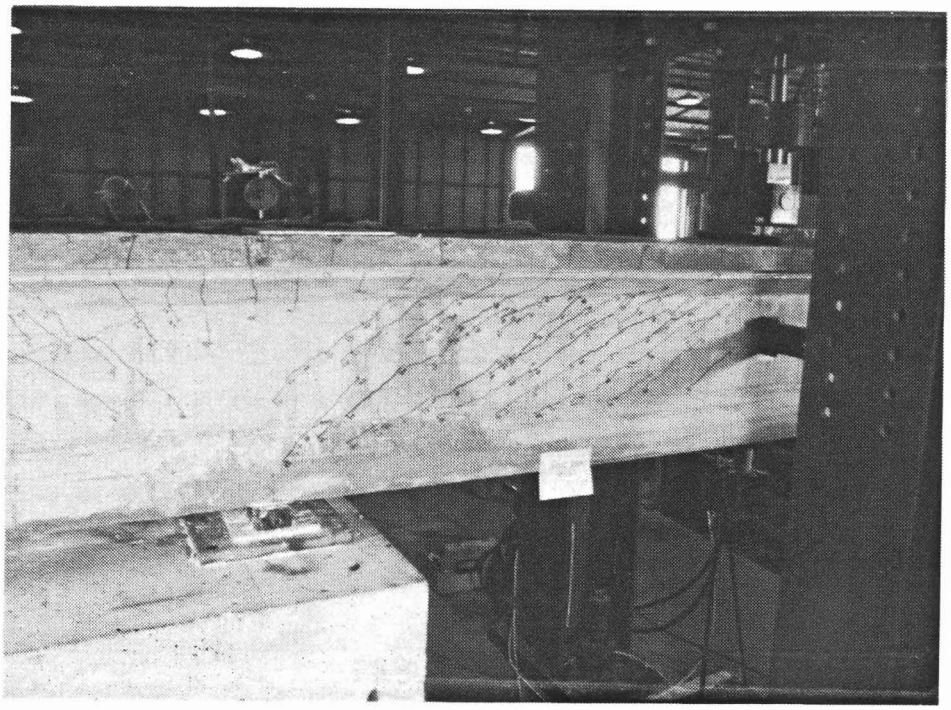

Figure 3.27 Test setup showing steel-pin bearing.

CHAPTER 4
TEST RESULTS

4.1 Introduction

This chapter contains results of the eight shear tests described in Chapter 3. Because the primary concern in this investigation is the effect of tendon profile on the shear behavior in negative moment regions, the tests are divided into three groups for discussion in this chapter. Series 1 consists of the two specimens with $d = 0.8h$ (Tests 1B-1-0.8 and 2B-8-0.8), where d is the centroid of the strands and h is the total height of the section (21.5"). Series 2 is made up of the two tests with $d = 0.6h$: 1A-1-0.6 and 2A-8-0.6. Series 3 includes the remaining four tests, all of which had strands draped from $d = 0.8h$ near the support to $d = 0.6h$ near the end. (Tendon profiles are shown in Chapter 3, Figures 3.4 through 3.15.)

Each series includes specimens with transverse reinforcement having a nominal contribution of $V_s = 1\sqrt{f_c'}\ b'd$ and $V_s = 8\sqrt{f_c'}\ b'd$. In addition, Series 3 has specimens with $V_s = 4\sqrt{f_c'}\ b'd$ and $V_s = 12\sqrt{f_c'}\ b'd$.

Because all specimens were loaded at the end of the cantilever, the applied load and shear on the cantilever are identical in all cases. When referring to the portion of the beam on the interior side of the support, a distinction will be made between the applied load, P, and the applied shear, or live-load shear. The shear on the interior was $0.39P$ in all tests except Test 2A-8-0.6, which had a much shorter back span that resulted in an applied shear of approximately $0.66P$ on the interior side of the support.

The maximum shear force due to dead load (V_d) and live load (V_i) occurred at the support. Because the loading arrangement introduced compression into the support region, the test beams were designed for the shear at a distance $h/2$ from the support in accordance with AASHTO Section 9.20.1.4. The dead load shear force at $h/2$ away from the support (to the cantilever side of the support) was 0.6 kips for all beams. Any reference to cracking or ultimate loads refers to the applied load plus the dead load ($V_i + V_d$) at a given load stage. Plots of load versus strain and load versus deflection, on the other hand, are based on applied load only.

4.2 Loading Procedure

All specimens were loaded in 2 kip increments until the first appearance of diagonal web-shear cracks, after which they were unloaded incrementally. Specimens were then reloaded in 2 to 4 kip increments until the applied load approached the design shear capacity of the specimen, at which time the load increment was reduced to 1 kip until failure occurred.

Two tests, 1A-1-0.6 and 2A-8-0.6, required three cycles of loading. Test 1A-1-0.6 required two load cycles to reach failure due to a bearing stability failure that occurred during the second load cycle at a load of 39 kips. After unloading, the failed elastomeric bearing was replaced with a steel-pin bearing, and the beam was loaded a third time until failure occurred at 42.0 kips.

After initial cracking, two load cycles were required to fail Specimen 2A-8-0.6 as the result of a premature bond failure of strands in the interior span at a load of 44 kips. This resulted due to extensive cracking near the hold-down that occurred during testing of the other end of the beam. The problem was rectified by moving the hold-down toward the support, to a more heavily reinforced area of the beam, effectively removing the poorly bonded portions of the strand from the test. This move reduced the back span from 141 in. to 82 in. resulting in more extensive shear cracking in the interior span during the remainder of the test.

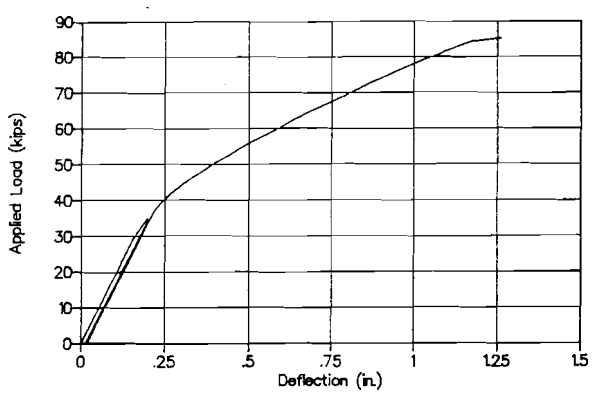

Figure 4.1 Applied load vs. load-point deflection for Test 1B-8-D.

4.3 Specimen Behavior

4.3.1 Load-Deflection Behavior. All specimens exhibited similar behavior up to the cracking load. The load versus deflection plot of Figure 4.1 shows the linear behavior prior to cracking at P = 35.6 kips. Load vs. deflection plots for all tests can be found in Appendix A.

The post-cracking behavior was more dependent upon the amount of shear

reinforcement than the strand profile. Specimens with higher levels of shear reinforcement exhibited nearly bi-linear behavior (Figure 4.1) while those with minimal shear reinforcement showed a continuing loss of stiffness from initial cracking until failure. This behavior is evidenced by the curved upper portion of the load-deflection plot shown in Figure 4.2, and is indicative of the smaller relative contribution of the stirrups in these specimens.

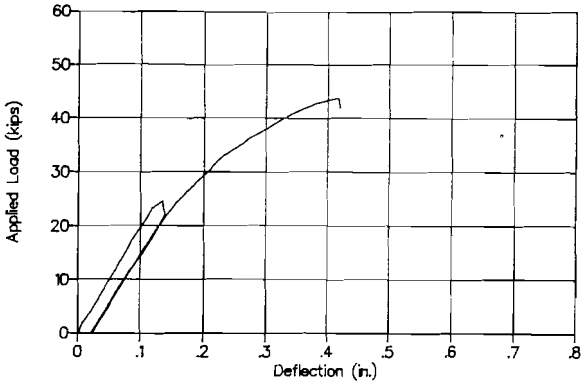

Figure 4.2 Applied load vs. load-point deflection for Test 1B-1-0.8.

Post-cracking strengths, as measured by the ratio of ultimate load, P_{ult}, to cracking load, P_{crack} (Table 4.1), were generally consistent with the amount of shear reinforcement, and in all cases were at least 1.5. The two exceptions to this observation were Tests 2B-8-0.8 and 2A-8-0.6, both of which cracked at lower-than-expected loads resulting in high ratios of ultimate to cracking load. In all cases, this post-cracking strength allowed for significant crack growth prior to failure. Although failure was rather sudden, cracks provided ample warning of impending failure. Deflections at failure ranged from 0.42 in. for Test 1B-1-0.8 to 1.25 in. for Test 1B-8-D.

Table 4.1 Test Results for All Specimens.

Test No.	P_{crack} for Shear (kips)	Angle of First Major Crack (°)	$P_{ult.}$ (kips)	Angle of Major Cracks @ Ult. (°)	Largest Diagonal Crack Opening (in.)	$P_{ult.}/P_{crack}$	P_{crack} for Flex. (kips)
1B-1-0.8	25.3	25	44.6	22	0.09	1.76	35
2B-8-0.8	20.1	30	63.8	26	0.04	3.17	43
1A-1-0.6	27.9	30	42.6	22	0.10	1.53	29
2A-8-0.6	18.6	10 - 25	62.4	30	0.01	3.35	31
1A-1-D	36.3	20	58.8	22	0.06	1.62	42
2B-4-D	38.6	20 - 35	67.1	25	0.05	1.74	49
1B-8-D	35.6	25 - 45	86.1	28	0.03	2.42	37
2A-12-D	36.4	25 - 30	79.4	30	0.01	2.18	39
Note: V_d = 0.6 kips is included in $P_{ult.}$ and P_{crack}.							

4.3.2 Cracking Loads. Observed cracking and ultimate loads for all specimens are given in Table 4.1. Initial cracking loads were not consistent for the beams with straight strands (Series 1 and Series 2). This may be explained by the subjectivity involved in detecting the first diagonal cracks. In particular, in the case of Test 2A-8-0.6, there were pre-existing cracks near the bottom of the web which propagated at a load of 18 kips. Additional cracks having small angles of inclination initiated near the bottom flange at loads between 18 and 28 kips, then the first large shear crack appeared. Since no change in slope of the load vs. deflection curve was evident before 28 kips, one might surmise that the cracks which initiated prior to 28 kips were due to local behavior related to the strands in the lower part of the web, and were not actually shear cracks. However, the cracks in Specimen 2B-8-0.8 that formed in the web at 19 kips were distributed throughout the central part of the shear-span and were inclined at approximately 25° from the horizontal; these were clearly web-shear cracks. An explanation for discrepancies in web cracking might be related to the general variability in tensile strength of concrete.

Specimens in Series 3 (with draped strands) had very consistent cracking loads, with only an 8% difference between the high and low cracking loads. Cracking loads for Series 3 ranged from 36 to 39 kips. This consistency would seem to indicate that the vertical component of the prestress provides some stabilizing influence to the effective tensile strength of the concrete in web.

4.3.3 Crack Patterns. Crack patterns, like load vs. deflection behavior, were primarily dependent on the amount of shear reinforcement. Inclination of major cracks for each test, measured from the horizontal, can be found in Table 4.1. In addition, Appendix B contains detailed crack diagrams for all specimens.

4.3.3.1 Initial Cracking. Two types of initial cracks were observed: short, shallow cracks at the junction of the web and the bottom flange with inclinations as low as 10°, and diagonal web-shear cracks inclined between 25 and 45°. Diagonal cracks with steeper inclination typically formed closer to the support, while those with a shallow angle were found in the central part of the shear span. In addition, the short, shallow cracks near the bottom flange were more common in specimens with less shear reinforcement, while steeper web-shear cracks were more common in specimens with heavy shear reinforcement. Figure 4.3 shows typical cracking patterns for lightly and heavily reinforced specimens ($V_s = 1\sqrt{f_c'}\ b'd$ and $V_s = 8\sqrt{f_c'}\ b'd$ respectively).

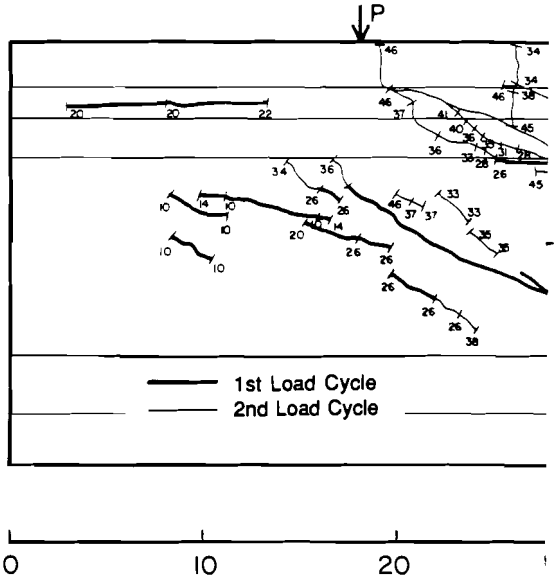
P
1st Load Cycle
2nd Load Cycle
0
10
20

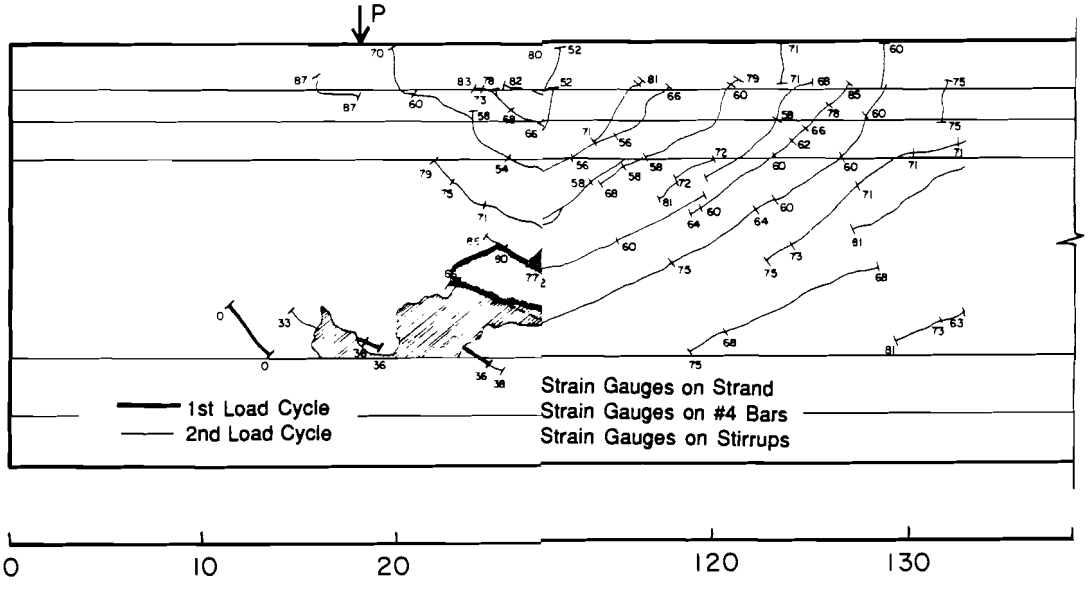
P
1st Load Cycle
2nd Load Cycle
Strain Gauges on Strand
Strain Gauges on #4 Bars
Strain Gauges on Stirrups
0
10
20
120
130

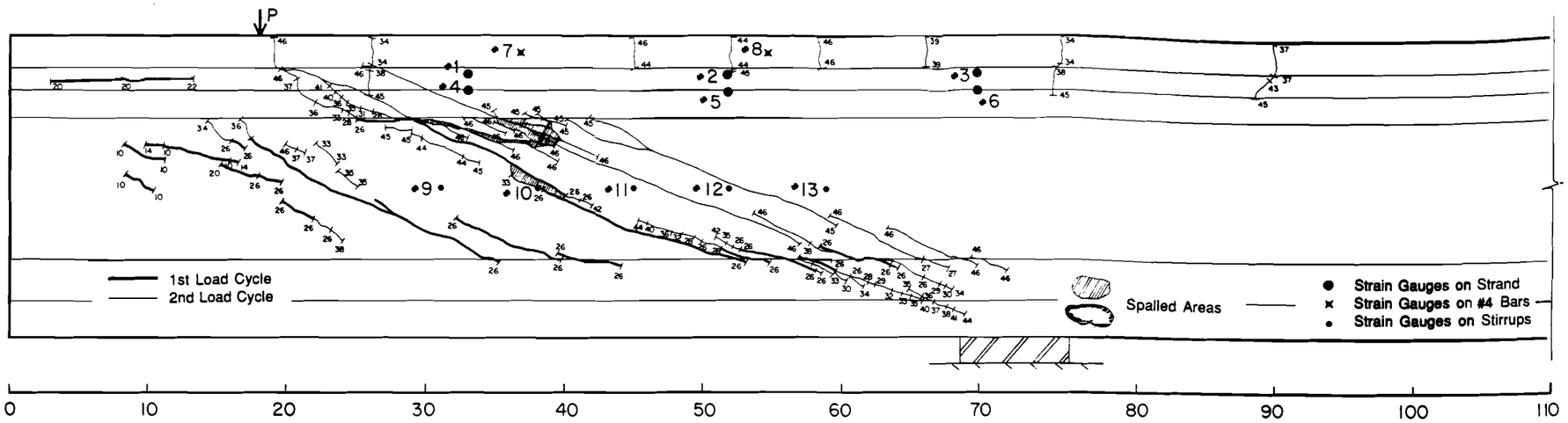

a) Specimen 1B-1-0.8

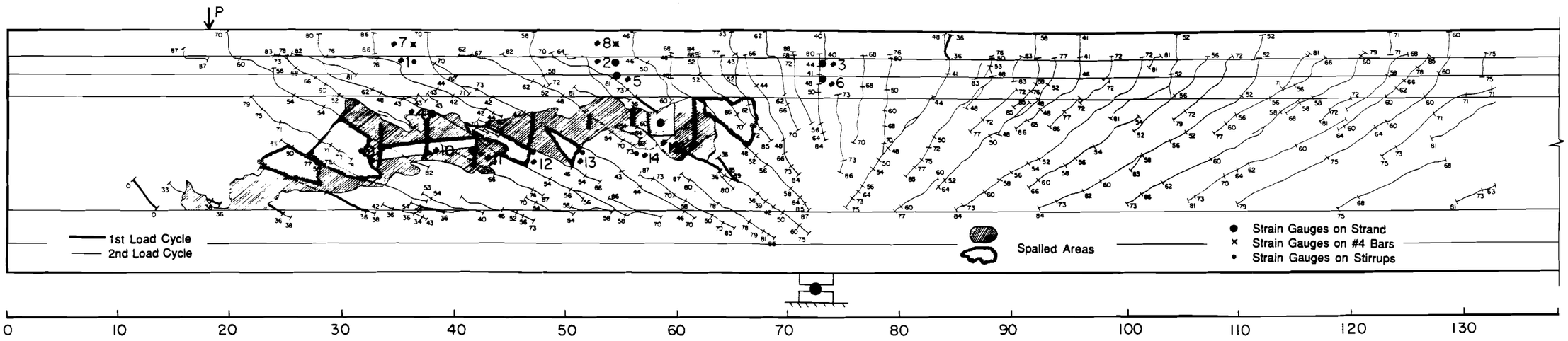

b) Specimen 1B-8-D

Figure 4.3 Crack diagram for Beam 1B.

Cracks were observed in four of the eight test specimens before loading. These cracks, generally short and shallow, occurred between the load point and the end of the cantilever. The one exception was Beam 2A-12-D, which had more extensive cracking. These cracks were inclined in the opposite direction of expected web shear cracks and pre-loading cracks observed in other specimens. In addition, two of these extended nearly from top to bottom of the web. In general, the majority of the pre-loading cracks in Specimen 2A-12-D were near the top of the web instead of the bottom. Because these cracks were oriented approximately perpendicular to the orientation of typical shear cracks, they did not propagate under load, and did not appear to affect the overall behavior of the beam. It is likely that cracks observed in other specimens prior to loading may be due to a shear lag effect at release of the prestress force, resulting from the difference in horizontal shear stress between the flange and the web.

4.3.3.2 Crack Growth to Failure. At loads beyond that of first cracking, web-shear cracks continued to propagate, generally extending into the bottom flange and through the top flange at failure. Initial cracks with shallow inclination propagated in many cases into the bottom flange, but propagated only a short distance into the web.

Flexural cracks were observed at loads ranging from 30 to 43 kips, generally agreeing with AASHTO/ACI cracking loads. Observed flexural cracking loads can be found in Table 4.1. Variation in the observed cracking loads can be explained by the difficulty in detecting flexural cracks before they appear.

The three specimens with $V_s = 1\sqrt{f_c'}\ b'd$ exhibited similar cracking patterns at failure. Each had three or four major diagonal shear cracks centered around a line between the load point and the support, and extending from the bottom flange into or through the top flange. The cracks closest to this line were inclined approximately 22° from the horizontal. Beams 1A-1-0.6 and 1B-1-0.8 had much simpler cracking patterns than Beam 1A-1-D, probably due to lower failure loads experienced by these two specimens as a result of the straight strand profiles. The largest diagonal crack openings at failure were on the order of 0.10 in. for Beams 1A-1-0.6 and 1B-1-0.8, and 0.06 in. for Beam 1A-1-D. The vertical component of the prestress force accounts for the difference.

The four specimens with the largest amount of shear reinforcement, 1B-8-D, 2A-8-0.6, 2A-12-D, and 2B-8-0.8 had consistent cracking patterns at failure. In all cases,

diagonal shear cracking was extensive throughout the shear span, with closely spaced cracks inclined at 26 to 32° extending from the bottom flange, through the web and top flange, to the slab. Web crack openings at failure ranged from 0.01 in. to 0.04 in. Flexure-shear cracks were well developed in all of these specimens at failure, but did not appear to be a significant factor in the failures.

Beam 2B-4-D experienced web-shear cracking patterns between those of the heavily reinforced and lightly reinforced specimens. Major web-shear cracks for this specimen were inclined approximately 25° at failure and opened to 0.05 in. Both of these parameters are consistent with the intermediate level of shear reinforcement.

4.3.3.3 Failure Modes. All specimens failed as a result of crushing of concrete compression struts in the web. The location where failure initiated appeared to coincide with the point of intersection of the critical strut and strands in the web. This point also corresponds with the location of highest compressive stress due to the prestress.

Failure of specimens with light shear reinforcement was characterized by limited spalling along the major web-shear cracks, and was accompanied by a relatively small drop in load. Figure 4.4 shows one of the lightly reinforced beams, Specimen 1B-1-0.8, at failure.

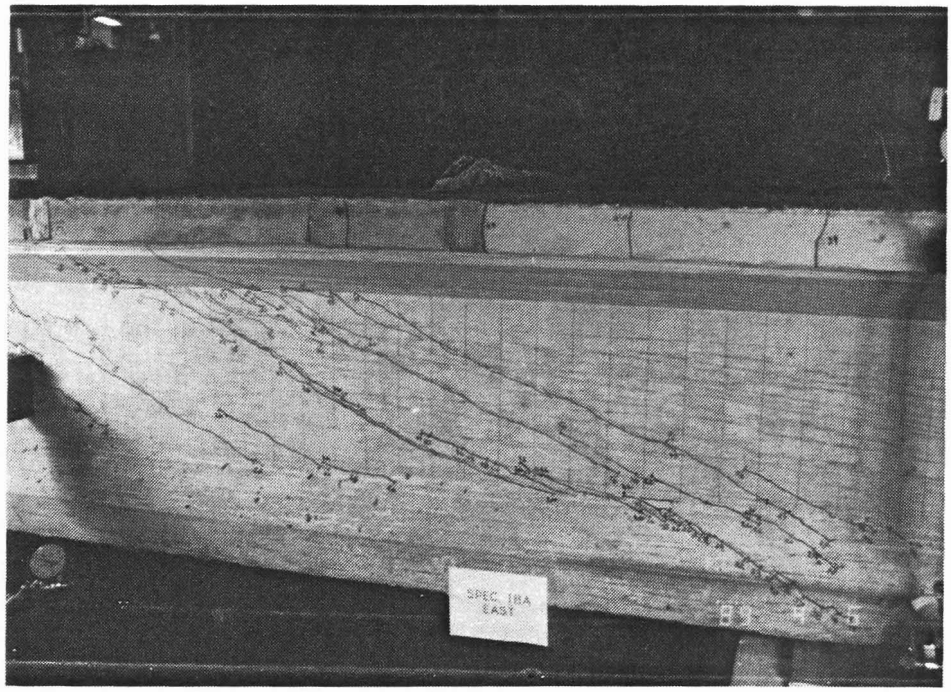

Figure 4.4 Specimen 1B-1-0.8 at failure ($V_s = 1\sqrt{f'_c}b'd$).

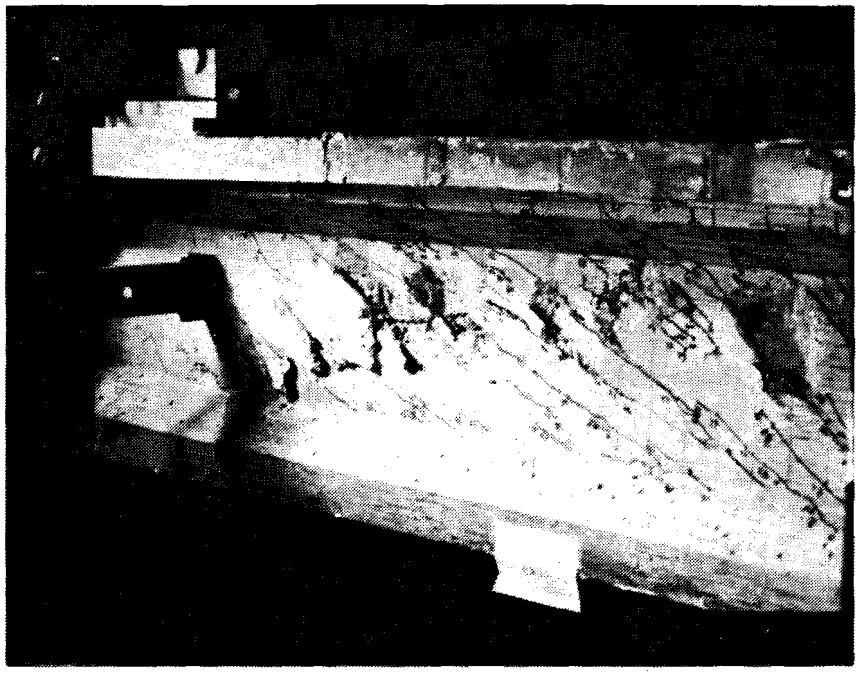

Figure 4.5 Specimen 1B-8-D at failure ($V_s = 8\sqrt{f'_c}b'd$).

Failure of specimens with high levels of shear reinforcement was typically explosive, characterized by a progressive crushing failure of the web throughout the shear span, large spalled areas, and a drop in load of 30 to 50 kips (approximately 70%). Beam 1B-8-D, one of the heavily reinforced specimens, is shown at failure in Figure 4.5.

4.3.4 Stirrups. Stirrup strains at first cracking were generally quite small, or zero. However, in cases where strain gauges were located very close to initial crack locations, measured strains were up to 50% of the yield strain. One gauge located at the crack location in Beam 1B-1-0.8 indicated yielding. A typical applied load vs. stirrup strain plot up to first cracking is shown in Figure 4.6.

Strain gauges generally indicated that stirrups in the shear span were at or near yield strain at failure. Gauges that did not indicate yielding were typically on stirrups closest to the support or closest to the load point, and were in regions of sound concrete away from any diagonal cracks. In almost all cases, the stirrups on

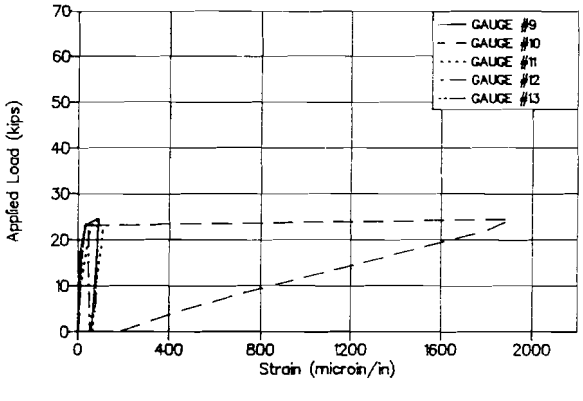

Figure 4.6 Applied load vs. stirrup strains during first load cycle for Test 1B-1-0.8.

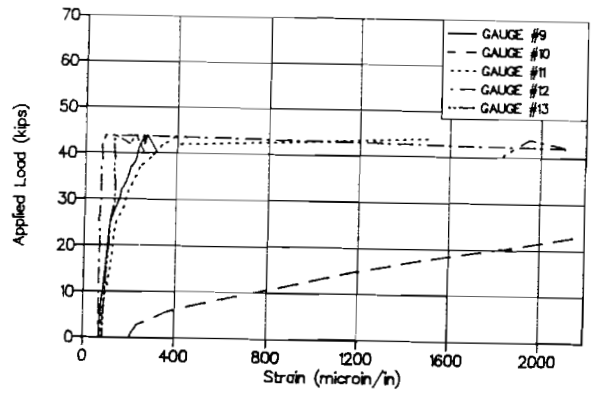

Figure 4.7 Applied load vs. stirrup strains during second load cycle for Test 1B-1-0.8.

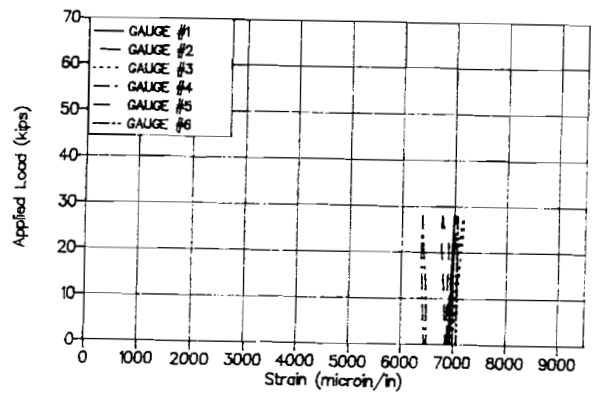

Figure 4.8 Applied load vs. strand strains during first load cycle for Test 2A-8-0.6.

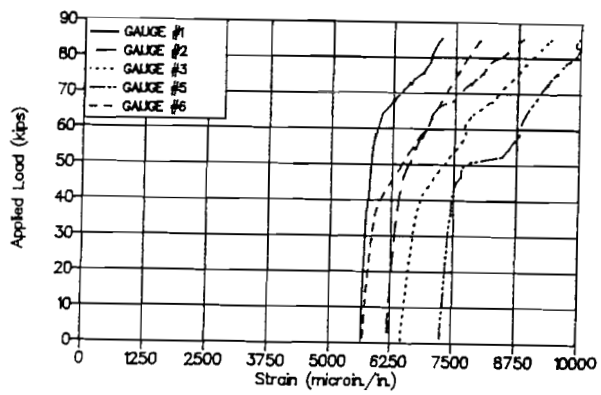

Figure 4.9 Applied load vs.strand strain during second load cycle for Test 1B-8-D.

which these gauges were attached crossed a major diagonal crack (one that caused another gauge to give an indication of yielding) away from the gauge, in which case yielding of the stirrup can be assumed. Figure 4.7 shows a typical plot of applied load vs. stirrup strains for the second cycle of loading. Plots for all tests can be found in Appendix C.

4.3.5 Strands. Increases in strand strain, as indicated by strain gauges on two strands in each specimen, were very small at first cracking load for all tests, as shown by the representative plot in Figure 4.8. In fact, because the lowest strands in Series 2 specimens were below the neutral axis of the uncracked section, strains at first cracking were less than before loading. End slip of up to 0.010 in. was recorded by dial gauges on strands anchored in the web. Only one strain gauge, at a location 33 in. from the end of the cantilever, indicated slip.

At failure, only one instrumented strand from any of the tests yielded. This was one of the upper strands in Beam 1B-8-D. However, the instrumented strand in the second layer from the top in this specimen (#6) was very near, if not at yield. Therefore, up to six strands in this specimen were at or above yield at failure. This specimen had the highest load at failure of any test. In addition, two other

beams, 2A-8-0.6 and 2A-12-D, had strands near yield at failure. Figure 4.9 contains the applied load vs. stirrup strain plot for Test 1B-8-D. All other specimens experienced strand strains well below yield. Plots for all tests can be found in Appendix D.

Maximum end slip at failure was 1/8 in. measured in Beam 1A-8-D. Six of eight specimens experienced end slip of strands anchored in the web prior to failure. Strain gauges approximately 36 in. from the end of the cantilever generally did not show evidence of strand slip (decreases in strain), indicating that sufficient bond was developed at that point along the strand.

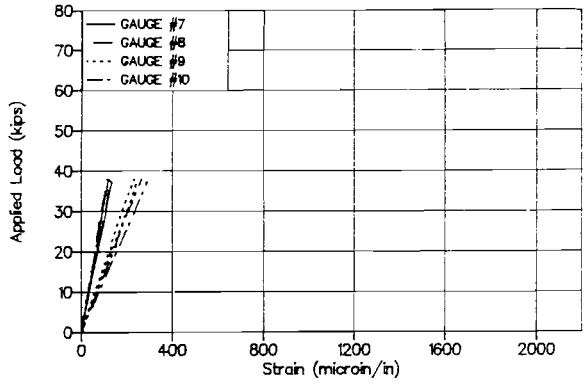

Figure 4.10 Applied load vs. #4 bar strain during first load cycle for Test 2B-4-D.

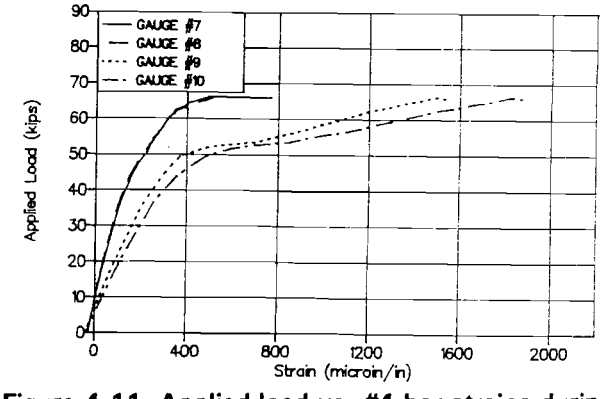

Figure 4.11 Applied load vs. #4 bar strains during second load cycle for Test 2B-4-D.

4.3.6 Non-prestressed Longitudinal Reinforcement. Up to initiation of cracking, non-prestressed slab reinforcement experienced small strains, reflecting the elastic stress distribution over the section prior to cracking, as shown by the typical plot in Figure 4.10. Strain gauge readings for the center slab bars indicated yielding at the support in the five most heavily reinforced specimens. Figure 4.11 shows a typical plot of applied load vs. longitudinal slab-bar strains for Specimen 2B-4-D with bars yielded at failure. Plots for all tests can be found in Appendix E. In Tests 1B-1-0.8 and 1A-1-0.6, maximum recorded strains 18 in. from the support were less than 50% of yield strain, and strains at the support were estimated at 70% of yield. No useable data was obtained from the gauges in Test 1A-1-D.

In the specimens with yielded #4 or #5 slab bars, the state of strain in the outer slab bars remains a question. Because half of the eight slab bars were outside the limits of the top flange, strains in these bars may be somewhat less than in the central four bars. However, cracking at the slab edges was nearly as well developed as over the center part of the section, so it will be assumed that strains in all slab bars were comparable.

CHAPTER 5
DISCUSSION OF TEST RESULTS

5.1 Introduction

The discussion of test results is divided into two parts. The first part deals with the effects of primary design variables on the test results. The influence of prestressing strand location and draping, and influence of amount of shear reinforcement on the behavior of the test specimens is discussed. In the second part, test results are compared with the AASHTO/ACI shear provisions for prestressed concrete, and with the generalized strut and tie model. In particular, the design assumptions and predictions of each model are discussed with reference to the test results.

5.2 Effects of Primary Variables

The primary design variables in this test program, as presented in Chapter 3, were the vertical position of the prestressing strands in the cross section, the slope of the strands, and the amount of shear reinforcement.

Although web-slenderness was not a variable in this study, webs of beams tested were slender, having a depth-to-width ratio of 5.0. Nevertheless, web-stability did not appear to influence specimen behavior.

5.2.1 Strand Location. Four of the eight shear tests were performed on specimens with straight prestressing strands in the cantilever. Of these four, two had the center of gravity of the strands located at eight-tenths the height of the beam ($d = 0.8h$) and two had it at six-tenths the height ($d = 0.6h$). AASHTO Section 9.20.2 allows the use of $0.8h$ in lieu of the actual distance from the extreme compression fiber to the centroid of the prestressing force, d, in Equation 5.1 (AASHTO Equation 9-27, ACI Equation 11-11) and Equation 5.2 (AASHTO Equation 9-29, ACI Equation 11-13) if d is less than $0.8h$.

$$V_{ci} = 0.6\sqrt{f_c'}\, b'd + V_d + V_i M_{cr} / M_{max} \quad (5.1)$$

where V_{ci} = flexure-shear cracking strength of concrete,
f_c' = 28 day compressive strength of concrete,
b' = width of web,
d = distance from extreme compression fiber to centroid of the prestressing force,
V_d = shear force at section due to unfactored dead load,
V_i = factored shear force at section due to externally applied loads occurring simultaneously with M_{max},
M_{cr} = moment that causes flexural cracking,
M_{max} = maximum factored moment at section due to externally applied loads.

$$V_{cw} = (3.5\sqrt{f_c'} + 0.3 f_{pc}) b'd + V_p \quad (5.2)$$

where V_{cw} = web-shear cracking strength of concrete,
f_{pc} = compressive stress in concrete at centroid of cross section resisting externally applied loads, or at junction of web and flange when the centroid lies within the flange,
V_p = vertical component of effective prestress force at section.

The shear capacities predicted by AASHTO/ACI design provisions (AASHTO1), adjusted for measured material properties, can be found in Table 5.1 The test results for all specimens were presented in Table 4.1 and repeated in Table 5.9.

The results for the four tests with straight strands show no apparent correlation between the position of the strands and the observed cracking loads. While the observed web-cracking loads for specimens 1A-1-0.6 and 1B-1-0.8 were above and within 15% of the AASHTO/ACI prediction, V_c, the cracking loads for specimens 2A-8-0.6 and 2B-8-0.8 were lower than the predicted values by 29 and 20%, respectively. All four of these specimens should have had nearly identical first-cracking loads according to AASHTO/ACI, with differences being due only to small variations in concrete strength. Beams 2A-8-0.6 and 2B-8-0.8, which displayed the two lowest ratios of cracking load to predicted cracking load in Figure 5.1, actually had higher concrete strengths (Table 3.3) than Specimens 1A-1-0.6 and 1B-1-0.8.

Table 5.1 Shear Capacity by AASHTO/ACI Method (AASHTO1), and Comparisons of Measured to Predicted Cracking and Ultimate Loads.

Test No.	V_c (kips)	V_s (kips)	V_p (kips)	V_n (kips)	V_{cr}/V_c	V_u/V_n
1A-1-0.6	24.2	3.3	0.0	27.5	1.15	1.55
2A-8-0.6	26.3	26.9	0.0	53.2	0.71	1.17
1B-1-0.8	24.1	3.3	0.0	27.4	1.05	1.63
2B-8-0.8	25.0	26.9	0.0	51.9	0.80	1.23
1A-1-D	36.7	3.3	12.5	40.0	0.99	1.47
2B-4-D	37.4	13.5	12.8	50.9	1.03	1.32
1B-8-D	36.3	26.9	12.2	63.2	0.98	1.36
2A-12-D	37.7	40.5	12.5	78.2	0.97	1.02
V_d = 0.6 kips added to measured V_u & V_{cr}				Ave.	0.96	1.34
				Std. Dev.	0.13	0.19

The most obvious difference between the two pairs of specimens was that the two specimens with minimum shear reinforcement ($V_s = 1\sqrt{f_c'}\ b'd$) experienced cracking loads reasonably consistent with those predicted by AASHTO/ACI, while the two with maximum reinforcement ($V_s = 8\sqrt{f_c'}\ b'd$) cracked at loads substantially below both the AASHTO/ACI predictions and the observed cracking loads of the two straight-strand specimens with minimum transverse reinforcement. This is evident in the plot shown in Figure 5.2. The reason for this discrepancy is not clear, since the amount of shear reinforcement should not effect the initial cracking load. However, the size of the transverse reinforcement in the web might have had some effect since the #2 stirrups used in the heavily reinforced specimens occupied 25% of the web width, while the #1-1/4 stirrups used in the lightly reinforced members occupied only 15% of the width. This explanation appears unsatisfactory, however, when the four draped-strand specimens are

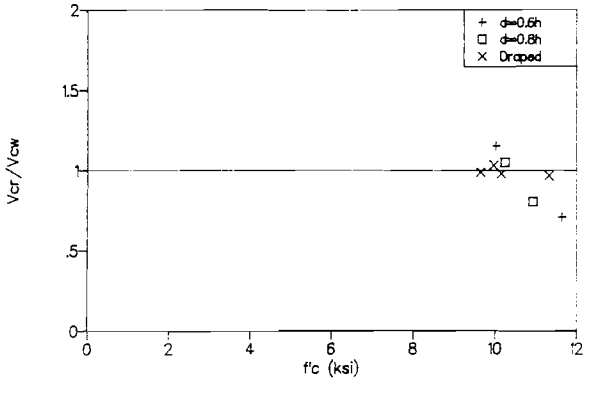

Figure 5.1 Ratio of measured cracking load to AASHTO/ACI calculated value versus f_c'.

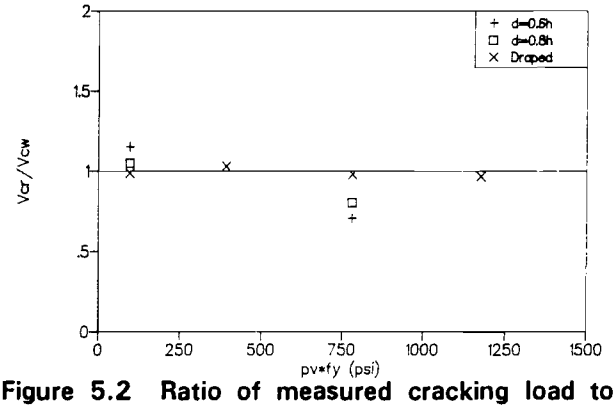

Figure 5.2 Ratio of measured cracking load to AASHTO/ACI calculated value versus $p_v f_y$.

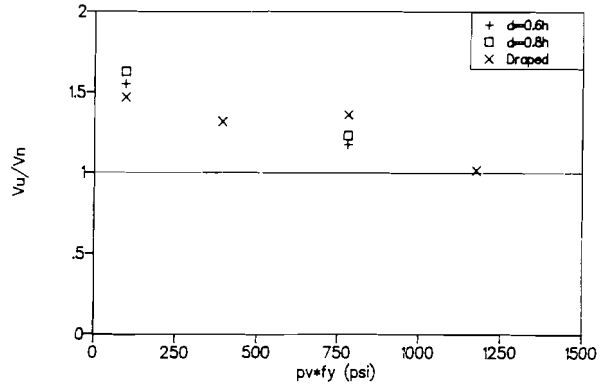

Figure 5.3 Ratio of measured ultimate load to AASHTO/ACI calculated value versus $p_v f_y$.

considered. All four of these employed the #2 stirrups, and had cracking loads within 8% of each other, and within 3% of those predicted by the AASHTO/ACI design equations.

The load capacity of straight-strand specimens, as seen in Figure 5.3, showed no clear indication of any dependance of shear strength on the location of the strands. For specimens with the same amount of shear reinforcement, the difference in ultimate load between the specimen with $d = 0.6h$ and the one with $d = 0.8h$ was less than 5%.

Cracking patterns also did not appear to be affected by the vertical location of the prestressing strands. Cracking patterns, like cracking loads and ultimate strengths, appear to be primarily dependent on the amount of shear reinforcement present.

5.2.2 Draped Prestressing Strands. Four of the eight shear tests were performed on specimens with draped prestressing strands. These had nominal levels of shear reinforcement, V_s equal to $1\sqrt{f_c'}$ b'd, $4\sqrt{f_c'}$ b'd, $8\sqrt{f_c'}$ b'd, and $12\sqrt{f_c'}$ b'd. All four specimens had the same strand profile in the cantilever, resulting in a calculated vertical component of the prestress force, V_p, between 12.0 and 13.0 kips. Since first cracking in all of these specimens consisted of diagonal cracks in the web, and since all failed as the result of crushing of concrete diagonals in the web, the cracking loads and ultimate capacities should reflect the vertical component of the prestress force (V_p in AASHTO Equation 9-29 for V_{cw}). Specimen 2A-12-D was designed for a flexure-shear failure on the interior side of the support, but, like the other specimens experienced a web-crushing failure in the cantilever at a load 36% higher than the predicted flexure-shear failure load for the interior span.

Cracking loads (Figure 5.2) for all four of these draped-strand specimens were very consistent, and averaged about 10 kips higher than the two straight-strand specimens from the first cast (1A-1-0.6 and 1B-1-0.8). This is another indication that the cracking loads for

the two specimens that cracked at 18.0 and 19.5 kips (2A-8-0.6 and 2B-8-0.8 respectively) were exceptionally low.

Ultimate loads for this group were less consistent than were the cracking loads. However, a comparison of specimens with identical shear reinforcement (Table 4.1 and Table 5.1) reveals that, in the two cases that can be compared ($V_s = 1\sqrt{f_c'}$ b'd: 1A-1-0.6, 1B-1-0.8, and 1A-1-D; $V_s = 8\sqrt{f_c'}$ b'd: 2A-8-0.6, 2B-8-0.8, and 1B-8-D), the difference between the ultimate strengths of beams with and without draped strands exceeded V_p. Transverse compression introduced into the struts by draped strands may account for this additional strength. Responsibility may also lie with inaccuracies in the measurement and estimation of prestress forces.

5.2.3 Shear Reinforcement. Four different nominal levels of shear reinforcement ranging from $V_s = 1\sqrt{f_c'}$ b'd to $V_s = 12\sqrt{f_c'}$ b'd were used in the cantilever regions of the eight test specimens. A comparison of cracking loads to ultimate loads shows that for all specimens the difference between the two was greater than predicted by the AASHTO V_s term. This is expressed as $(V_u\text{-}V_{cr})/V_s$ in Figure 5.4, where V_u is the measured ultimate load, V_{cr} is the observed first web-shear cracking load, and V_s is the AASHTO design transverse steel contribution. This may be explained in part by the presence of additional closely-spaced #2 bars in the region extending 6 in. on either side of the load point. Supporting this explanation is the observation that the ratio of measured ultimate load to AASHTO predicted ultimate load (Figure 5.3) was generally greater for the specimens with lesser amounts of shear reinforcement. The additional #2 bars provided a greater percentage increase in stirrup area and capacity for lightly reinforced specimens. The contribution of these additional stirrups is considered in the modified AASHTO/ACI predicted loads (AASHTO2) presented in Table 5.2, and in the strut-and-tie model predictions that will be discussed later in this chapter. However, for the AASHTO design method, the increase in capacity assuming the first two pairs of #2 stirrups to be fully effective is between 9 and 15%, which

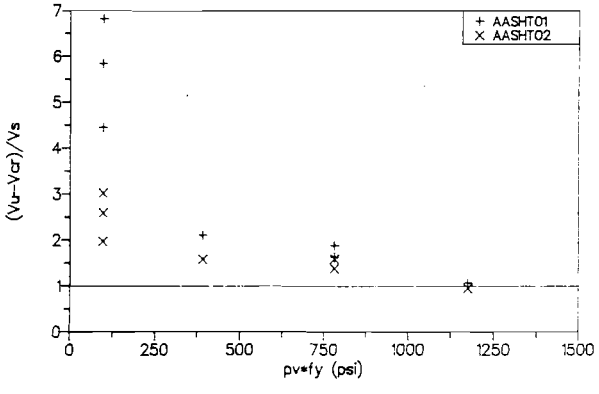

Figure 5.4 Ratio of difference between measured ultimate and cracking loads to AASHTO/ACI V_s vs. $p_v f_y$.

Table 5.2 Revised Design Shear Capacity (AASHTO2) Adjusted for Total Transverse Steel Provided.

Test No.	V_c (kips)	V_s (kips)	V_p (kips)	V_n (kips)	V_u/V_n
1A-1-0.6	24.2	7.4	0.0	31.6	1.35
2A-8-0.6	26.3	31.8	0.0	58.1	1.07
1B-1-0.8	24.1	7.4	0.0	31.5	1.41
2B-8-0.8	25.0	31.8	0.0	56.8	1.12
1A-1-D	36.7	7.4	12.5	44.1	1.33
2B-4-D	37.4	18.0	12.8	55.4	1.21
1B-8-D	36.3	31.8	12.2	68.1	1.26
2A-12-D	37.7	45.5	12.5	83.2	0.95
V_d = 0.6 kips added to measured V_u.				Ave.	1.22
				Std. Dev.	0.15

is not enough to account for the full capacity. The additional strength is likely due to the unaccounted for shear transfer mechanisms of arching, dowel action, and aggregate interlock. The ratio $(V_u\text{-}V_{cr})/V_s$ for the lightly reinforced specimens plotted in Figure 5.4 supports this assertion since arching action (essentially a direct strut and tie) as indicated by the cracking patterns of these beams is more likely in the lightly reinforced specimens.

5.3 Comparison with Model Assumptions

The AASHTO/ACI shear provisions and the generalized strut-and-tie model are generally based on similar assumptions. Comparison of the observed test results to the model assumptions can give an indication of the applicability of these models.

5.3.1 AASHTO/ACI Model Assumptions. Because all of the tests exhibited web shear cracking failures, only the V_{cw} concrete capacity term of the AASHTO/ACI provisions can be evaluated, although flexural-shear cracking will be discussed briefly.

The AASHTO/ACI model assumes that at failure both the transverse and longitudinal steel have yielded. In addition, compressive stresses in the concrete diagonals (struts) of a 45° truss are implicitly limited to a fraction of the 28-day compressive strength, f'_c, to prevent brittle failure by crushing of the web. Strain gauges on stirrups confirmed the

validity of the assumption that the stirrups yield. However, due to the desire to prevent a flexural failure, an excessive amount of longitudinal steel was used in the top slab, preventing yield of the tension tie prior to failure in most cases.

Finally, crack angles at failure were in all cases less than the assumed 45° (except in regions near the load point and support – D regions). In most cases the inclination of cracks was approximately one half of this value. These reduced angles resulted from the prestressing and a combination of the loading arrangement and the shear reinforcement. In the specimens with small amounts of shear reinforcement, a direct strut, or a single arch and tie, was required to carry the applied load, resulting in very low crack inclinations. The 45° assumption, however, is still conservative because the higher angle requires more transverse reinforcement in design than does the observed lower angle.

5.3.2 Strut-and-Tie Model Assumptions. Assumptions for the generalized strut-and-tie model are similar to those described for the 45° truss model except that the strut angle is no longer restricted to 45°. Various restrictions on the strut angle have been proposed which generally limit the angle α to a range between 30 and 60° to ensure that redistribution of forces can occur as required by crack inclinations deviating from those experienced at initial cracking. Collins and Mitchell[14] proposed limits of

$$15° < \alpha < 60° \tag{5.3}$$

for the principal compression stresses at failure. The lower limit is particularly applicable to prestressed concrete since the precompression force tends to increase the ratio of longitudinal to vertical compressive stresses, thus lowering the angle of the strut. Observed crack patterns in the current test program confirm this low angle, both at failure and at initial cracking. The large ratio of longitudinal to transverse reinforcement area also contributed to the observed small crack inclinations.

Because the strut-and-tie model assumes that all struts and ties are loaded uniaxially, only compressive stresses should be experienced by the struts. However, tension ties crossing the struts, aggregate interlock forces, slender webs, and the coming together of forces near concentrated loads can result in tensile stresses and cracking across the struts, reducing the compressive capacity of the struts below f'_c. It is therefore necessary to consider this reduced effective concrete strength by introducing an efficiency factor, ν, when

checking compressive stresses in the struts. Numerous values for this strength reduction, or softening, have been proposed.[14, 18, 34, 38, 39, 41, 42] Later in this chapter, an efficiency factor proposed by Bergmeister[8] will be considered in light of the current test data.

As with the AASHTO/ACI model, the assumption of yielded stirrups appears to be appropriate for these tests. Due to the heavy longitudinal reinforcement provided to preclude a flexural failure, the longitudinal reinforcement did not appear to have yielded prior to crushing of the web, except in Test 1B-8-D. This observation could not be absolutely confirmed, but, nevertheless, was not critical because failures were all of the web-crushing variety. The crushing failure in the struts allowed a more precise analysis of the strut behavior at failure. This analysis will be discussed later in this chapter.

A very important assumption of the strut-and-tie model is that all reinforcement is properly detailed so as to prevent a local bond or compression failure at the nodes connecting the struts and ties. All non-prestressed reinforcement used in this test program proved to be adequately detailed, and no node failures were observed. In rectangular beams the nodes can be more critical than in flanged sections like those tested in this program which have the nodes located in the relatively large flanges. As a result, the critical sections are isolated in the thin web. However, some of the prestressing strands, especially those anchored in the web, experienced end slip prior to failure; but strain gauges on the strands indicated that in all cases strand stresses were maintained in the shear-span. The ultimate behavior of the specimens did not appear to be affected by the end slip; shear-tension failures were not observed in any of the specimens.

5.4 Comparison of Design Models to Test Results

Test specimens were designed for shear by the 1983 AASHTO specifications (and applicable revisions through 1987).[1] Design calculations were updated following completion of the testing program to reflect measured material properties. Predicted cracking (V_c) and ultimate (V_n) loads based on the design calculations are referred to as "AASHTO1" in Table 5.1. Strut-and-tie models, also based on measured material properties, were developed for all specimens. This section includes a comparison of predicted strengths based on both of these models to the test results. In addition, details of both models will be examined to explain, where possible, inconsistencies between the models and observed behavior.

5.4.1 AASHTO/ACI Shear Provisions.

5.4.1.1 Web-Shear Cracking Behavior. Cracking loads as predicted by the AASHTO V_c term can be found in Table 5.1. In all cases this represents V_{cw}, the web-shear capacity. It can be concluded from Figure 5.2 that, in general, AASHTO/ACI values were adequate; five of eight observed cracking loads were within 5% of their respective predicted values. However, they were not, in general, conservative, and Specimens 2A-8-0.6 and 2B-8-0.8 cracked at 71% and 80% of predicted cracking loads. Both specimens had a straight tendon layout and the same level of shear reinforcement, but the centroid of the prestressing force was not identical. However, the other two specimens with straight tendons had higher-than-predicted cracking loads.

Cracking behavior of the draped-strand specimens was considerably more consistent than for those with straight strands; all had measured cracking loads within 3% of AASHTO/ACI predicted values. For these four specimens, the average ratio of predicted to measured cracking loads was 0.99 with a standard deviation of 0.02; well within acceptable limits.

5.4.1.2 Ultimate Load Predictions. Ultimate load predictions by AASHTO/ACI provisions were much less accurate than were the cracking load predictions, but were in all cases conservative. Design of the specimens included additional stirrups from the end of the beam to a point 6 in. inside the load point to prevent local failure of the web under the concentrated load. In the original calculation of shear capacities this reinforcement was ignored. However, cracking patterns and strain gage readings provided reason to suspect that at least the first two pairs of detail stirrups were active (and in some cases yielded) at failure. Consequently, shear capacities for all specimens were calculated a second time using this additional contribution to the V_s term, and assuming that it was uniformly distributed throughout the shear span. The resulting revised predictions are identified as AASHTO2 in Table 5.2.

The inclusion of these additional stirrups in the shear calculations necessarily affected those specimens with minimum shear reinforcement more than those with maximum reinforcement. As can be seen in Figure 5.5, the average increase in predicted load was not significantly different between those with minimum and maximum reinforcement. For the first set of design calculations, AASHTO1 (Table 5.1), the average ratio of measured

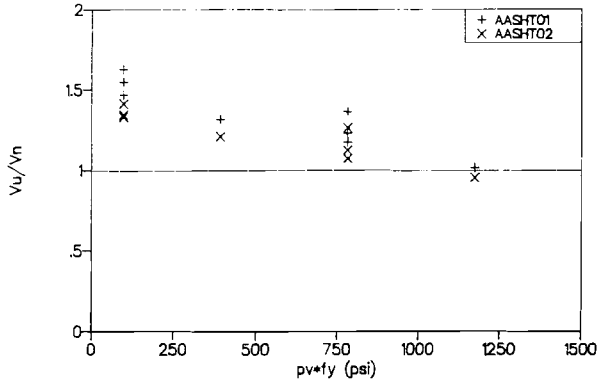

Figure 5.5 Ratio of ultimate load to predicted failure load versus $p_v f_y$.

ultimate load to predicted ultimate load was 1.34 with a standard deviation of 0.19 (high of 1.63 and low of 1.02). The values for the recalculation considering the two extra pairs of stirrups, AASHTO2 (Table 5.2), were more accurate and less scattered, having an average ratio of measured to predicted load of 1.22, and a standard deviation of 0.15 (high of 1.41 and low of 0.95). However, in practice, it would not be normal procedure to consider any detail bars as contributing to the overall shear capacity of a beam using the AASHTO/ACI equations, even for a relatively short cantilever such as that tested in this program. It is more realistic to make a comparison using the values based on the typical shear span reinforcement.

As discussed earlier in Section 5.2.1, there was no clear relationship between the location of the prestressing strands and the accuracy of the AASHTO/ACI predictions. Likewise, a relationship between draping of strands and prediction accuracy was not evident.

AASHTO/ACI predictions were conservative but less accurate for specimens with minimum shear reinforcement than for specimens with greater amounts of transverse reinforcement. This reflects the fact that the steel contribution at ultimate is more easily predicted than is the post-cracking concrete strength. In specimens with minimum shear reinforcement, the concrete contribution is a much greater percentage of the beam capacity than it is in heavily-reinforced specimens. Furthermore, the concrete contribution prescribed by the AASHTO/ACI provisions does not account for the shear transfer mechanisms of aggregate interlock, dowel action by the longitudinal reinforcement, or arching action, which further contributes to the conservatism.

5.4.1.3 Flexure-Shear Cracking. Although flexure-shear cracking did not dominate the behavior of any of the beams in this program, all except Specimen 1B-1-0.6 experienced flexure-shear cracks prior to failure. According to the AASHTO/ACI design equations, flexure-shear cracks could be expected inside the support prior to formation of web-shear cracks in the same area. For Beam 2A-12-D this was the predicted failure mode. However, web-shear cracking in the cantilever controlled the failure of this specimen.

Table 5.3 Calculated and Observed Flexure-Shear Cracking Capacity, Adjusted for Measured Material Properties.

Test No.	Predicted V_{ci}*		Observed V_{cr} Flex.-Shear		V_{cr}/V_{ci}	
	Cant. (1) (kips)	Interior (2) (kips)	Cant. (3) (kips)	Int. (4) (kips)	Cant. (3)/(1)	Int. (4)/(2)
1A-1-0.6	34.9	14.4 16.0 17.3	36.6	14.9 16.4 16.4	1.05	1.03 1.03 0.95
1A-1-D	50.4	20.5 20.9	54.6	22.3 22.3	1.08	1.09 1.07
1B-1-0.8	No flexural-shear cracking observed.					
1B-8-D	46.6	19.2 22.5	48.6	23.8 20.7	1.04	1.24 0.92
2A-8-0.6	41.6	32.1	38.6	28.6	0.93	0.89
2A-12-D	--	19.7 20.5 21.7	--	23.0 27.7 22.3	--	1.17 1.35 1.03
2B-8-0.8	--	22.9	--	24.7	--	1.08
2B-4-D	54.7	23.9	53.6	25.0	0.98	1.05
* AASHTO/ACI 318-83				Ave. Std. Dev.	1.02 0.05	1.07 0.12

Due to the difficulty in determining the origin of inclined cracks in the presence of flexural cracks, it was often difficult to ascertain the load at which flexural cracks turned into shear cracks. Consequently, selected well-defined flexural-shear cracks from each specimen were chosen to compare to AASHTO/ACI predictions. Table 5.3 shows the excellent correlation between these observed cracking loads and predicted values. Again, since only those cracks that were obviously flexural-shear cracks were considered, these results may not be representative of the overall accuracy of the V_{ci} predictions. It is also possible that web-shear cracks were misidentified as flexural-shear cracks, especially since the predicted loads were relatively close for the two types of cracks in the interior span. Nevertheless, the fact that shears 40% greater than the design capacity were experienced on the inside of the support prior to failure in the cantilever, strongly suggests that the AASHTO/ACI provisions for flexure-shear behavior are appropriate for use in negative-moment regions similar to those tested in this program.

5.4.2 Strut-and-Tie Model. A strut-and-tie model was developed for the cantilever region of each specimen at ultimate load. Due to the nature of the strut-and-tie model, a post-cracking mechanism model assuming that concrete functions only in uniaxial

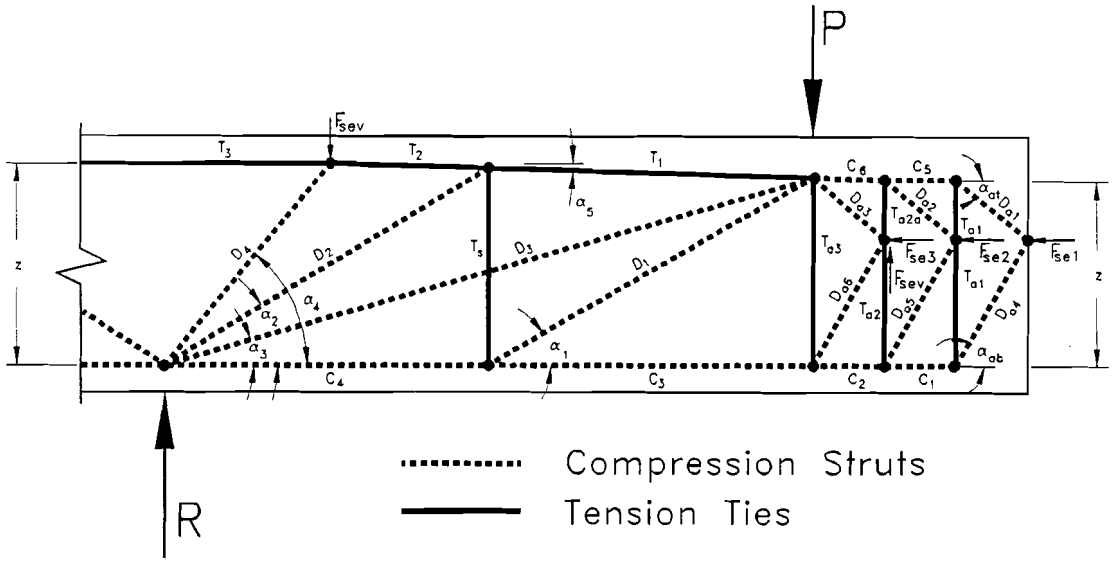

Figure 5.6 Basic strut-and-tie model used for all specimens.

compression, it is not well-suited for crack prediction. Consequently, a comparison will be made only between predicted and actual ultimate loads.

One basic strut-and-tie model was developed, variations of which were used for all specimens. The basic model shown in Figure 5.6 consisted of a two-panel truss between the load point and support. An additional three panels of *K*-truss extended from the load point to the end of the beam to carry the prestress force into the main truss. Variations of this basic model were necessary to account for direct strut behavior in lightly reinforced specimens and variations in tendon profiles. The direct strut, D_3, was only included in models for lightly reinforced specimens which did not contain sufficient shear reinforcement to carry the entire vertical load from the top to bottom chord. An additional inclined strut, D_4, necessary to equilibrate the vertical component of the prestress at the drape point was added to the basic model in specimens with inclined prestressing.

Dead load was introduced into the strut-and-tie model as a single concentrated load placed conservatively at the point of application of the applied load. This was done to avoid complicating the model for the benefit of less than 2% of the total load.

Four variations of the basic model were investigated for each specimen. The variables in the four versions of each model were the location of the vertical tie representing the total stirrup force (T_s), and the magnitude of this tie force. For each specimen, the four models will be referred to as ST1, ST2, ST3 and ST4. Details of the four strut-and-tie models for each specimen are presented in Tables 5.4 through 5.7.

Table 5.4 Strut-and-Tie Model Details for Specimens 1A-1-0.6 and 1A-1-D.

Note: Forces in kips Angles in Degrees		Specimen 1A-1-0.6 End, z = 15.62 in. Support, z = 15.62 in. Efficiency v = .390 Eq 5.6 Fse1, 2 & 3 = 46.3 kips Fsev = .0 kips				Specimen 1A-1-D End, z = 15.62 in. Support, z = 16.95 in. Efficiency v = .392 Eq 5.6 Fse1, 2 & 3 = 48.0 kips Fsev = 12.7 kips			
Strut-&-Tie Model		ST1	ST2	ST3	ST4	ST1	ST2	ST3	ST4
Ultimate Load:	P	40.2	32.0	34.0	34.0	51.9	44.5	45.6	45.6
Angles:	α1	29.8	49.0	29.8	30.1	30.5	49.3	30.5	30.4
	α2	29.8	20.9	29.8	29.6	30.5	21.6	30.5	31.0
	α3	16.0	16.0	16.0	16.0	16.2	16.2	16.2	16.2
	α4	--	--	--	--	50.8	50.8	50.8	50.8
	α5	0.0	0.0	0.0	0.0	1.6	1.6	1.6	1.6
	αat	39.7	39.7	39.7	39.7	39.7	39.7	39.7	39.7
	αab	60.6	60.6	60.6	60.6	60.6	60.6	60.6	60.6
Diag. Struts:	D1	47.5	31.3	18.7	18.6	46.5	31.1	18.3	18.4
(Compression +)	D2	47.5	66.2	18.7	18.6	44.3	59.8	17.5	17.3
	D3	60.0	30.5	89.6	11.5	60.2	37.9	88.5	88.5
	D4	--	--	--	--	17.7	16.8	16.9	16.9
	Da1	41.0	41.0	41.0	41.0	42.5	42.5	42.5	42.5
	Da2	41.0	41.0	41.0	41.0	42.5	42.5	42.5	42.5
	Da3	41.0	41.0	41.0	41.0	48.1	48.1	48.1	48.1
	Da4	30.0	30.0	30.0	30.0	31.2	31.2	31.2	31.2
	Da5	30.0	30.0	30.0	30.0	31.2	31.2	31.2	31.2
	Da6	30.0	30.0	30.0	30.0	23.3	23.3	23.3	23.3
Vertical Ties:	Ts	23.6	23.6	9.3	9.3	23.6	23.6	9.3	9.3
(Tension +)	Ta1	26.2	26.2	26.2	26.2	27.1	27.1	27.1	27.1
	Ta2	26.2	26.2	26.2	26.2	27.1	27.1	27.1	27.1
	Ta2a	26.2	26.2	26.2	26.2	25.3	25.3	27.1	27.1
	Ta3	26.2	26.2	26.2	26.2	20.5	20.5	20.5	20.5
Top Chord:	T1	4.3	-44.8	7.7	7.5	-3.7	-44.9	-0.7	-0.6
(Tension +)	T2	45.5	17.0	24.0	23.9	34.6	10.8	14.4	14.2
	T3	45.5	17.0	24.0	23.9	45.7	21.4	25.1	24.8
	C5	31.6	31.6	31.6	31.6	32.7	32.7	32.7	32.7
	C6	63.1	63.1	63.1	63.1	65.5	65.5	65.5	65.5
Bottom Chord:	C1	14.8	14.8	14.8	14.8	15.3	15.3	15.3	15.3
(Compression +)	C2	29.5	29.5	29.5	29.5	30.6	30.6	30.6	30.6
	C3	44.3	44.3	44.3	44.3	42.1	42.1	42.1	42.1
	C4	85.5	64.8	60.5	60.3	82.2	62.4	57.9	58.0

Table 5.5 Strut-and-Tie Model Details for Specimens 1A-1-0.8 and 1A-8-D.

Note: Forces in kips Angles in Degrees		Specimen 1B-1-0.8 End, z = 16.95 in. Support, z = 16.95 in. Efficiency v = .389 Eq 5.6 Fse1, 2 & 3 = 46.0 kips Fsev = .0 kips				Specimen 1B-8-D End, z = 15.6 in. Support, z = 17.0 in. Efficiency v = .4 Eq 5.6 Fse1, 2 & 3 = 45.6 kips Fsev = 12.1 kips			
Strut-&-Tie Model		ST1	ST2	ST3	ST4	ST1	ST2	ST3	ST4
Ultimate Load:	P	45.1	35.2	39.1	39.1	68.4	67.3	68.4	66.2
Angles:	α1	31.9	51.3	31.9	32.2	30.5	34.5	30.5	28.5
	α2	31.9	22.5	31.9	31.6	30.5	27.6	30.5	33.2
	α3	17.3	17.3	17.3	17.3	--	--	--	--
	α4	0.0	0.0	0.0	0.0	50.8	50.8	50.8	50.8
	α5	0.0	0.0	0.0	0.0	1.6	1.6	1.6	1.6
	αat	18.4	18.4	18.4	18.4	39.7	39.7	39.7	39.7
	αab	68.1	68.1	68.1	68.1	60.6	60.6	60.6	60.6
Diag. Struts:	D1	44.7	30.2	17.6	17.5	111.0	98.3	111.0	113.1
(Compression +)	D2	44.7	61.7	17.6	17.5	105.9	114.1	105.9	94.7
	D3	72.4	39.1	100.3	100.3	--	--	--	--
	D4	0.0	0.0	0.0	0.0	19.0	18.8	19.0	18.7
	Da1	42.8	42.8	42.8	42.8	40.4	40.4	40.4	40.4
	Da2	42.8	42.8	42.8	42.8	40.4	40.4	40.4	40.4
	Da3	42.8	42.8	42.8	42.8	45.7	45.7	45.7	45.7
	Da4	14.6	14.6	14.6	14.6	29.6	29.6	29.6	29.6
	Da5	14.6	14.6	14.6	14.6	29.6	29.6	29.6	29.6
	Da6	14.6	14.6	14.6	14.6	22.3	22.3	22.3	22.3
Vertical Ties:	Ts	23.6	23.6	9.3	9.3	56.3	55.7	56.3	54.0
(Tension +)	Ta1	13.5	13.5	13.5	13.5	25.8	25.8	25.8	25.8
	Ta2	13.5	13.5	13.5	13.5	25.8	25.8	25.8	25.8
	Ta2a	13.5	13.5	13.5	13.5	24.0	24.0	24.0	24.0
	Ta3	13.5	13.5	13.5	13.5	19.4	19.4	19.4	19.4
Top Chord:	T1	-14.7	-65.5	-11.0	-11.2	-0.8	-15.5	-0.8	2.9
(Tension +)	T2	23.2	-8.6	4.0	4.0	90.4	85.7	90.4	82.2
	T3	23.2	-8.6	4.0	4.0	102.3	97.5	102.3	93.9
	C5	40.6	40.6	40.6	40.6	31.1	31.1	31.1	31.1
	C6	81.2	81.2	81.2	81.2	62.2	62.2	62.2	62.2
Bottom Chord:	C1	5.4	5.4	5.4	5.4	14.5	14.5	14.5	14.5
(Compression +)	C2	10.9	10.9	10.9	10.9	29.1	29.1	29.1	29.1
	C3	16.3	16.3	16.3	16.3	40.0	40.0	40.0	40.0
	C4	54.2	35.2	31.2	31.1	135.6	121.0	135.6	139.4

Table 5.6 Strut-and-Tie Model Details for Specimens 2A-8-0.6 and 2A-12-D.

Note: Forces in kips Angles in Degrees		Specimen 2A-8-0.6 End, z = 15.62 in. Support, z = 15.62 in. Efficiency v = .383 Eq 5.6 Fse1, 2 & 3 = 50.0 kips Fsev = .0 kips				Specimen 2A-12-D End, z = 15.62 in. Support, z = 16.95 in. Efficiency v = .385 Eq 5.6 Fse1, 2 & 3 = 48.5 kips Fsev = 12.9 kips			
Strut-&-Tie Model		ST1	ST2	ST3	ST4	ST1	ST2	ST3	ST4
Ultimate Load:	P	60.1	55.4	60.1	58.1	75.0	76.6	75.0	72.7
Angles:	α1	29.8	34.2	29.8	28.3	30.5	31.9	30.5	28.5
	α2	29.8	26.4	29.8	31.5	30.5	29.3	30.5	33.2
	α3	--	--	--	--	--	--	--	--
	α4	--	--	--	--	50.8	50.8	50.8	50.8
	α5	--	--	--	--	1.6	1.6	1.6	1.6
	αat	39.7	39.7	39.7	39.7	39.7	39.7	39.7	39.7
	αab	60.6	60.6	60.6	60.6	60.6	60.6	60.6	60.6
Diag. Struts:	D1	120.9	98.5	120.9	122.7	122.2	120.7	122.2	124.8
(Compression +)	D2	120.9	124.8	120.9	111.1	116.6	123.7	116.6	104.4
	D3	--	--	--	--	--	--	--	--
	D4	--	--	--	--	20.5	20.6	20.5	20.1
	Da1	44.3	44.3	44.3	44.3	42.9	42.9	42.9	42.9
	Da2	44.3	44.3	44.3	44.3	42.9	42.9	42.9	42.9
	Da3	44.3	44.3	44.3	44.3	48.6	48.6	48.6	48.6
	Da4	32.5	32.5	32.5	32.5	31.5	31.5	31.5	31.5
	Da5	32.5	32.5	32.5	32.5	31.5	31.5	31.5	31.5
	Da6	32.5	32.5	32.5	32.5	23.7	23.7	23.7	23.7
Vertical Ties:	Ts	60.1	55.4	60.1	58.1	62.0	63.7	62.0	59.6
(Tension +)	Ta1	28.3	28.3	28.3	28.3	27.4	27.4	27.4	27.4
	Ta2	28.3	28.3	28.3	28.3	27.4	27.4	27.4	27.4
	Ta2a	28.3	28.3	28.3	28.3	25.5	25.5	25.5	25.5
	Ta3	28.3	28.3	28.3	28.3	20.6	20.6	20.6	20.6
Top Chord:	T1	2.7	-20.7	2.7	5.8	2.7	-0.1	2.7	7.0
(Tension +)	T2	107.7	91.1	107.7	100.5	103.2	107.8	103.2	94.5
	T3	107.7	91.1	107.7	100.5	116.1	120.8	116.1	107.2
	C5	34.1	34.1	34.1	34.1	33.1	33.1	33.1	33.1
	C6	68.1	68.1	68.1	68.1	66.1	66.1	66.1	66.1
Bottom Chord:	C1	15.9	15.9	15.9	15.9	15.5	15.5	15.5	15.5
(Compression +)	C2	31.9	31.9	31.9	31.9	30.9	30.9	30.9	30.9
	C3	47.8	47.8	47.8	47.8	42.5	42.5	42.5	42.5
	C4	152.7	129.3	152.7	155.8	147.8	145.1	147.8	152.2

Table 5.7 Strut-and-Tie Model Details for Specimens 2B-8-0.8 and 2B-4-D.

Note: Forces in kips Angles in Degrees		Specimen 2B-8-0.8 End, z = 16.95 in. Support, z = 16.95 in. Efficiency v = .386 Eq 5.6 Fse1, 2 & 3 = 47.7 kips Fsev = .0 kips				Specimen 2B-4-D End, z = 15.62 in. Support, z = 16.95 in. Efficiency v = .390 Eq 5.6 Fse1, 2 & 3 = 47.3 kips Fsev = 12.6 kips			
Strut-&-Tie Model		ST1	ST2	ST3	ST4	ST1	ST2	ST3	ST4
Ultimate Load:	P	64.2	59.7	64.2	62.2	65.0	64.7	61.4	61.1
Angles:	α1	31.9	36.4	31.9	30.3	30.5	34.7	30.5	28.5
	α2	31.9	28.3	31.9	33.7	30.5	27.4	30.5	33.1
	α3	--	--	--	--	--	--	16.2	--
	α4	--	--	--	--	50.8	50.8	50.8	50.8
	α5	--	--	--	--	1.6	1.6	1.6	1.6
	αat	18.4	18.4	18.4	18.4	39.7	39.7	39.7	39.7
	αab	68.1	68.1	68.1	68.1	60.6	60.6	60.6	60.6
Diag. Struts:	D1	121.5	100.6	121.5	123.4	98.3	87.5	84.2	89.5
(Compression +)	D2	121.5	126.1	121.5	112.2	93.7	102.7	80.3	75.1
	D3	--	--	--	--	13.4	13.4	25.8	24.3
	D4	--	--	--	--	19.2	19.1	18.7	18.7
	Da1	44.3	44.3	44.3	44.3	41.9	41.9	41.9	41.9
	Da2	44.3	44.3	44.3	44.3	41.9	41.9	41.9	41.9
	Da3	44.3	44.3	44.3	44.3	47.4	47.4	47.4	47.4
	Da4	15.1	15.1	15.1	15.1	30.7	30.7	30.7	30.7
	Da5	15.1	15.1	15.1	15.1	30.7	30.7	30.7	30.7
	Da6	15.1	15.1	15.1	15.1	23.1	23.1	23.1	23.1
Vertical Ties:	Ts	64.2	59.7	64.2	62.2	49.9	49.9	42.8	42.8
(Tension +)	Ta1	14.0	14.0	14.0	14.0	26.7	26.7	26.7	26.7
	Ta2	14.0	14.0	14.0	14.0	26.7	26.7	26.7	26.7
	Ta2a	14.0	14.0	14.0	14.0	24.9	24.9	24.9	24.9
	Ta3	14.0	14.0	14.0	14.0	20.1	20.1	20.1	20.1
Top Chord:	T1	-23.1	-45.3	-23.1	-19.6	-2.6	-15.3	-2.7	1.9
(Tension +)	T2	80.1	65.7	80.1	73.8	78.2	76.0	66.5	64.8
	T3	80.1	65.7	80.1	73.8	90.3	88.0	78.3	76.6
	C5	42.1	42.1	42.1	42.1	32.2	32.2	32.2	32.2
	C6	84.2	84.2	84.2	84.2	64.5	64.5	64.5	64.5
Bottom Chord:	C1	5.6	5.6	5.6	5.6	15.1	15.1	15.1	15.1
(Compression +)	C2	11.3	11.3	11.3	11.3	30.1	30.1	30.1	30.1
	C3	16.9	16.9	16.9	16.9	41.5	41.5	41.5	41.5
	C4	120.0	97.8	120.0	123.5	126.1	113.4	114.0	120.1

5.4.2.1 Model ST1. For model ST1, the same total stirrup contribution as was assumed in the revised AASHTO predictions (AASHTO2) was assumed as a limit for the total force carried by the stirrups in the shear span. This assumption required full participation of the first two pairs of detail stirrups in addition to the design shear-span reinforcement. It should be noted that the AASHTO V_s term represents the stirrup force over a design region of length d because the shear provisions are based on a 45° truss model, whereas the tie force in the strut-and-tie model represents the total vertical force carried by the stirrups in the shear-span. For the three specimens with $V_s = 1\sqrt{f_c'}\ b'd$ and the one with $V_s = 4\sqrt{f_c'}\ b'd$, the tie force was taken as this limiting value; a direct strut (D_3 in Figure 5.6) between the load point and the support was introduced to account for the remainder of the vertical load. The remaining four specimens did not require a direct strut, and were therefore determinate trusses. Consequently, the tie force was determined by the model geometry, and was less than the assumed limit in all cases. Models without a direct strut were investigated for Specimen 2B-4-D, but this resulted in either a tie force, T_s, approximately 10% over the assumed limit or, if the limit was assumed, concrete strut stresses too low to be capable of producing the observed web-compression failures.

In the interest of simplicity, the inclinations of the two diagonal compression struts, α_1 and α_2, measured from the horizontal (not including the direct strut when present), were assumed equal for model ST1. In specimens with straight strands this resulted in the single vertical tie being located at midpoint of the shear-span. In specimens with draped strands, the vertical tie was located closer to the point of load application.

5.4.2.2 Model ST2. Model ST2 was the same as Model ST1 except that instead of arbitrarily assuming equal angles of inclination for the major compression struts, the vertical tie was located at the horizontal centroid of the assumed participating stirrups. This resulted in the tie being located closer to the load point than in Model ST1, and in the inclinations of the main struts not being equal.

5.4.2.3 Model ST3. This model had the same geometry as Model ST1, but assumed a total stirrup force based on the design shear reinforcement in the shear-span as was done for the AASHTO1 predictions. In other words, only those stirrups counted in the design V_s were considered here. The end detail stirrups were ignored in the assumed vertical tie force. The end detail was, however, relied upon in anchoring the strands. For Specimens 2A-8-0.6, 2B-8-0.8, 1B-8-D, and 2A-12-D, Model ST3 was identical to Model ST1 because

the total tie force required at ultimate load was less than the design force. In other words, the compression struts determined the dimensions of this model for these specimens.

5.4.2.4 Model ST4. This model was based on the same limiting total stirrup force as Model ST3, but had the vertical tie located at the centroid of the design stirrups. As for the previous models, the total available stirrup force for the heavily reinforced specimens was never reached.

5.4.2.5 Prestressing. Prestressing was regarded as an externally applied compression force applied over the transfer length for the strands. The prestressing strand was then treated as passive reinforcement, and was combined with non-prestressed reinforcement to comprise the tension chord, the location of which was the centroid of all tension reinforcement. The only difference between the prestressing strand and the mild reinforcement in this model was that in checking stresses in the strand it was necessary to add the effective prestress to the stress induced by the applied load. Where strands were draped, the top chord was inclined to remain at the centroid of all tension reinforcement at any location.

The vertical component of the prestress force was modeled as a single point load (F_{sev}) at the drape point. At the drape point nearest the load point, this required splitting the central tension tie of the *K*-truss into two separate ties, T_{a2a} and T_{a2}, above and below the application of the prestress force, respectively. At the drape point closer to the support, an additional compression strut, D_4, was added to carry the vertical load directly to the support. The overall effect of modeling the vertical component in this manner was to lower the effect of the applied load on the shear span by the amount of the vertical component of the prestress. This is analogous to the effect of the V_p term in the AASHTO/ACI equation for V_{cw}.

5.4.2.6 Anchorage Zone. The total effective prestress force after all losses, F_{se}, was divided into three equal forces, F_{se1}, F_{se2}, and F_{se3}, which were applied at the mid-height nodes of the *K*-truss panels. The vertical location of the mid-height nodes was at the centroid of the nine prestressing strands. The three *K*-truss panels covered a length approximately equal to the estimated transfer length, $50d_b$.[1, 27] This section of truss has very steep struts resulting in compressive stresses of up to $0.5f'_c$. This full-depth truss was used because it provided a relatively simple means of distributing the prestress force over the

depth of the section to the chords of the truss. In addition, the actual strand layout covered 5 in. or more of the beam height, so the actual force distribution would be over a depth of nearly 8 in. if a 12° strut-and-tie model as proposed by Bergmeister[8] was applied to the outermost strands. Other refinements to the model in the anchorage region are possible. In general, these would include flatter strut angles, effectively lowering both the compressive force in the struts and the tensile force in the ties. However, these refinements also result in a considerably more complex model without significantly changing the distribution of forces in the shear-span portion of the model. It should be noted, however, that adequate design of the transfer zone at the end of the beam is extremely important to ensure that redistribution of forces can occur as required to develop the strut-and-tie model.

5.4.2.7 Compression Chord. The location of the compression chord was taken as the centroid of the transformed bottom flange section and the compression reinforcement in the flange. Checking stresses in the bottom flange and compression reinforcement then required satisfying compatibility between the strains in the steel and concrete to determine the portion of the total chord force carried by each.

5.4.2.8 Ties. Each strut-and-tie model contained one vertical tension tie located near the center of the shear-span that modeled all of the stirrups in the shear-span. This is a simplification of the model shown in Figure 5.7 which represents each stirrup with a discrete tie that is connected to a compression strut at the top and bottom chords. In Figure 5.7, the heavy dashed lines represent the discrete struts, the heavy solid lines represent the

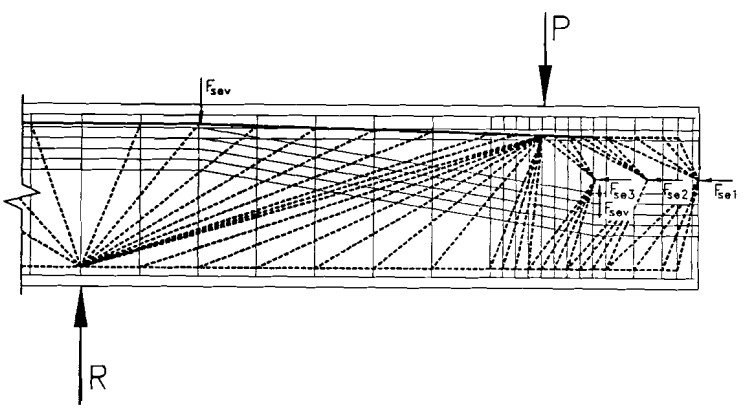

Figure 5.7 Strut-and-tie model assuming each stirrup to be a discreet vertical tension tie.

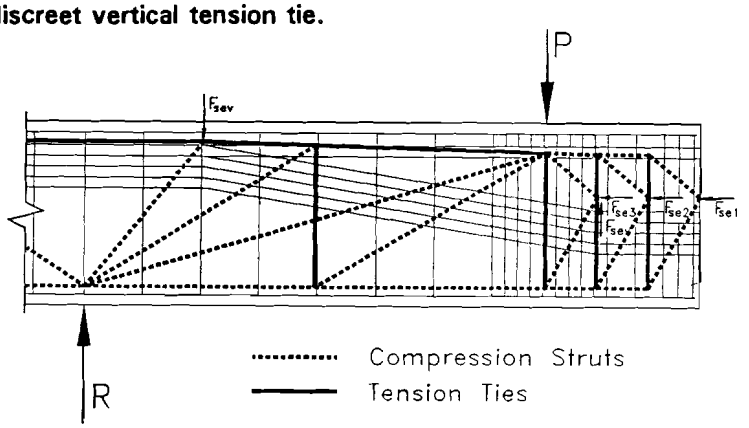

Figure 5.8 Simplified strut-and-tie model showing corresponding reinforcement.

tension chord, and the thin lines are the actual reinforcement, the stirrups assumed to be the discrete vertical tension ties. Figure 5.8 shows the simplified model developed from the complex model in Figure 5.7, along with the actual reinforcement. This discrete tie model is more accurate than the simplified one, but is also complicated and unwieldy, requiring iteration as the model was necessarily redundant. Calculation of strut sizes and stresses is also relatively difficult in this model. However, the complex model is quite useful in demonstrating the applicability of the simple model. It provides a vivid picture of the flow of forces through the section, evincing the gradual increase of forces along the length of the chords and the relatively even distribution of forces in the web which fan from the load point and support to the center of the shear-span.

In the simplified model, the single tie can be located in one of three manners: 1) by geometry, 2) by distribution of stirrup area, or 3) by distribution of stirrup force. Models ST1 and ST3 employed a geometric tie location definition as described in Sections 5.4.2.1 and 5.4.2.3. This has the advantage of simplicity and presents a relatively even distribution of force throughout the shear-span.

Models ST2 and ST4 employed the second method of determining the tie location. This consisted of assuming stirrup yield at failure for a given number of stirrups, then using the centroid of the resultant vertical force as the tie location. This approach allowed explicit consideration of two of the detail stirrup pairs near the load point as described in Sections 5.4.2.2 and 5.4.2.4. The difficulty in this method lies in determining which stirrup pairs to assume as yielded at failure. It is also not necessarily more accurate than the geometric definition; it predicts higher compressive stresses in the area of the web near the support, contradicting the evidence provided by the crack patterns and failure modes which indicated a more uniform distribution of stress throughout the shear span (Figure 5.9).

Determining the tie location by the third method is more difficult than by either of the first two methods because it requires determination of the actual or assumed stirrup force distribution over the shear-span. Consequently, this method was not used in any of the models considered.

5.4.2.9 Nodes. The components of strut-and-tie models where forces are concentrated and redirected are referred to as nodes. In a rectangular beam they are the locations of highest compressive stress. In I-beams, on the other hand, they are not

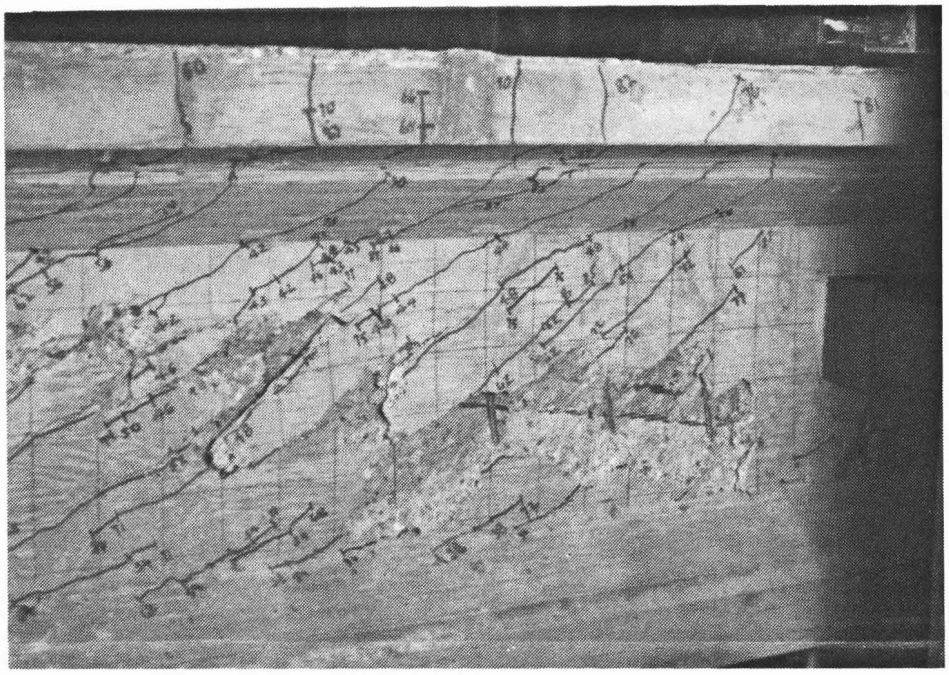

Figure 5.9 Crack pattern for specimen 1B-8-D at failure.

necessarily critical because they tend to be confined to the flanges. Because the flanges are so much greater in width than the web, the web becomes the location of highest compressive stress. The specimens tested in this program were all thin-webbed I-beams. As a result, none experienced node failures or even significant distress in the nodal regions.

The particular loading arrangement and chosen strut-and-tie models used in this study resulted in a number of extremely congested nodes. For example, the support region of Beam 1A-1-D, shown in Figure 5.8, has a C-C-C-C-C-C-C node in the bottom flange. As one might expect, dimensioning of a node such as this by geometric methods results in either an extremely large or extremely complex node. Neither choice is desirable. The present state of knowledge of node behavior does not permit a reasonable understanding of the behavior of such complex nodes as were encountered here. However, research into the behavior of nodes is currently underway at The University of Texas at Austin.[7,9]

5.4.2.10 Struts. The strut-and-tie models developed for the beams tested in this program included two, three, or four struts in the shear-span. Two of these were used to equilibrate the tie force of the stirrups in each specimen. Because there were never sufficient stirrups to carry the applied load more than once from the top to bottom chord, a two panel truss was used in all models. Specimens 1A-1-0.6, 1A-1-D, 1B-1-0.8, and 2B-4-D

could not carry the full vertical load by stirrup action, thus requiring an additional direct strut from the load point to the support. The use of this modified model was corroborated by crack patterns and strain gauge readings which indicated both full development of the stirrups and the existence of a direct strut from load to support. A fourth minor strut was needed to transmit the vertical component of the prestress force from the drape point to the support in the four beams with draped strands in the cantilever.

5.4.2.11 Strut Definition. As was previously mentioned, in flanged beams, particularly I-beams, struts are generally the critical location for checking compressive stresses in the concrete. This being the case, it is necessary to define the strut width at the point where compressive stresses are critical. However, this point is not necessarily at the point of maximum compressive stress because transverse stresses on the struts affect the effective compressive strength. For example, the biaxial compression experienced by the bottom flange near the support results in an effective concrete strength greater than f'_c, while the transverse tension and resultant cracking applied to the web struts by the stirrups, in conjunction with the lack of confinement extant in a thin web, can result in "softening" of the concrete,[13] effectively reducing the compressive strength as shown in Figure 5.10.[13] So, although struts may narrow as they enter the flange, the transverse stresses have less of a detrimental effect in this region than they do in the central part of the web, in many cases making the center of the web the critical region in the strut.

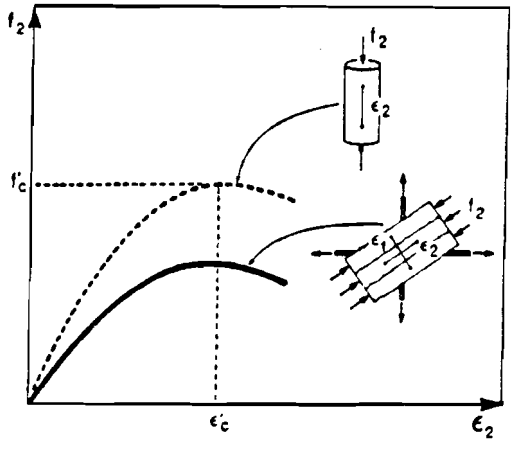

Figure 5.10 Softening of concrete due to transverse tensile strain.[12]

Since all failures in this testing program were of the web-crushing variety, a geometric strut definition was chosen, and calculated compressive strengths were then compared to the appropriate efficiency factor. Efficiency factors will be discussed in Section 5.4.2.12. Two different strut width definitions were used depending on the geometry of the strut-and-tie model. For models with main struts parallel to each other, the strut width, *w*, was

$$w = z \cos \alpha \tag{5.4}$$

where z is the distance between top and bottom chord and α is the strut angle. For cases where struts are not parallel, and more than one inclined strut enters a single node (for example, where a direct strut is required) it is proposed that the width of each strut be proportioned according to the relative magnitude of the forces carried by adjacent struts. This case is shown in Figure 5.11. The width, w, of the main strut, D_3, is defined as follows:

$$w = \frac{2 z \tan\left[\dfrac{(\alpha_2 - \alpha_3)D_3}{D_2+D_3}\right]}{\tan \alpha_2 \cos \alpha_3} \tag{5.5}$$

where z is the distance between the top and bottom chord at the location of the vertical tie, α_1 is the angle measured from horizontal to the adjacent strut D_1, and α_3 is the angle measured from horizontal to the main strut D_3. This equation assumes that the two struts adjacent to the one under consideration are parallel and carry equal loads. For cases where this is not true, Equation 5.5 can be used twice to independently consider the effect of each adjacent strut, the calculated values of w being each divided by 2 and added together to obtain the total strut width. If no adjacent inclined strut exists on one side of the strut in question, it is conservative to assume symmetry based on the adjacent strut on the other side.

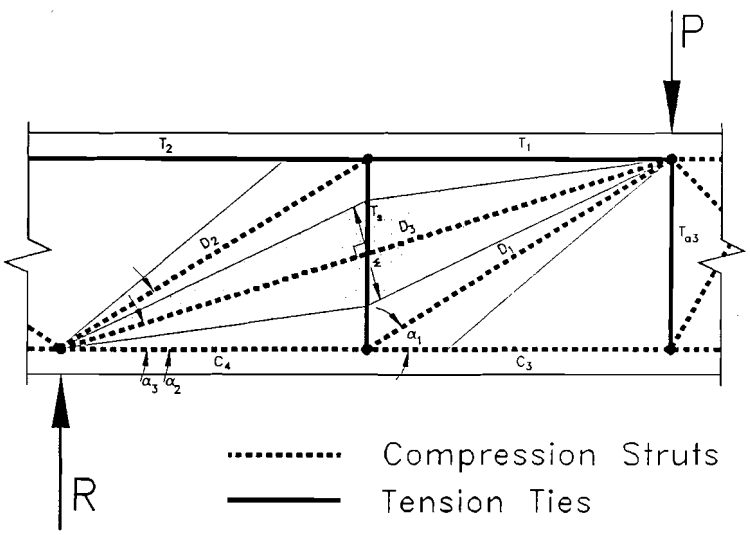

Figure 5.11 Proposed strut-width definition for models with diagonals crossing vertical ties.

5.4.2.12 Concrete Efficiency in Compression Struts. Using the strut-width definition presented above and the strut-and-tie models described in Sections 5.4.2.1 through 5.4.2.4, experimental efficiency factors for the major diagonal struts were calculated as $\nu_e = f_d/f'_c$, where f_d is the compressive stress in the strut at failure. These experimental efficiency factors for the major diagonal struts of the four models considered are tabulated in Table

Table 5.8 Experimental Efficiency Factors for Struts in All Strut-and-Tie Models.

Test Desig.	f_c' (ksi)	Effic. Factor Eq. 5.6 (A)	Strut	Model ST1 f_d / f_c'		Model ST2 f_d / f_c'		Model ST3 f_d / f_c'		Model ST4 f_d / f_c'	
				(1)	(1)/(A)	(2)	(2)/(A)	(3)	(3)/(A)	(4)	(4)/(A)
1A-1-0.6	10.024	.390	D1	.434	1.113	.449	1.152	.511	1.311	.508	1.303
			D2	.434	1.113	.623	1.598	.511	1.311	.514	1.318
			D3	.435	1.116	.457	1.172	.515	1.321	.514	1.318
1A-1-D	9.646	.392	D1	.466	1.190	.475	1.213	.542	1.384	.542	1.384
			D2	.432	1.103	.615	1.570	.496	1.266	.490	1.251
			D3	.450	1.149	.483	1.233	.523	1.335	.519	1.325
1B-1-0.8	10.246	.389	D1	.383	0.985	.405	1.041	.446	1.147	.444	1.142
			D2	.383	0.985	.547	1.406	.446	1.147	.449	1.154
			D3	.384	0.987	.412	1.059	.450	1.157	.450	1.157
1B-8-D	10.155	.389	D1	.500	1.284	.471	1.210	.500	1.284	.519	1.333
			D2	.476	1.223	.508	1.305	.476	1.223	.455	1.169
			D3								
21-8-0.6	11.640	.383	D1	.398	1.038	.369	0.962	.398	1.038	.411	1.072
			D2	.398	1.038	.431	1.124	.398	1.038	.385	1.004
			D3								
2A-12-D	11.325	.385	D1	.411	1.069	.402	1.045	.411	1.069	.426	1.108
			D2	.392	1.019	.401	1.043	.392	1.019	.374	0.973
			D3								
2B-8-0.8	10.927	.386	D1	.383	0.992	.359	0.930	.383	0.992	.394	1.020
			D2	.383	0.992	.412	1.067	.383	0.992	.372	0.963
			D3								
2B-4-D	9.965	.390	D1	.419	1.074	.416	1.066	.457	1.171	.464	1.189
			D2	.396	1.015	.409	1.048	.429	1.100	.418	1.071
			D3	.405	1.038	.403	1.033	.441	1.130	.436	1.117
Average of all struts:					1.078		1.171		1.174		1.171
Standard Dev. of all struts:					0.085		0.181		0.125		0.130
Average of all critical struts:					1.094		1.273		1.177		1.198
Standard Dev. of critical struts:					0.095		0.216		0.133		0.125

5.8. Figures 5.12 and 5.13 are comparisons of the experimental efficiency factors to those calculated using the formula that follows, which was proposed by Bergmeister et al.[8]

$$\nu = 0.6 \left[0.5 + \frac{15}{\sqrt{f_c'}} \right] \qquad (5.6)$$

The term *0.6* in this expression is applied to account for the reduced compressive strength caused by transverse tensile stresses in severely cracked beams or slender webs, as demonstrated by MacGregor.[30] As proposed, the parenthetical portion of this expression applies to confined concrete in compression and nodal zones.

In Figure 5.12 and Figure 5.13, the ratio of experimental to theoretical efficiency factors is plotted versus $\rho_v f_y$, the actual shear reinforcement ratio multiplied by the yield stress of the shear reinforcement. In this expression, $\rho_v = A_v/b's$ where A_v is the area of vertical shear reinforcement over a distance s, and b' is the width of the web. The experimental efficiency factors plotted are for the critical strut in each model for each specimen. The various strut-and-tie models were included to demonstrate the applicability of both the strut-and-tie models and the efficiency factor formula. Since the strut-and-tie model is based on the lower bound theorem, experimental values of the efficiency factor at ultimate load should always be greater than theoretical values if the strut in question is truly critical and the theoretical efficiency factor is valid. All but three of the experimental values plotted in Figures 5.12 and 5.13 were greater than their theoretical counterparts. The three that fell below were all within 2% of the theoretical values.

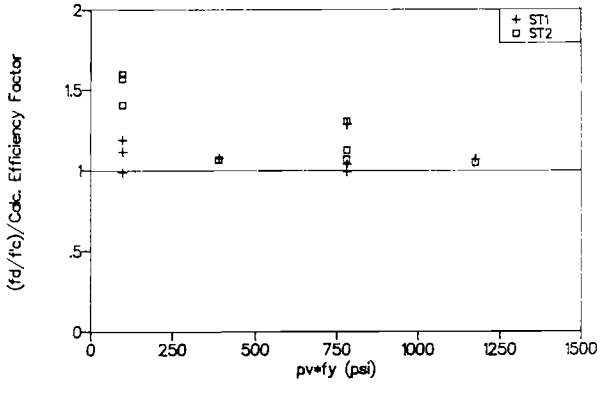

Figure 5.12 Comparison of experimental strut efficiency, f_d/f'_c, to factors calculated by Eq. 5.6.

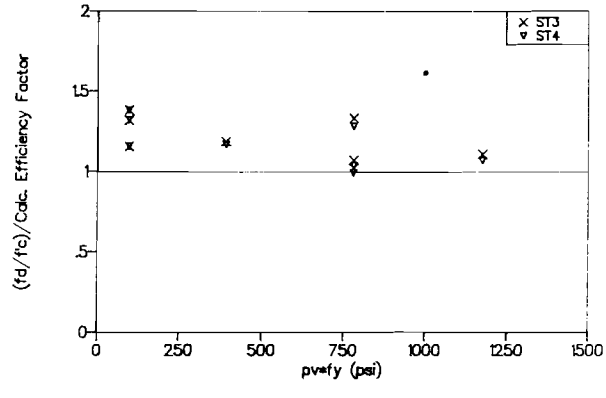

Figure 5.13 Comparison of experimental strut efficiency, f_d/f'_c, to factors calculated by Eq.5.6.

Model ST1 showed the best correlation with the values from Equation 5.6. The mean value of the ratio of experimental to calculated critical strut efficiency factors was 1.09 for model ST1, with a standard deviation of 0.10. This model provided the best results primarily because it most accurately modeled the total stirrup force by including all of the effective stirrups in the tie force, and by placing the tie near the center of the

shear-span, allowing the diagonal struts to best match the flow of forces as indicated by cracking patterns.

Other models also agreed well with Equation 5.6. For the range of values of $\rho_v f_y$ covered by this test program, there seems to be a trend toward increasing accuracy with increasing amounts of shear reinforcement. This effect could be due to the decreasing proportion of the total load carried by the concrete as the level of shear reinforcement is increased. However, it could also be related to the choice of models, because specimens having large concrete contributions due to direct strut action are more difficult to accurately model than those relying heavily on shear reinforcement.

5.4.2.13 Model Predictions. All of the beams in this test program experienced web-crushing failures and as such, the strut-and-tie models applied to these beams should predict diagonal strut stresses reaching their limiting values, $\nu f'_c$, as failure becomes imminent. At the same time, stresses in the compression chord and reinforcement should be at or below their limiting values. Due to the size of the bottom flange and the large amount of compression reinforcement it contained, it was never a critical component in the strut-and-tie models for these beams.

Failure loads as predicted by the four strut-and-tie models for each specimen are tabulated in Table 5.9.

Stirrup yielding was assumed in developing the redundant strut-and-tie models (those with minimal reinforcement and thus a direct strut from load point to support). Models for specimens without direct struts were controlled by compression failure in the diagonals. Stresses were then checked in the longitudinal and transverse reinforcement. For the four beams with lowest values of $\rho_v f_y$, 1A-1-0.6, 1A-1-D, 1B-1-0.8, and 2B-4-D, the tensile chord forces were well below capacity. However, the three specimens with the highest ratios of shear strength to flexural strength (1B-8-D, 2A-8-0.6, and 2A-12-D) had flexural

Table 5.9 Predicted Failure Loads by Strut-and-Tie Models Using Efficiency Factors Calculated From Equation 5.6.

Test Desig.	V_{crack}	Ultimate Load					Stirrup Contribution					Comparison			
	V_{cr} Meas. (kips)	V_n1 ST1 (kips)	V_n2 ST2 (kips)	V_n3 ST3 (kips)	V_n4 ST4 (kips)	V_u Meas. (kips)	T_s ST1 (kips)	T_s ST2 (kips)	T_s ST3 (kips)	T_s ST4 (kips)	V_u-V_{cr} Meas. (kips)	V_u(act) / V_n1	V_u(act) / V_n2	V_u(act) / V_n3	V_u(act) / V_n4
1A-1-0.6	27.9	40.2	32.0	34.0	34.0	42.6	23.6	23.6	9.30	9.30	14.7	1.06	1.33	1.25	1.25
2A-8-0.6	18.6	60.1	55.4	60.1	58.1	62.4	60.1	55.4	60.1	58.1	43.8	1.04	1.13	1.04	1.07
1B-1-0.8	25.3	45.1	35.2	39.1	39.1	44.6	23.6	23.6	9.30	9.30	19.3	0.99	1.27	1.14	1.14
2B-8-0.8	20.1	64.2	59.7	64.2	62.2	63.8	64.2	59.7	64.2	62.2	43.7	0.99	1.07	0.99	1.03
1A-1-D	36.3	51.9	44.5	45.6	45.6	58.8	23.6	23.6	9.30	9.30	22.5	1.13	1.32	1.29	1.29
2B-4-D	38.6	65.0	64.7	61.4	61.1	67.1	49.9	49.9	42.8	42.8	28.5	1.03	1.04	1.09	1.10
1B-8-D	35.6	68.4	67.3	68.4	66.2	86.1	56.3	55.7	56.3	54.0	50.5	1.26	1.28	1.26	1.30
2A-12-D	36.4	75.0	76.6	75.0	72.7	79.4	62.0	63.7	62.0	59.6	43.0	1.06	1.04	1.06	1.09
Note: V_d = 0.6 kips added to measured V_{cr} & V_u.											Ave.	1.07	1.18	1.14	1.16
											Std.	0.08	0.12	0.11	0.10

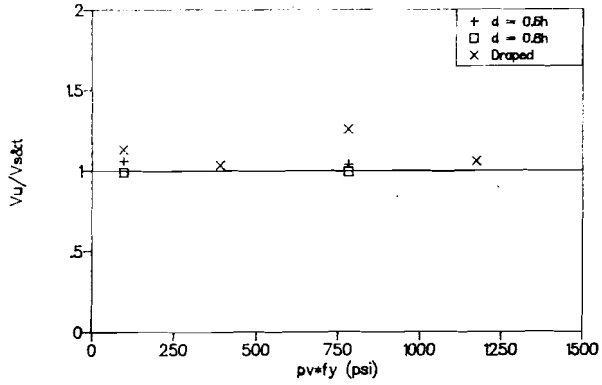

Figure 5.14 Comparison of experimental ultimate loads to those predicted by strut-and-tie model ST1.

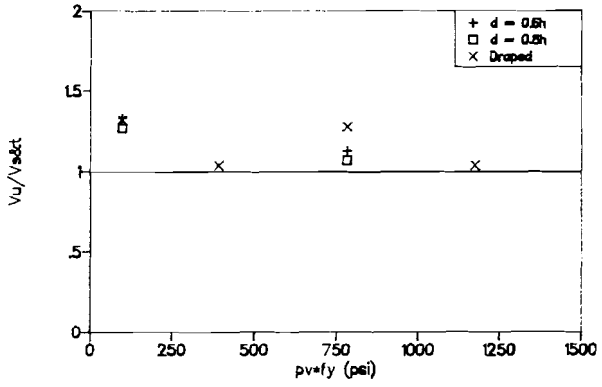

Figure 5.15 Comparison of experimental ultimate loads to those predicted by strut-and-tie model ST2.

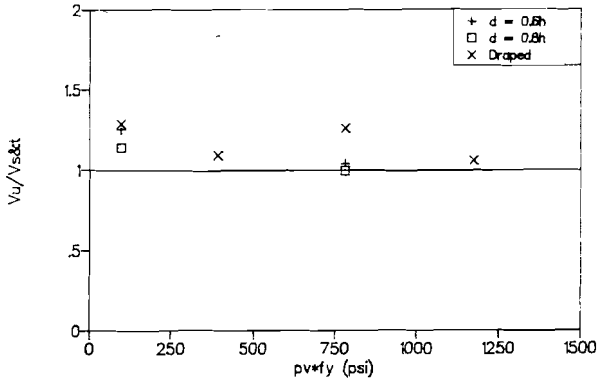

Figure 5.16 Comparison of experimental ultimate loads to those predicted by strut-and-tie model ST3.

reinforcement at or near yield at failure according to the models. This agrees with the strain measurements recorded during testing. Models for the remaining specimen, 2A-8-0.8, were controlled by compression failure in the diagonals. However, transverse reinforcement forces were close to those required to yield the vertical tie. In cases where either the vertical or longitudinal tie yielded before compression failure in the diagonal, the strut-and-tie model prediction for the diagonal strut force at failure is still applicable because compression failure initiates following yielding of the tension tie.

In Figures 5.14 to 5.17 the ratio of experimental failure loads (shears) to predicted failure loads using the strut-and-tie are plotted versus $\rho_v f_y$ for each of the four basic models. From these plots it is apparent that model *ST1* provides the best correlation between experimental and theoretical values, although *ST1* is slightly unconservative in two cases (less than 1%). Use of models ST2, ST3, and ST4 results in slightly more scatter in results, but in all cases the predicted values are conservative. This demonstrates the relative insensitivity of the predictions to minor changes in model geometry.

5.5 Summary of Design Implications

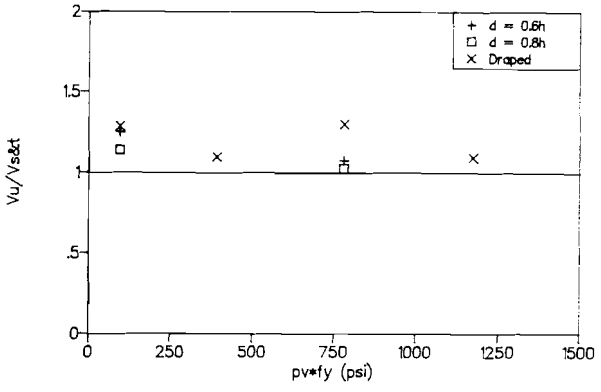

Figure 5.17 Comparison of experimental ultimate loads to those predicted by strut-and-tie model ST4.

Test results presented in Chapter 4 and discussed in this chapter indicate that current AASHTO/ACI design provisions can be applied to pretensioned, thin-webbed, I-beams subject to shear and negative-moment bending. More particularly, for beams having draped strands, or straight strands with $d = 0.6h$ or $d = 0.8h$, AASHTO/ACI equations conservatively predicted the ultimate shear capacity. Conservatism decreased with increasing values of $\rho_v f_y$ from 100 to 1180 psi, and increased slightly with an increase in d from $0.6h$ to $0.8h$.

Flexure-shear cracking was observed in all but one specimen. However, because of the thin web and large amount of flexural reinforcement, none of the specimens experienced a flexure-shear failure. One specimen which was designed to fail in the flexure-shear mode developed shears exceeding the *Specifications*' predicted capacity by 40% before failing in a web-crushing mode. Web instability also was not observed in any of the tests, even though the typical web had a slenderness ratio of 5.0. Investigation into the design of slender-web test specimens by AASHTO/ACI methods indicated that, for beams with ratios of longitudinal to transverse reinforcement more typically found in practice, flexural capacity controlled the design.

The general strut-and-tie model provided a better estimate of shear strength, and a better understanding of the observed behavior than the AASHTO/ACI equations for shear. Because the number of tests conducted in this study was very limited, the general strut-and-tie model should be further confirmed against a large body of test data from thin-web specimens[23, 29, 32, 33] in order to permit general application of the model.

CHAPTER 6
SUMMARY AND CONCLUSIONS

6.1 Summary

The primary objective of the research described herein was to evaluate the suitability of the current AASHTO/ACI design provisions for shear as applied to thin-web pretensioned I-beams subject to shear and negative-moment bending. Eight tests were performed on four pretensioned beams with varying tendon profiles and amounts of shear reinforcement. Behavior was measured and observed to collect information on cracking loads, inclination and size of diagonal cracks, failure modes and loads, steel strains, and end slip of prestressing strands. Observed behavior was compared to predicted behavior based on the *1983 AASHTO Specifications for Highway Bridges*[1] and the *1983 ACI Building Code.*[4]

A secondary objective was to examine the application of strut-and-tie models to thin-web, pretensioned I-beams. Four variations of a basic strut-and-tie model were evaluated for each test beam. Based on observed web-crushing failures, a strut-width definition for non-parallel diagonal struts was proposed in conjunction with a concrete efficiency factor definition proposed for thin webs by Bergmeister et al.[8]

6.2 Conclusions

Based on measured and observed behavior of the beams tested, the following conclusions can be made concerning the behavior of thin-web I-beams subjected to shear and negative-moment bending, the appropriateness of the current AASHTO/ACI design provisions for shear, and the application of strut-and-tie models.

6.2.1 Overall Behavior.

1) Cracking loads did not show a clear dependance on location of the centroid of strands in straight-strand beams.
2) Measured initial crack inclinations were in all cases less than 45° and for lightly reinforced beams were as shallow as 10 to 15°.

3) Crack inclinations at failure were primarily dependent on the amount of web reinforcement; inclinations ranged from approximately 20° for lightly reinforced beams to 30° for heavily reinforced specimens.
4) Stirrups yielded at or before failure due to web-crushing in all beams. Flexural reinforcement generally did not yield prior to failure.
5) A direct compression strut between the load point and support (arch action) was observed in lightly reinforced beams.

6.2.2 Comparison of Observed Behavior to AASHTO Models.

1) AASHTO design equations for shear conservatively predicted ultimate loads for the eight beams tested in shear and negative-moment bending when $d = 0.8h$ was used in lieu of the actual distance from the extreme compression fiber to the center of gravity of the prestress force.
2) AASHTO/ACI predicted ultimate loads were slightly less conservative for straight-strand specimens with center of gravity of strands at $0.6h$ than for specimens with center of gravity at $0.8h$ and having equal amounts of shear reinforcement.
3) AASHTO/ACI predicted ultimate loads for draped-strand specimens underestimated shear strength of specimens by 2 to 47%.
4) The strongest trend evident from comparing AASHTO/ACI predictions to measured failure loads was the decreasing conservatism of the code predictions with increasing $\rho_v f_y$. This can be interpreted either as a higher effectiveness of the stirrups or as a greater "concrete contribution" in lightly reinforced members, perhaps due to the formation of a direct strut (arch action) between the applied load and the support reaction.
5) The AASHTO/ACI V_c term did not provide an accurate prediction of cracking load for straight-strand specimens. Measured cracking loads ranged from 15% above to 29% below the AASHTO/ACI predicted load.
6) In contrast, observed initial cracking loads for beams with draped strands were within 3% of AASHTO/ACI predicted values.
7) Observed flexure-shear cracking loads were very close to AASHTO predicted values, even though they occurred after web-shear cracking.
8) Although no flexure-shear failures were observed in this study, one specimen which was designed to fail in the flexure-shear mode developed shears exceeding the *Specifications'* capacity by 40% before failing in a web-crushing mode.

6.2.3 Comparison of Observed Behavior to Strut-and-Tie Models.

1) Ultimate load predictions based on strut-and-tie models were in all cases conservative.
2) Ultimate load predictions based on strut-and-tie models were generally more accurate and less variable than AASHTO/ACI predictions.
3) The level of accuracy did not show significant dependence on either tendon profile or amount of web-reinforcement. Small variations in model geometry did not have a significant effect on model accuracy.

6.3 Concluding Remarks

The AASHTO design equations for shear, using $d = 0.8h$ in lieu of the actual distance from the extreme compression fiber to the center of gravity of the prestress force, provided conservative to over-conservative predictions of ultimate loads for thin-web I-beams tested in shear and negative-moment bending. This was true for specimens with nominal values of V_s ranging from $1\sqrt{f_c'}$ b'd to $12\sqrt{f_c'}$ b'd, and strand layouts having center of gravity at $0.6h$, $0.8h$, or draped between $0.6h$ and $0.8h$.

In addition, this study demonstrated that the strut-and-tie model can be effectively applied to local regions of pretensioned I-beams having straight or draped tendon profiles. Aspects of the strut-and-tie model requiring further study include complex nodal regions at the intersection of more than three struts and ties, nodal regions with triaxial states of stress as found in flanged beams, introduction of prestress forces into the overall model, evaluation of the compressive stress regions containing nonparallel struts, and development of efficiency factors more consistent with the physical nature of the model.

APPENDIX A

This Appendix contains plots of applied load vs. load-point deflection for all tests. All plots show load cycles to first cracking and to failure. In addition, Figures A.1 and A.5 show a third load cycle required to reach failure during Tests 1A-1-0.6 and 2A-8-0.6.

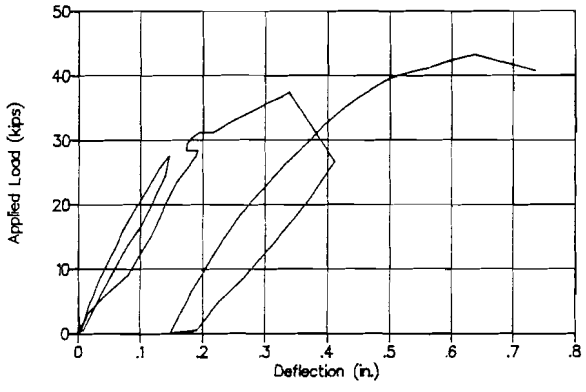

Figure A.1 Applied load vs. load-point deflection for Test 1A-1-0.6.

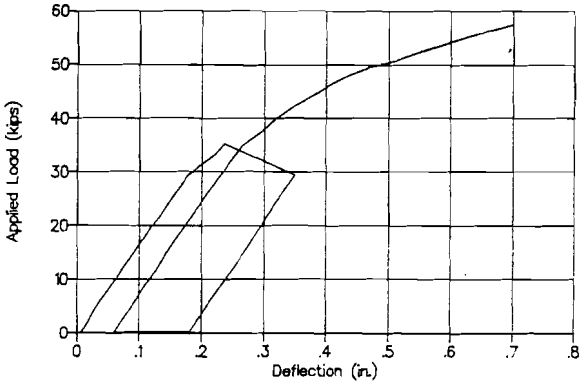

Figure A.2 Applied load vs. load-point deflection for Test 1A-1-D.

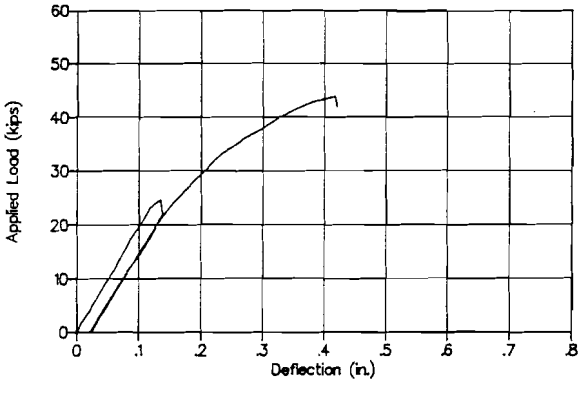

Figure A.3 Applied load vs. load-point deflection for Test 1B-1-0.8.

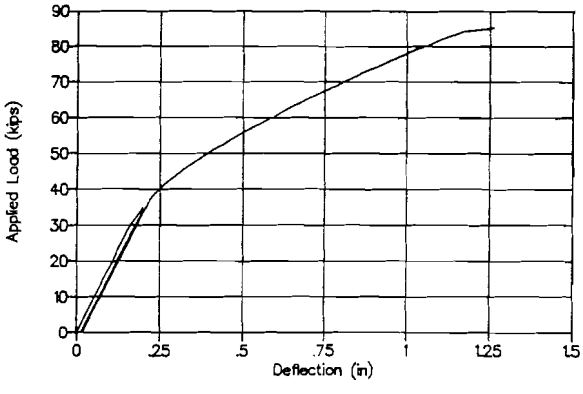

Figure A.4 Applied load vs. load-point deflection for Test 1B-8-D.

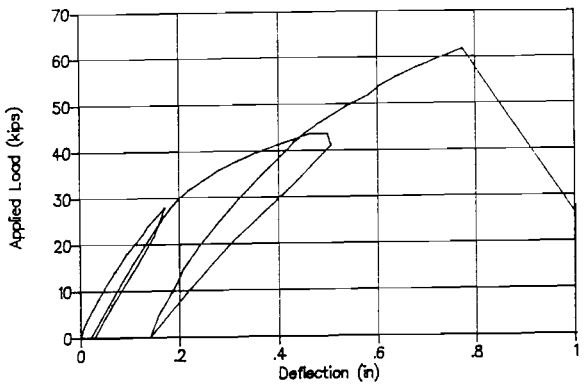

Figure A.5 Applied load vs. load-point deflection for Test 2A-8-0.6.

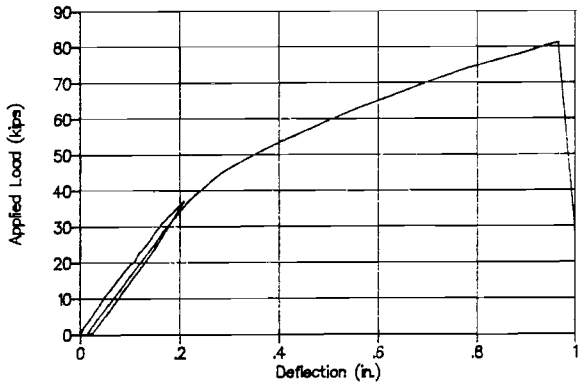

Figure A.6 Applied load vs. load-point deflection for Test 2A-12-D.

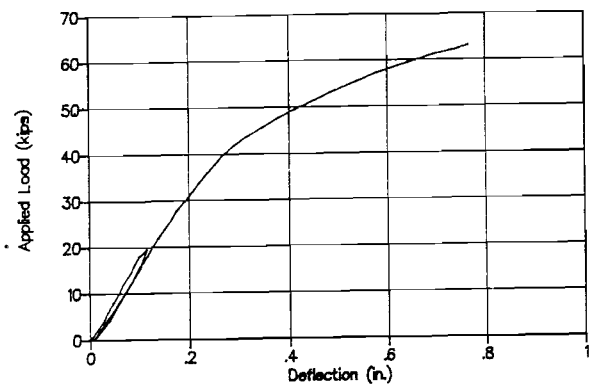

Figure A.7 Applied load vs. load-point deflection for Test 2B-8-0.8.

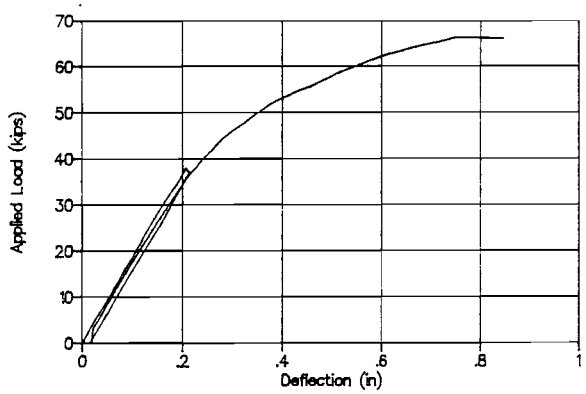

Figure A.8 Applied load vs. load-point deflection for Test 2B-4-D.

APPENDIX B

Crack diagrams showing the East side of each specimen (as it was positioned in the test setup) are included in this appendix. Thick lines indicate the cracks observed at the first cracking load. Thin lines indicate cracks at failure. Numbers along cracks indicate the load in kips at which the crack propagated to the corresponding tick mark. A medium weight line appears in Figures B.1a and B.2a and indicates the crack propagation during the intermediate load cycle required in Tests 1A-1-0.6 and 2A-8-0.8.

Shaded areas indicate regions where concrete spalled off the beam. Outlined areas represent regions where spalled concrete remained in place. The scale across the bottom of each drawing defines distances along the beams in inches.

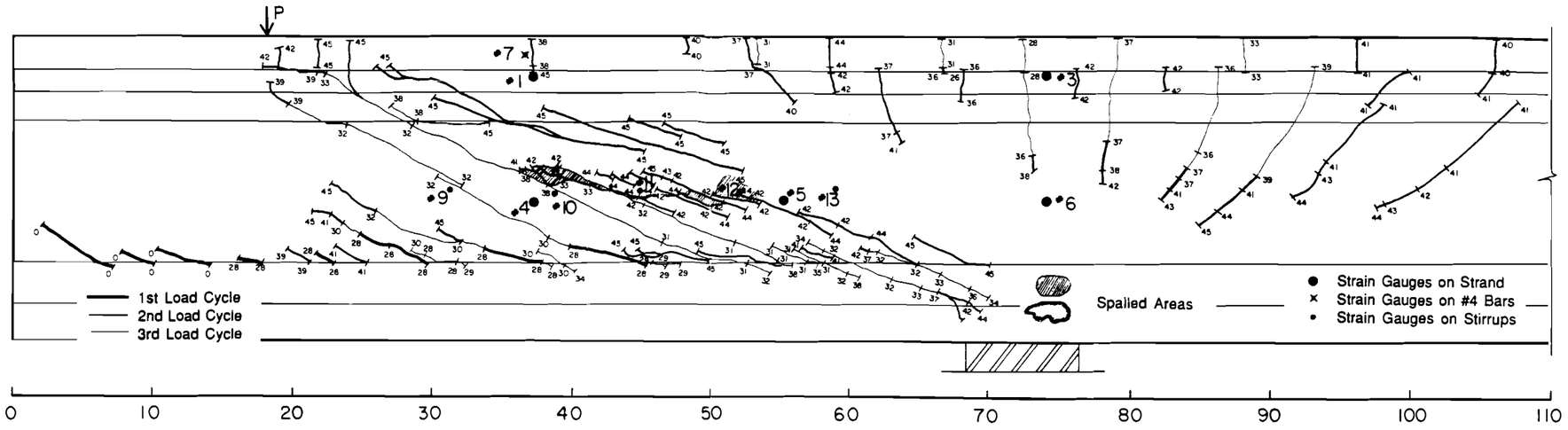

a) Specimen 1A-1-0.6

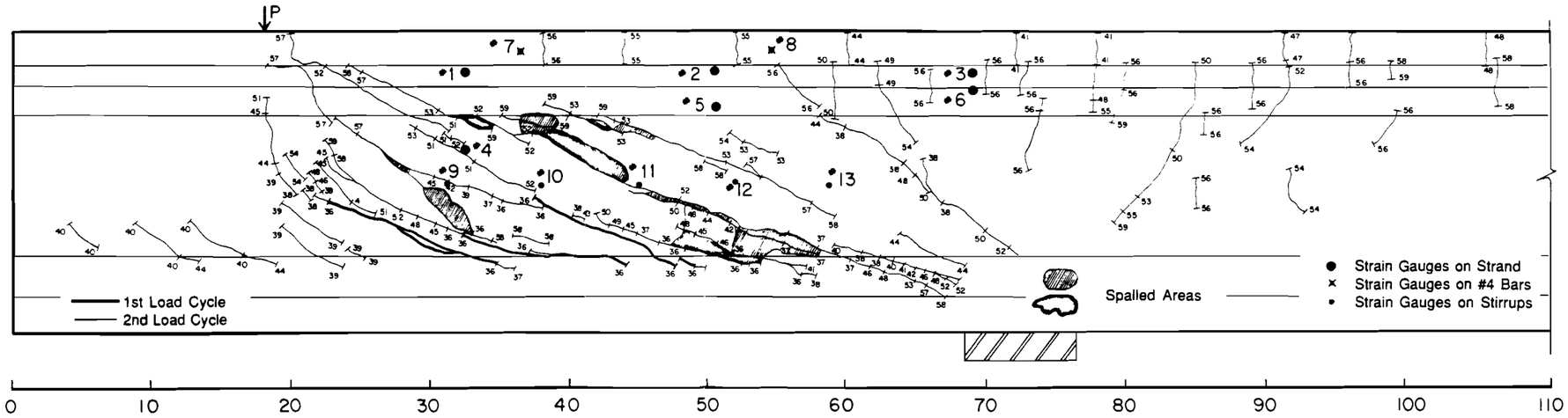

b) Specimen 1A-1-D

Figure B.1 Crack diagrams for Beam 1A.

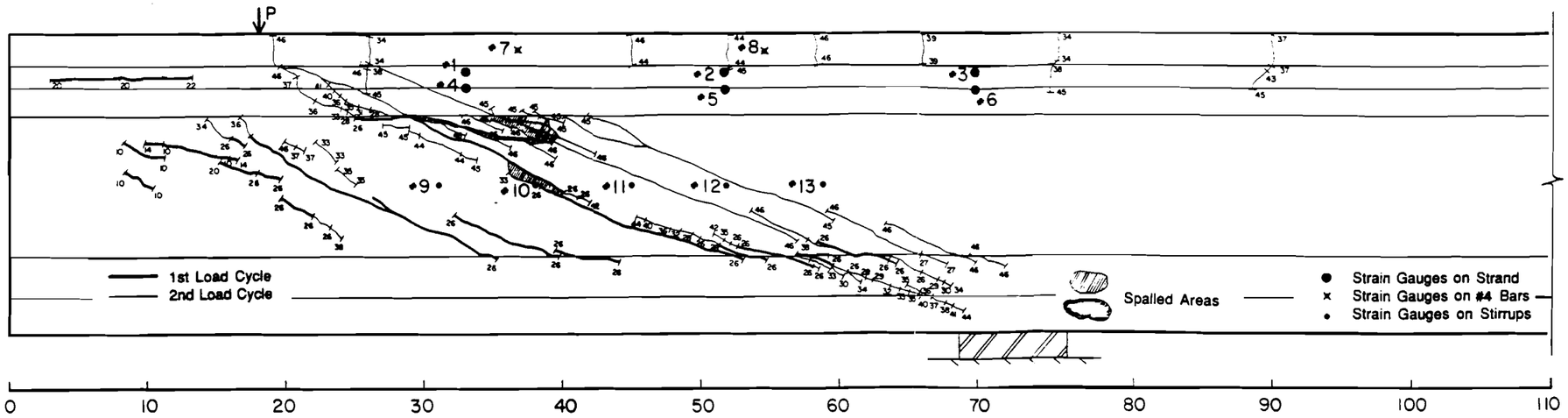

a) **Specimen 1B-1-0.8**

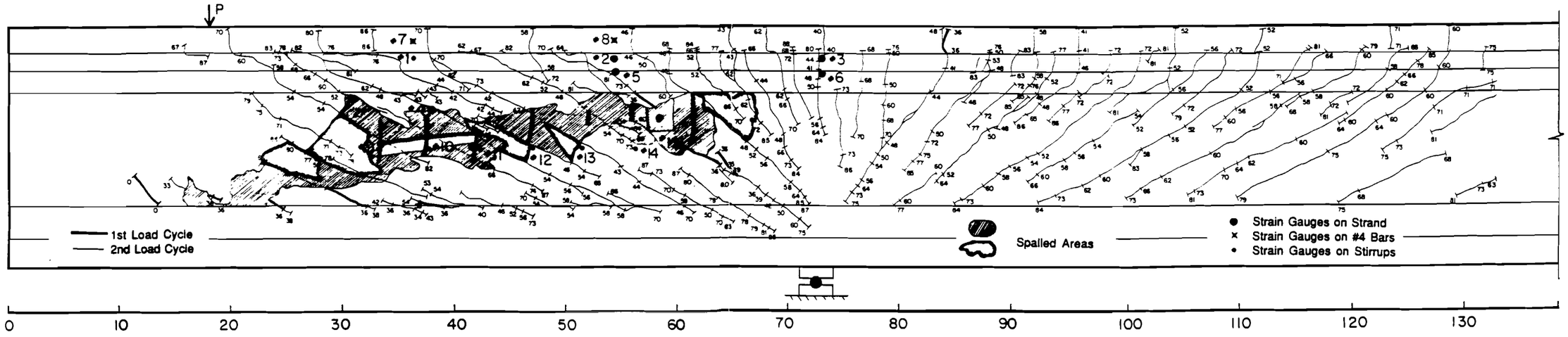

b) **Specimen 1B-8-D**

Figure B.2 Crack diagrams for Beam 1B.

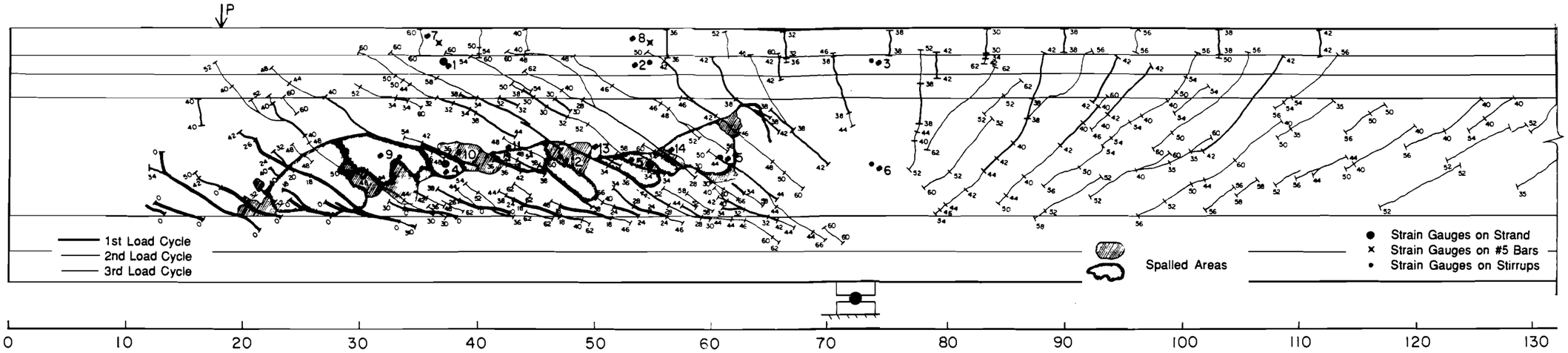

a) **Specimen 2A-8-0.6**

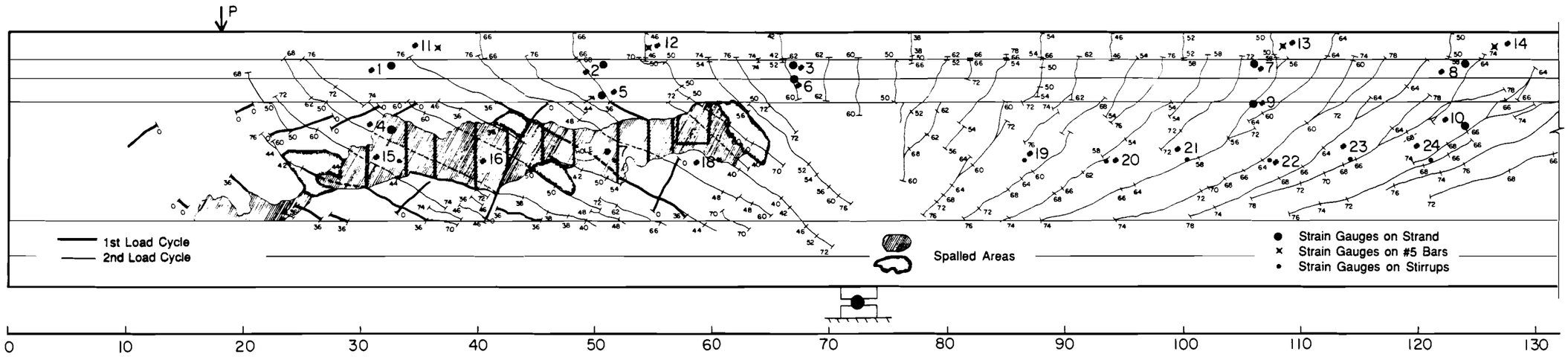

b) **Specimen 2A-12-D**

Figure B.3 Crack diagrams for Beam 2A.

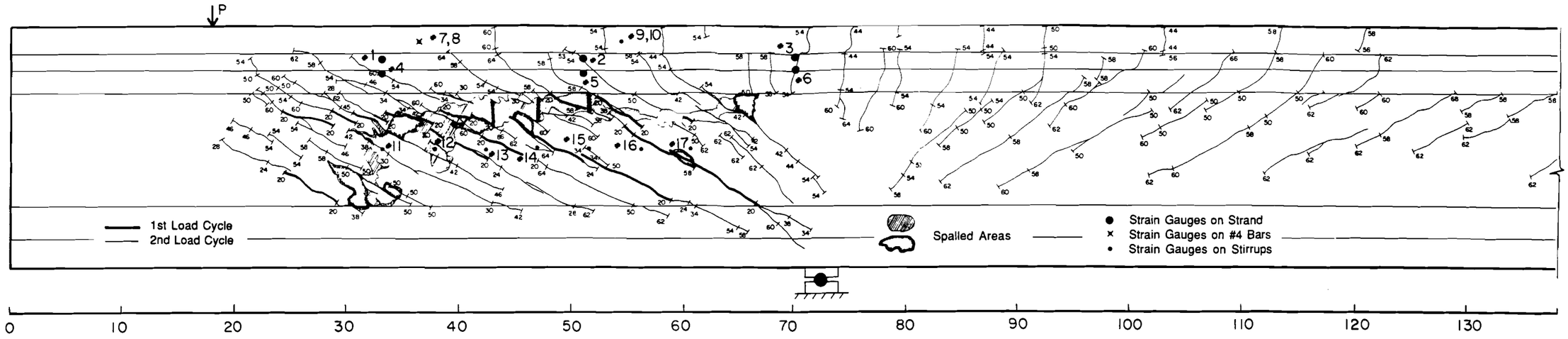

a) **Specimen 2B-8-0.8**

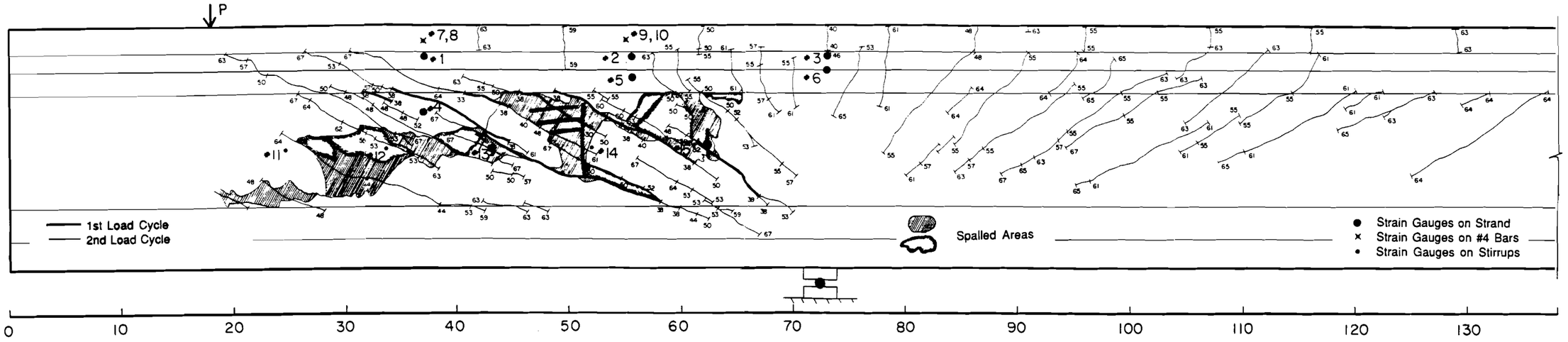

b) **Specimen 2B-4-D**

Figure B.4 Crack diagrams for Beam 2B.

APPENDIX C

This appendix contains plots of applied load vs. stirrup strain measured by electronic resistance strain gauges. Strains are plotted separately for each load cycle. Strain gauge numbers refer to numbers in Figures 3.18 through 3.22. Specimen 2A-12-D contained both #1¼ gauged stirrups in the interior span and #2 gauged stirrups in the cantilever. Strains for these are plotted separately.

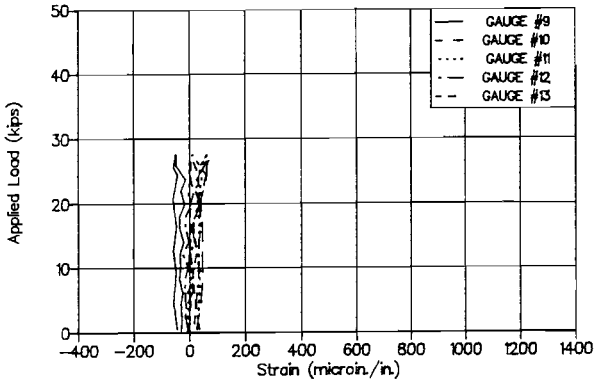

Figure C.1 Applied load vs. stirrup strains for first load cycle of Test 1A-1-0.6.

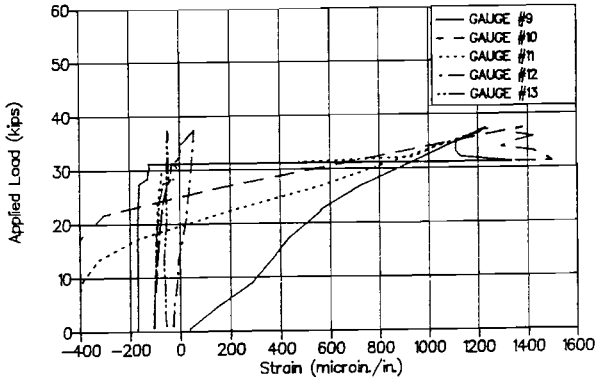

Figure C.2 Applied load vs. stirrup strains for second load cycle of Test 1A-1-0.6.

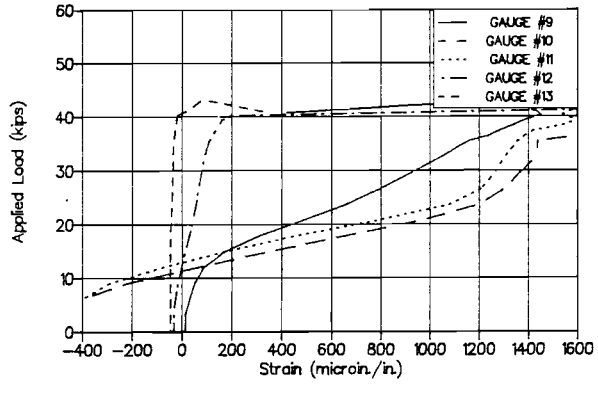

Figure C.3 Applied load vs. stirrup strains for final load cycle of Test 1A-1-0.6.

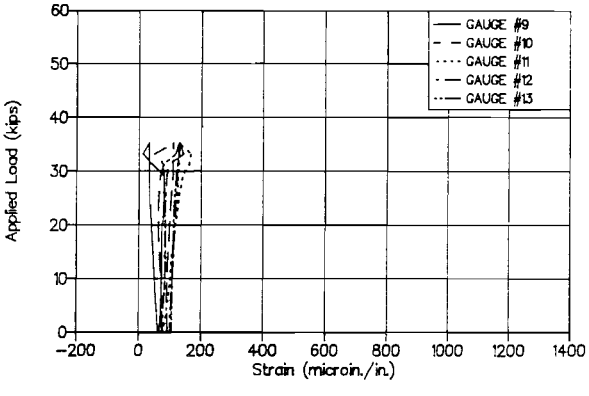

Figure C.4 Applied load vs. stirrup strains for first load cycle of Test 1A-1-D.

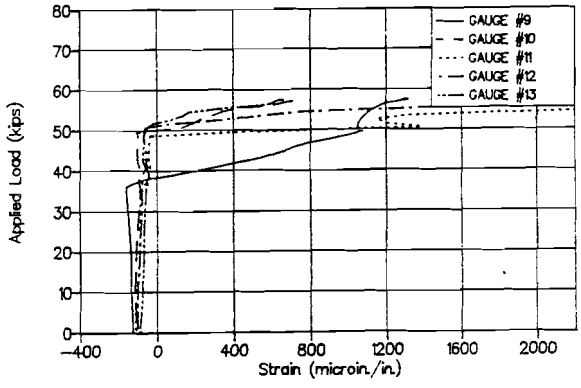

Figure C.5 Applied load vs. stirrup strains for second load cycle of Test 1A-1-D.

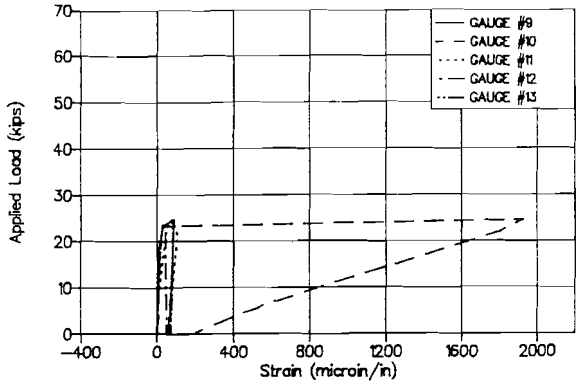

Figure C.6 Applied load vs. stirrup strains for first load cycle of Test 1B-1-0.8.

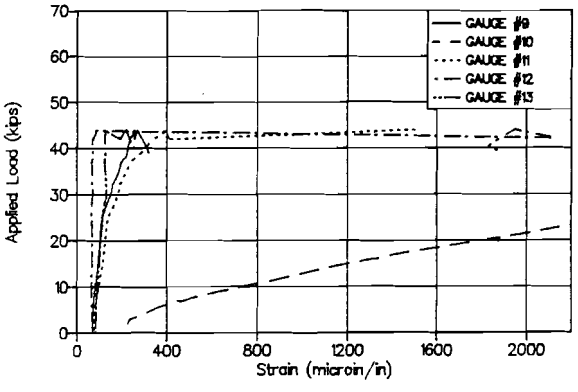

Figure C.7 Applied load vs. stirrup strains for second load cycle of Test 1B-1-0.8.

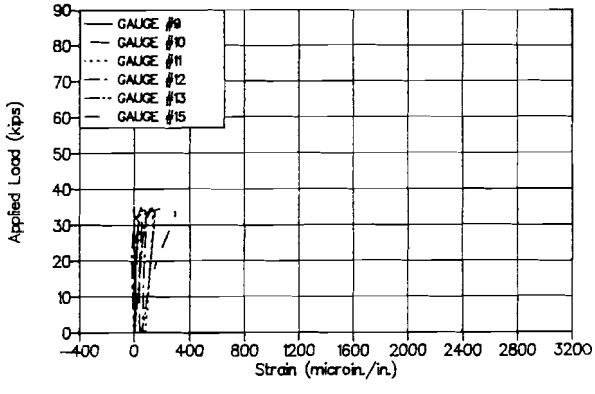

Figure C.8 Applied load vs. stirrup strains for first load cycle of Test 1B-8-D.

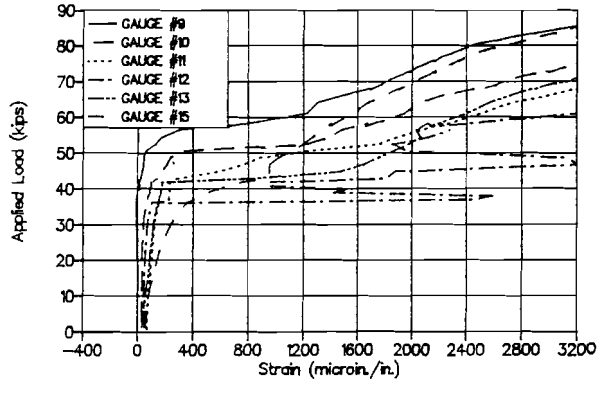

Figure C.9 Applied load vs. stirrup strains for second load cycle of Test 1B-8-D.

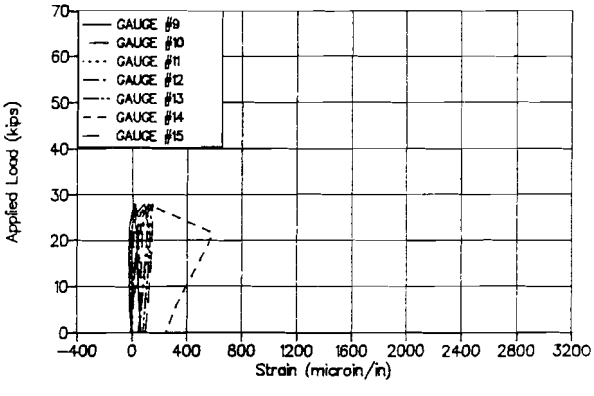

Figure C.10 Applied load vs. stirrup strains for first load cycle of Test 2A-8-0.6.

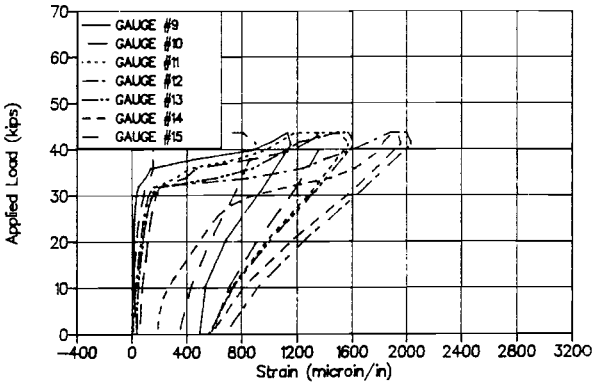

Figure C.11 Applied load vs. stirrup strains for second load cycle of Test 2A-8-0.6.

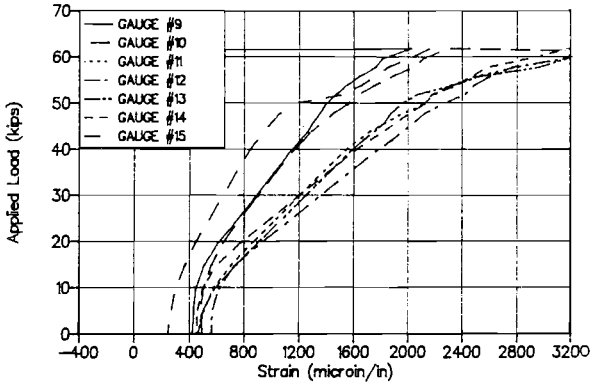

Figure C.12 Applied load vs. stirrup strains for final load cycle of Test 2A-8-0.6.

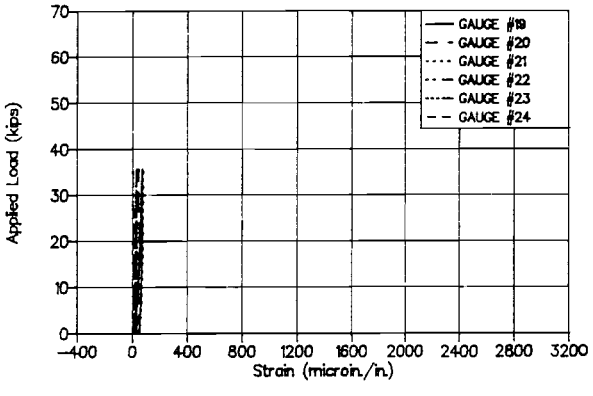

Figure C.13 Applied load vs. #1-1/4 stirrup strains for first load cycle of Test 2A-12-D.

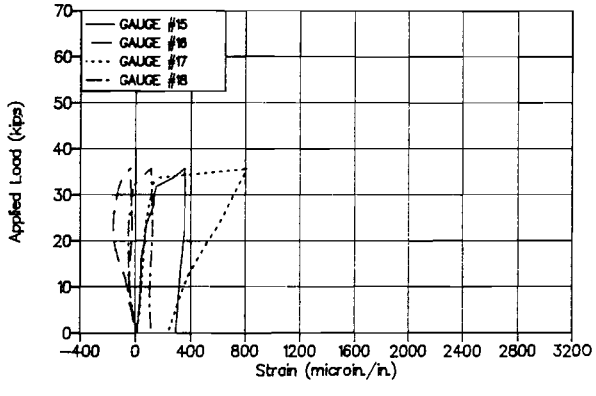

Figure C.14 Applied load vs. #2 stirrup strains for first load cycle of Test 2A-12-D.

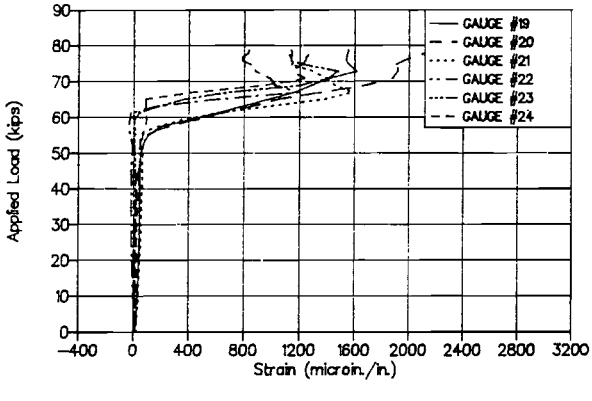

Figure C.15 Applied load vs. #1-1/4 stirrup strains for second load cycle of Test 2A-12-D.

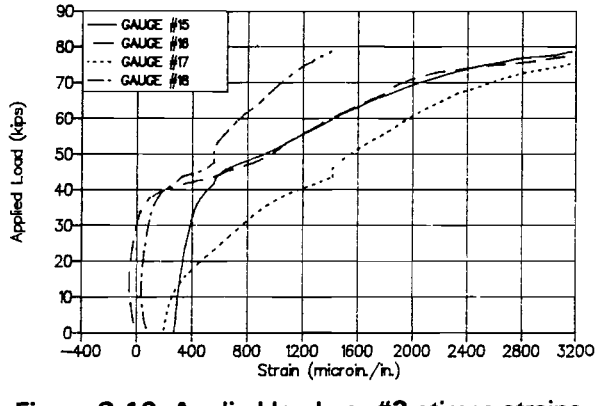

Figure C.16 Applied load vs. #2 stirrup strains for second load cycle of Test 2A-12-D.

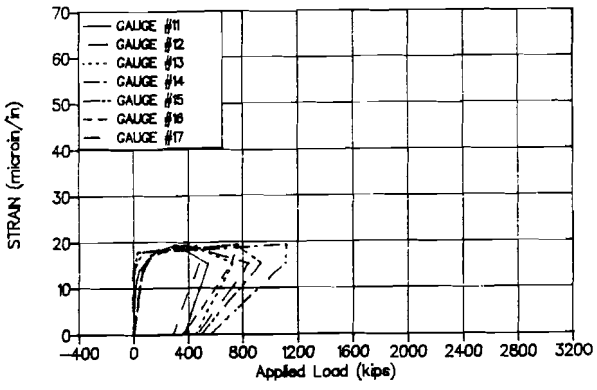

Figure C.17 Applied load vs. stirrup strains for first load cycle of Test 2B-8-0.8.

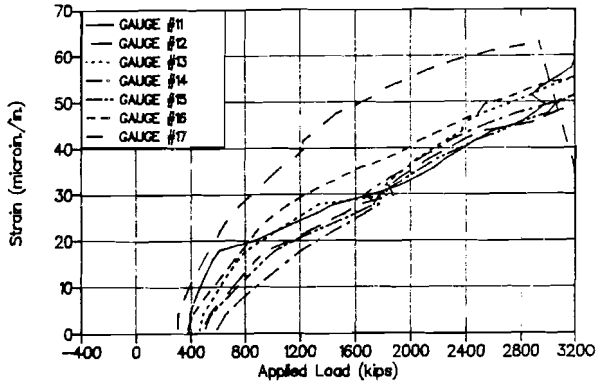

Figure C.18 Applied load vs. stirrup strains for second load cycle of Test 2B-8-0.8.

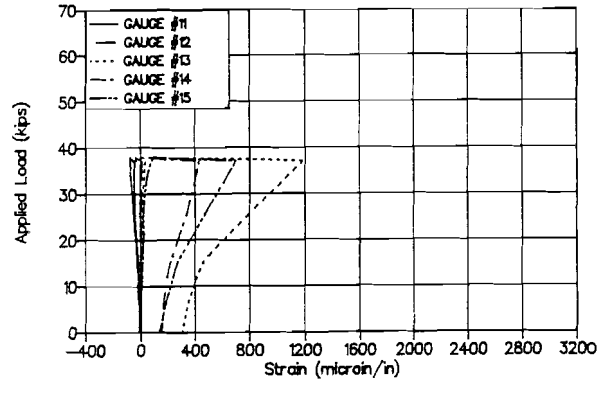

Figure C.19 Applied load vs. stirrup strains for first load cycle of Test 2B-4-D.

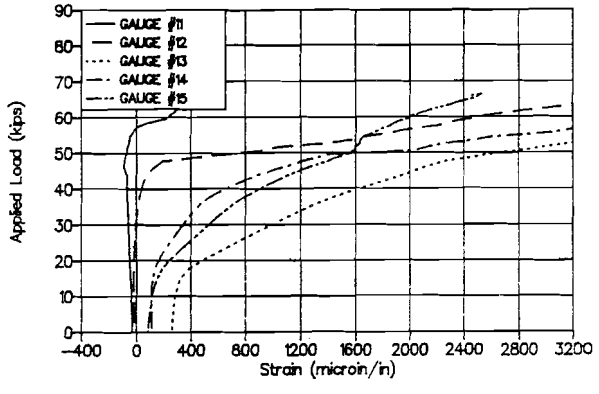

Figure C.20 Applied load vs. stirrup strains for second load cycle of Test 2B-4-D.

APPENDIX D

This appendix contains plots of applied load vs. strand strain measured by electronic resistance strain gauges. Strains are plotted separately for each load cycle. Strain gauge numbers refer to numbers in Figures 3.18 through 3.22. Because Specimen 2A-12-D contained strand gauges both in the interior span and in the cantilever, strains for draped and straight strands are plotted separately.

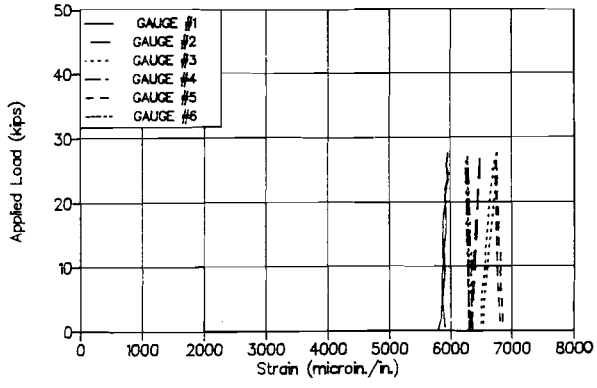

Figure D.1 Applied load vs. strand strains for first load cycle of Test 1A-1-0.6.

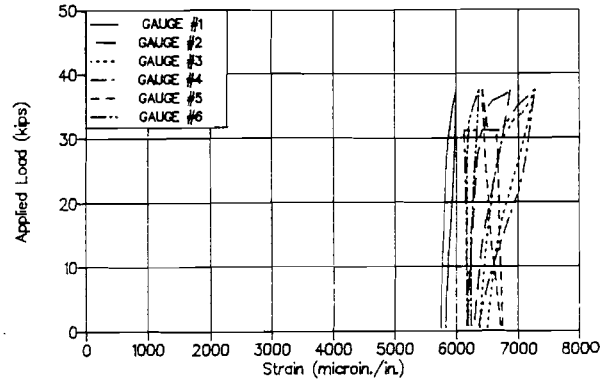

Figure D.2 Applied load vs. strand strains for second load cycle of Test 1A-1-0.6.

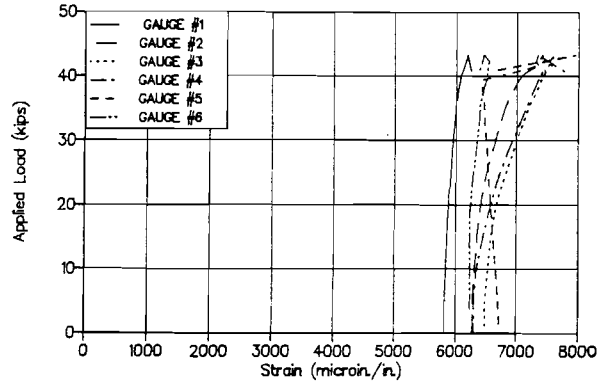

Figure D.3 Applied load vs. strand strains for final load cycle of Test 1A-1-0.6.

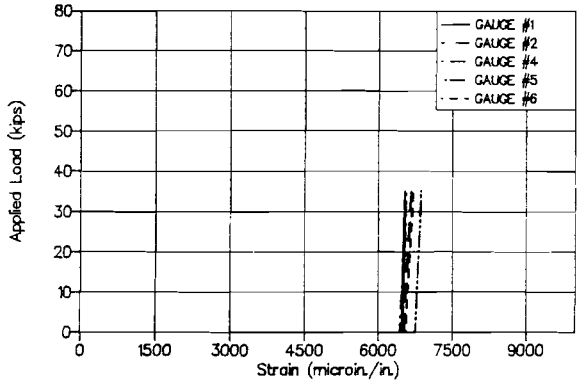

Figure D.4 Applied load vs. strand strains for first load cycle of Test 1A-1-D.

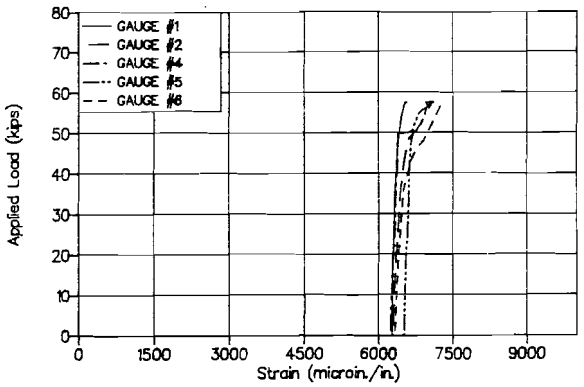

Figure D.5 Applied load vs. strand strains for second load cycle of Test 1A-1-D.

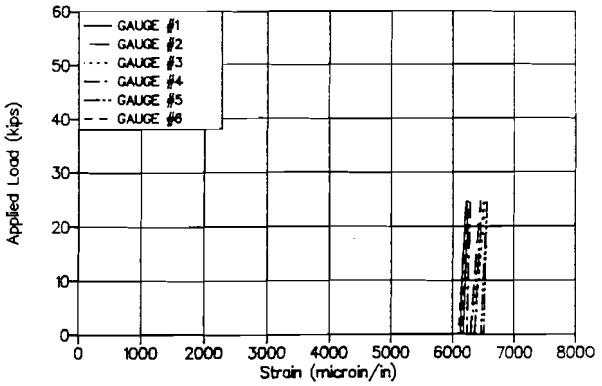

Figure D.6 Applied load vs. strand strains for first load cycle of Test 1B-1-0.8.

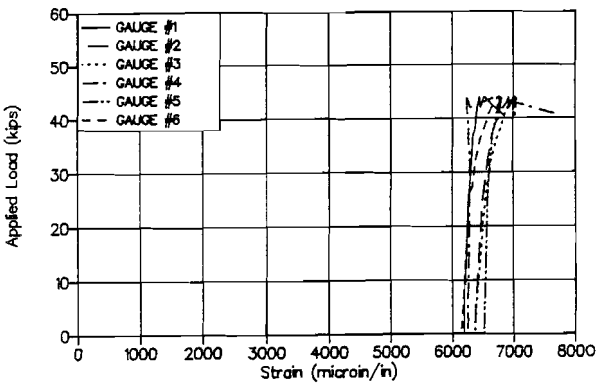

Figure D.7 Applied load vs. strand strains for second load cycle of Test 1B-1-0.8.

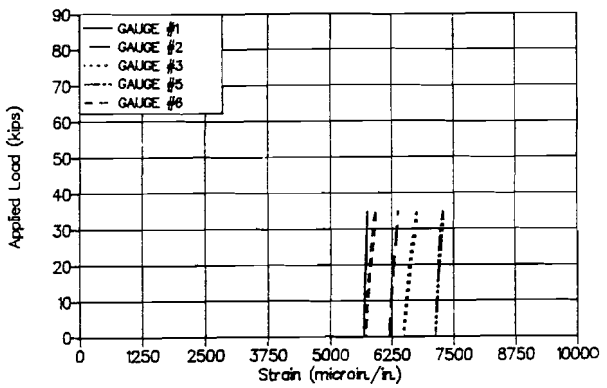

Figure D.8 Applied load vs. strand strains for first load cycle of Test 1B-8-D.

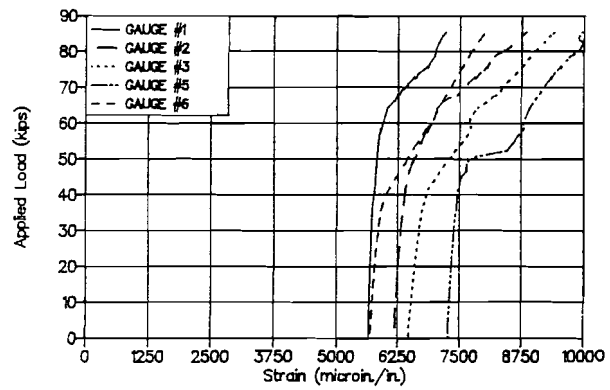

Figure D.9 Applied load vs. strand strains for second load cycle of Test 1B-8-D.

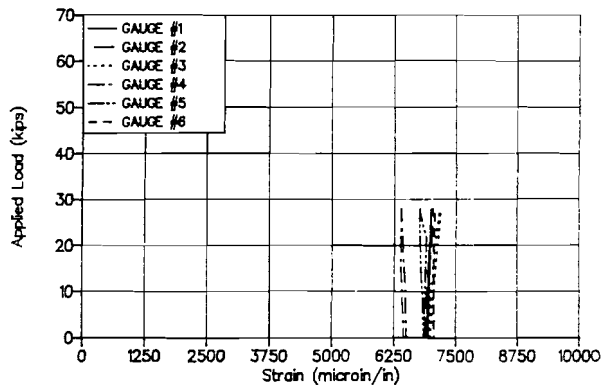

Figure D.10 Applied load vs. strand strains for first load cycle of Test 2A-8-0.6.

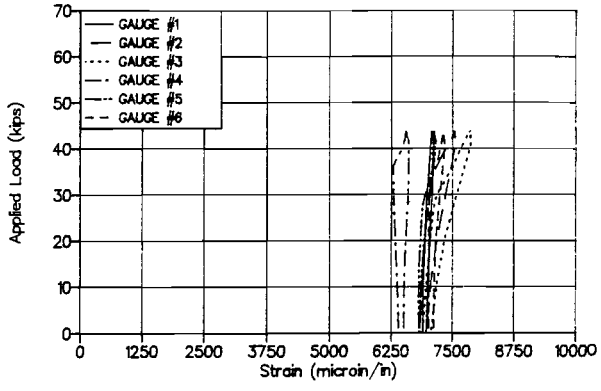

Figure D.11 Applied load vs. strand strains for second load cycle of Test 2A-8-0.6.

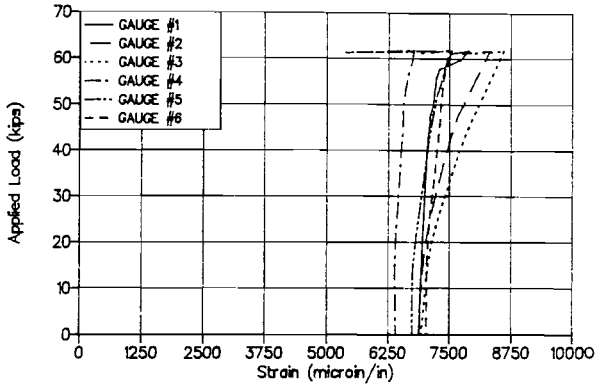

Figure D.12 Applied load vs. strand strains for final load cycle of Test 2A-8-0.6.

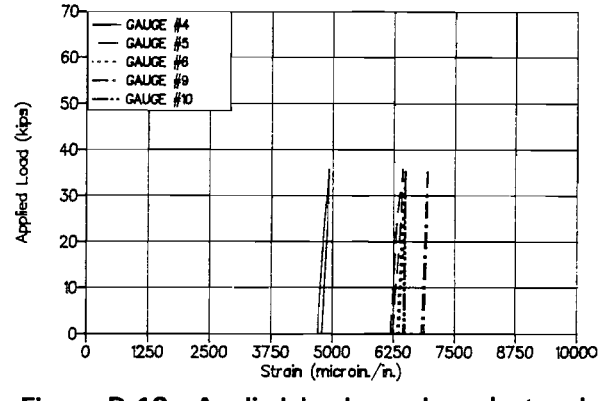

Figure D.13 Applied load vs. draped strand strains for first load cycle of Test 2A-12-D.

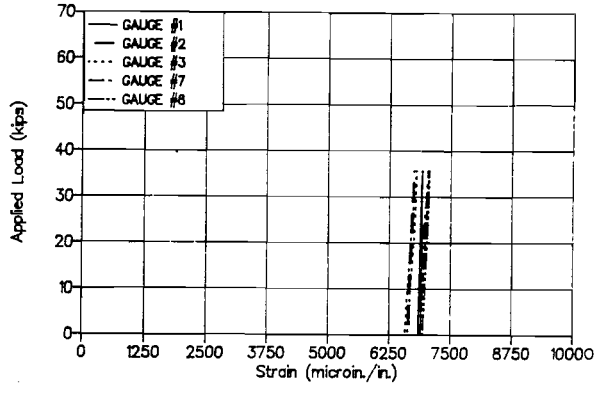

Figure D.14 Applied load vs. straight strand strains for first load cycle of Test 2A-12-D.

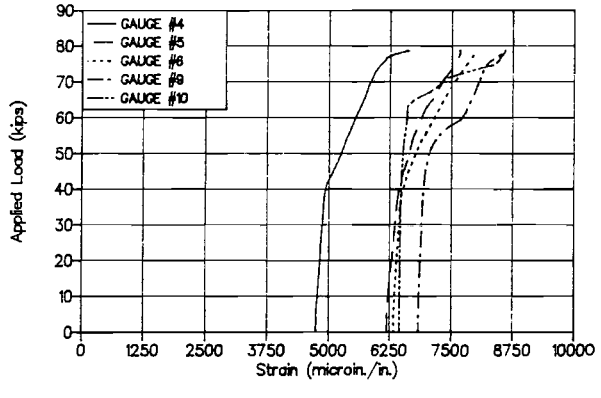

Figure D.15 Applied load vs. draped strand strains for second load cycle of Test 2A-12-D.

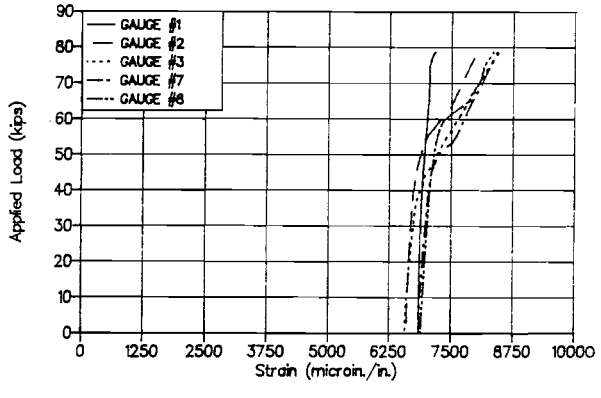

Figure D.16 Applied load vs. straight strand strains for second load cycle of Test 2A-12-D.

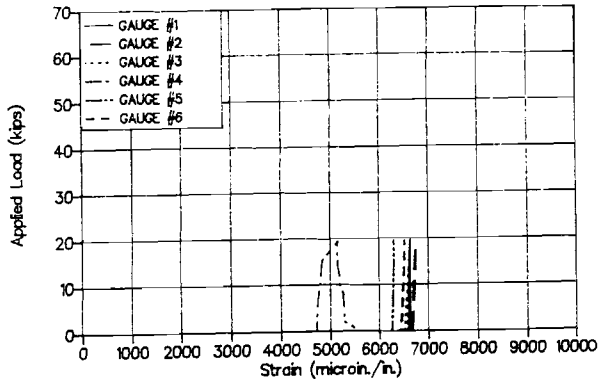

Figure D.17 Applied load vs. strand strains for first load cycle of Test 2B-8-0.8.

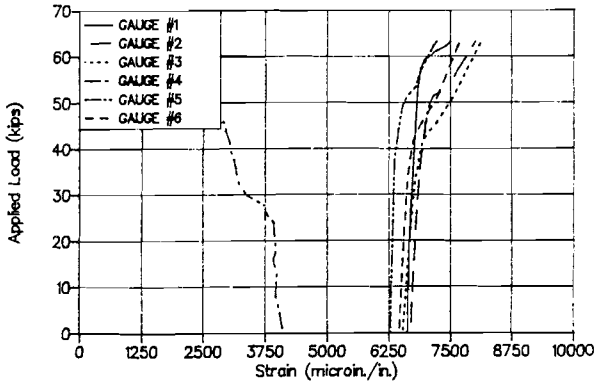

Figure D.18 Applied load vs. strand strains for second load cycle of Test 2B-8-0.8.

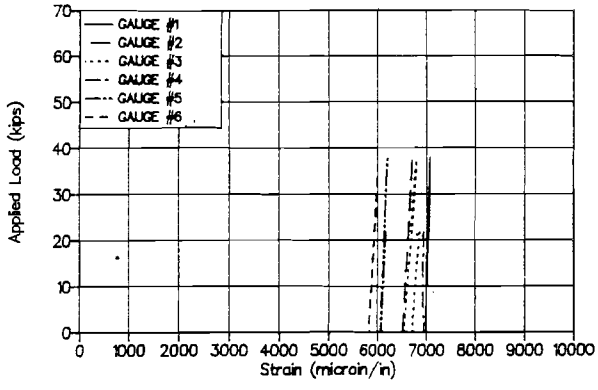

Figure D.19 Applied load vs. strand strains for first load cycle of Test 2B-4-D.

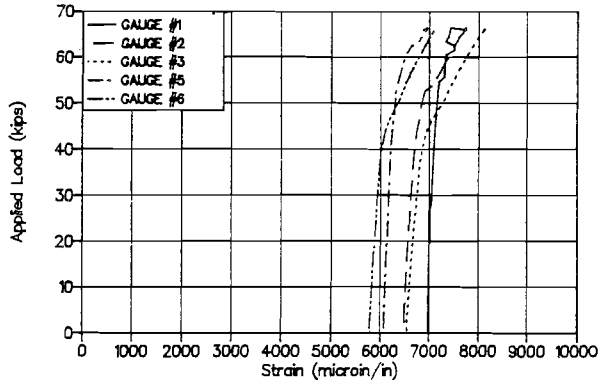

Figure D.20 Applied load vs. strand strains for second load cycle of Test 2B-4-D.

APPENDIX E

This appendix contains plots of applied load vs. strain in the non-prestressed longitudinal bars in the slab, measured by electronic resistance strain gauges. Strains are plotted separately for each load cycle. Strain gauge numbers refer to numbers in Figures 3.18 through 3.22. In Specimen 2A-8-0.6 and 2A-12-D the gauged longitudinal bars were #5 bars. In all other specimens they were #4 bars. No useable data were obtained from longitudinal bar gauges in Specimen 1A-1-0.6.

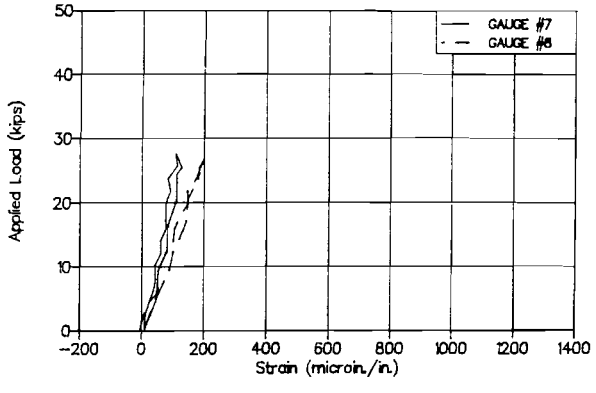

Figure E.1 Applied load vs. #4 bar strains for first load cycle of Test 1A-1-0.6.

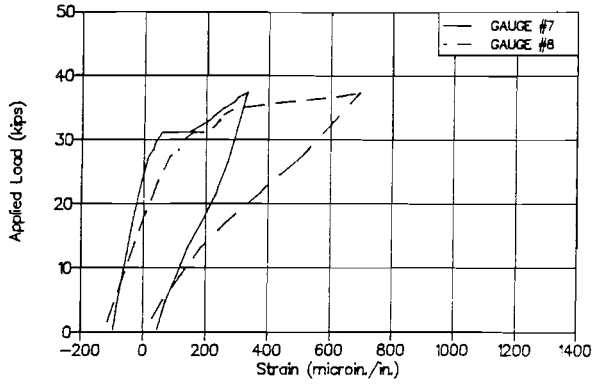

Figure E.2 Applied load vs. #4 bar strains for second load cycle of Test 1A-1-0.6.

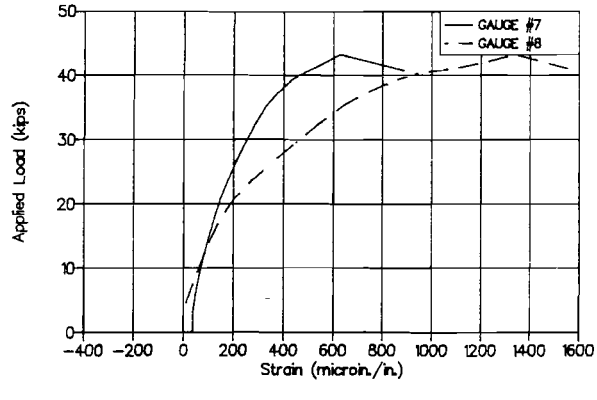

Figure E.3 Applied load vs. #4 bar strains for final load cycle of Test 1A-1-0.6.

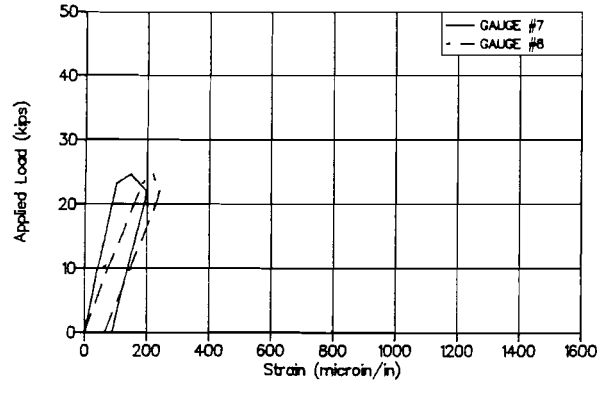

Figure E.4 Applied load vs. #4 bar strains for first load cycle of Test 1B-1-0.8.

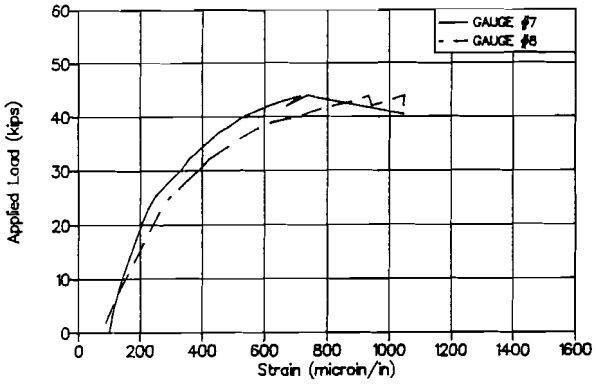

Figure E.5 Applied load vs. #4 bar strains for second load cycle of Test 1B-1-0.8.

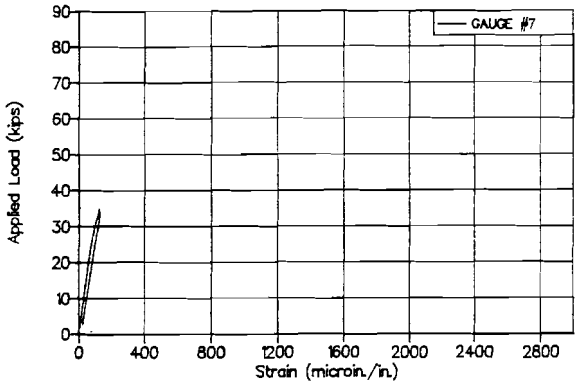

Figure E.6 Applied load vs. #4 bar strains for first load cycle of Test 1B-8-D.

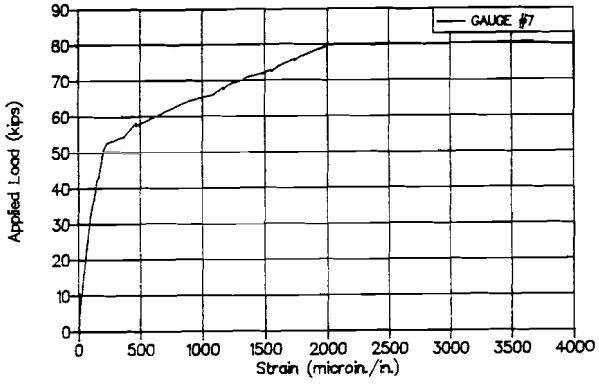

Figure E.7 Applied load vs. #4 bar strains for second load cycle of Test 1B-8-D.

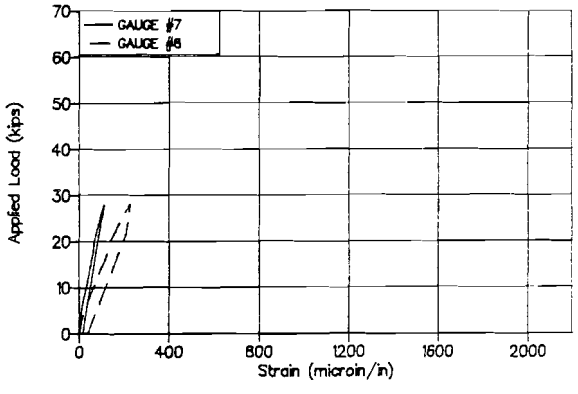

Figure E.8 Applied load vs. #5 bar strains for first load cycle of Test 2A-8-0.6.

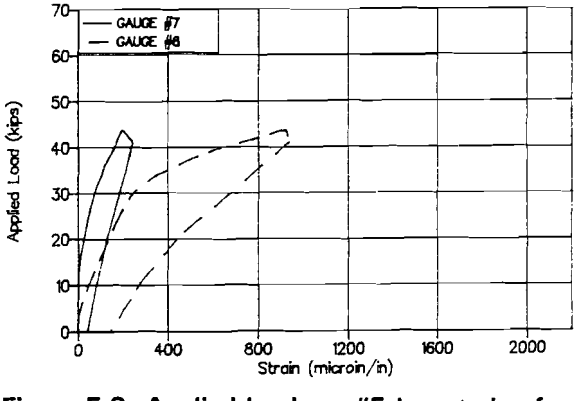

Figure E.9 Applied load vs. #5 bar strains for second load cycle of Test 2A-8-0.6.

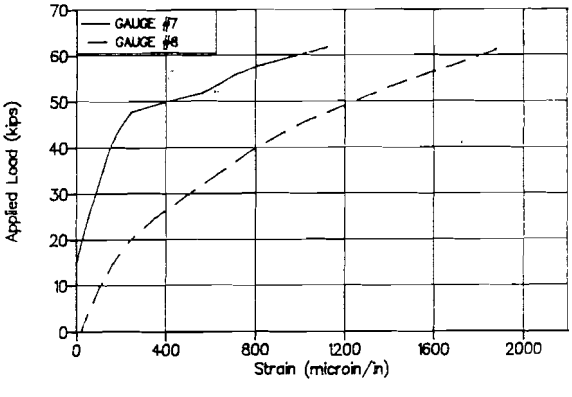

Figure E.10 Applied load vs. #5 bar strains for final load cycle of Test 2A-8-0.6.

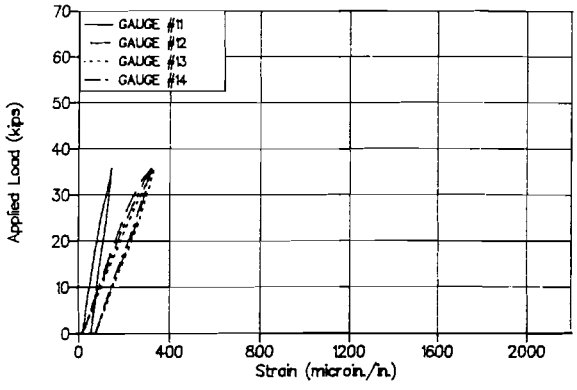

Figure E.11 Applied load vs. #5 bar strains for first load cycle of Test 2A-12-D.

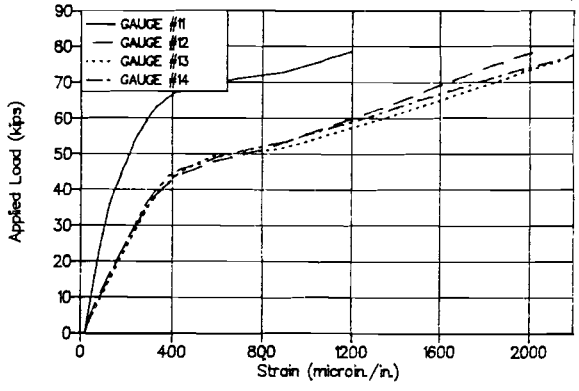

Figure E.12 Applied load vs. #5 bar strains for second load cycle of Test 2A-12-D.

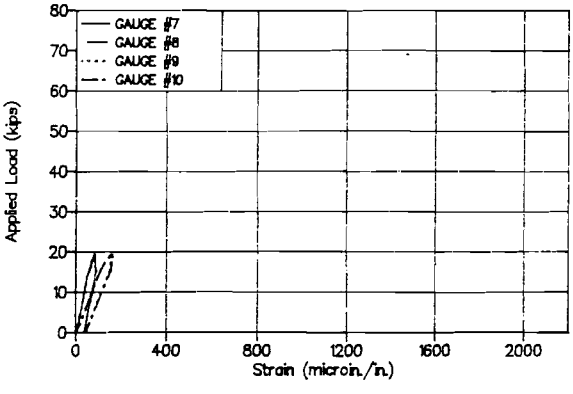

Figure E.13 Applied load vs. #4 bar strains for first load cycle of Test 2B-8-0.8.

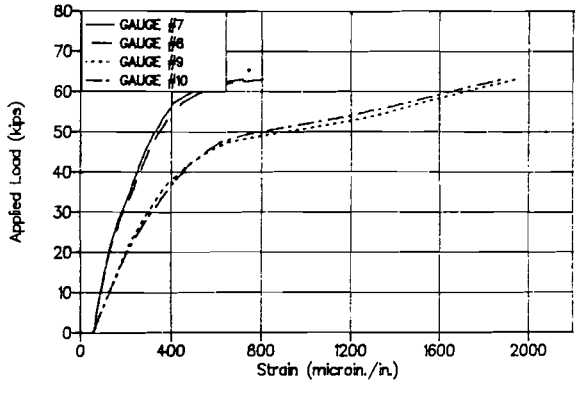

Figure E.14 Applied load vs. #4 bar strains for second load cycle of Test 2B-8-0.8.

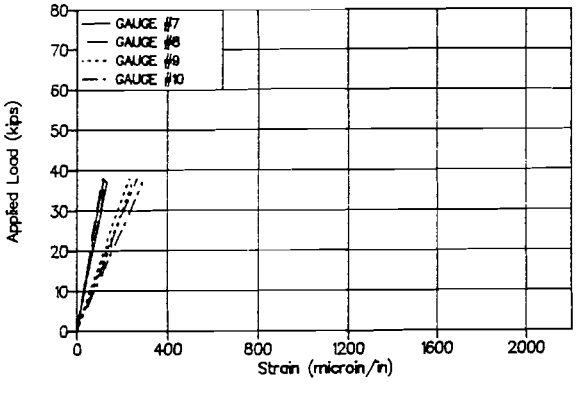

Figure E.15 Applied load vs. #4 bar strains for first load cycle of Test 2B-4-D.

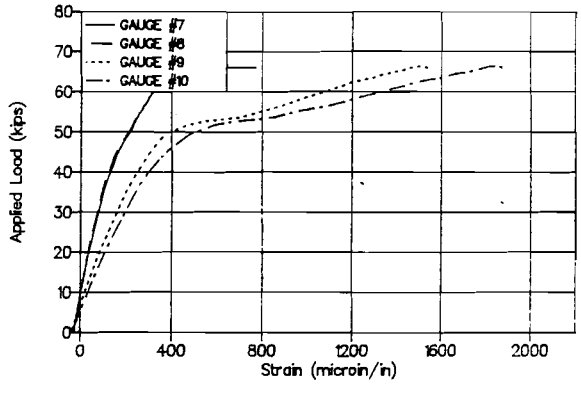

Figure E.16 Applied load vs. #4 bar strains for second load cycle of Test 2B-4-D.

REFERENCES

1. American Association of State Highway and Transportation Officials, *Standard Specification for Highway Bridges*, Thirteenth Edition, Washington, D.C., 1983 and Supplements through 1987.

2. American Concrete Institute – American Society of Civil Engineers Committee 426, "The Shear Strength of Reinforced Concrete Members," Journal of the Structural Division, *Proceedings*, American Concrete Institute, Vol. 99, No. ST6, June 1973, pp. 1091-1187.

3. American Concrete Institute, *Building Code Requirements for Reinforced Concrete (ACI 318-71)*, Detroit, 1971, 78 pp.

4. American Concrete Institute, *Building Code Requirements for Reinforced Concrete (ACI 318-83)*, Detroit, 1983, 111 pp.

5. American Concrete Institute, *Commentary on Building Code Requirements for Reinforced Concrete (ACI 318-63)*, SP10 Detroit, 1965, 91 pp.

6. American Concrete Institute, *Commentary on Building Code Requirements for Reinforced Concrete (ACI 318-71)*, Detroit, 1971, 96 pp.

7. Anderson, R.B., "Behavior of CTT-Nodes in Reinforced Concrete Strut-and-Tie Models," Unpublished Masters Thesis, The University of Texas at Austin, Dec. 1988.

8. Bergmeister, K., Breen, J.E., Jirsa, J.O., and Kreger, M.E., "Detailing for Structural Concrete – Draft Report," *Research Report 1127-3F*, Center for Transportation Research, The University of Texas at Austin, Sept. 1989.

9. Bouadi, Abdelhakim, "Behavior of CCT-Nodes in Structural Concrete Strut-and-Tie Models," Unpublished Masters Thesis, The University of Texas at Austin, Dec. 1989.

10. Carino, N.J., and Lew, H.S., "Re-examination of the Relation Between Splitting Tensile and Compressive Strength of Normal Weight Concrete," ACI Journal, *Proceedings*, Vol. 79, No. 3, May/June 1982, pp. 214-219.

11. Castrodale, R.W., "A Study of Pretensioned High Strength Concrete Girders in Composite Highway Bridges," Unpublished Ph.D. Dissertation, The University of Texas at Austin, 1988.

12. Cerruti, L.M., and Marti, P., "Staggered Shear Design of Concrete Beams: Large-Scale Tests," *Canadian Journal of Civil Engineering*, Vol. 14, 1987, pp. 257-268.

13. Collins, M.P., and Mitchell, D., "A Rational Approach to Shear Design: The 1984 Canadian Code Provisions," *ACI Journal*, Nov./Dec. 1986, pp. 925-933.

14. Collins, M.P., and Mitchell, D., "Shear and Torsion Design of Prestressed and Non-Prestressed Concrete Beams," *PCI Journal*, Vol. 25, No. 5, Sept./Oct. 1980, pp. 32-100.

15. Comite Europeen du Beton, "Members Design," *Information Bulletin No. 146*, Paris, France, Jan. 1982.

16. CEB-FIP, *Model Code for Concrete Structures*, CEB-FIP International Recommendations, Third Edition, Comite Euro-International du Beton, Paris, France, 1978, 348 pp.

17. Cook, W.D., and Mitchell, D., "Studies of Disturbed Regions Near Discontinuities in Reinforced Concrete Members," *ACI Structural Journal*, Mar./Apr. 1988, 11 pp.

18. *Design of Concrete Structures for Buildings (CAN3-A23.3-M84)*, Canadian Standards Association, Rexdale, 1984, 281 pp.

19. Elzanaty, A.H., Nilson, A.H., and Slate, F.O., "Shear Capacity of Prestressed Concrete Beams Using High-Strength Concrete," *ACI Journal*, May/June 1986, pp. 359-368.

20. Ferguson, P.M., *Reinforced Concrete Fundamentals*, Fourth Edition, John Wiley and Sons, New York, 1979, 724 pp.

21. Haddadin, M.J., Hong, S.T., and Mattock, A.H., "Stirrup Effectiveness in Reinforced Concrete Beams with Axial Force," *Proceedings*, ASCE, Vol. 97, ST9, Sept. 1971, pp. 2227-2297.

22. Hartmann, D.L., Breen, J.E., and Kreger, M.E., "Shear Capacity of High-Strength Prestressed Concrete Girders," *Research Report 381-2*, Center for Transportation Research, The University of Texas at Austin, Jan. 1988.

23. Hawkins, N.M., "Strength and Behavior of Two-Span Continuous Prestressed Concrete Beams," Ph.D. Thesis, University of Illinois at Urbana, Oct. 1961.

24. Hawkins, N.M., Sozen, M.A., and Siess, C.P., "Behavior of Continuous Prestress Concrete Beams," *Proceedings of International Symposium on Flexural Mechanics of Reinforced Concrete, ACI Special Publication No. 12*, 1965.

25. Kaufman, M.K., and Ramirez, J.A., "Re-evaluation of the Ultimate Shear Behavior of High-Strength Concrete Prestressed I-Beams," *ACI Structural Journal*, May/June 1988.

26. Leonhardt, I.F., *Prestressed Concrete Design and Construction*, Wilhelm Ernst and Son, Berlin, 1964, pp. 79-84.

27. Libby, J.R., *Modern Prestressed Concrete: Design Principles and Construction Methods*, Third Edition, Van Nostrand Reinhold Company, New York, 1971, pp. 166-171.

28. Lin, T.Y., and Burns, N.H., *Design of Prestressed Concrete Structures*, Third Edition, John Wiley and Sons, 1981, pp. 268-278.

29. MacGregor, J.G., "Strength and Behavior of Prestressed Concrete Beams with Web Reinforcement," Ph.D. Thesis, University of Illinois at Urbana, Oct. 1960.

30. MacGregor, J.G., *Reinforced Concrete: Mechanisms and Design*, Prentice Hall, Englewood Cliffs, NJ, 1988, pp. 169-200.

31. MacGregor, J.G., and Hanson, J.M., "Proposed Changes in Shear Provisions for Reinforced and Prestressed Concrete Beams," *ACI Journal*, April 1969, pp. 276-288.

32. MacGregor, J.G., Sozen, M.A., and Siess, C.P., "Strength of Prestressed Concrete with Web Reinforcement," *ACI Journal*, Dec. 1965, pp. 1503-1517.

33. MacGregor, J.G., Sozen, M.A., and Siess, C.P., "Effect of Draped Reinforcement on Behavior of Prestressed Concrete Beams," *ACI Journal*, Vol. 32, No. 6, Dec. 1960, pp. 649-677.

34. Marti, P., "Basic Tools of Reinforced Concrete Beam Design," *ACI Journal*, Jan./Feb. 1985, pp. 46-56.

35. Marti, P., "Truss Models in Detailing," *Concrete International*, Dec. 1985, pp. 66-73.

36. Marti, P., "Staggered Shear Design of Simply Supported Concrete Beams," *ACI Journal*, Jan./Feb. 1986, pp. 36-42.

37. Naaman, A.E., "Ultimate Analysis of Prestressed and Partially Prestressed Sections by Strain Compatibility," *PCI Journal*, Vol. 22, No. 1, Jan./Feb. 1977, pp. 32-51.

38. Nielsen, M.P., Braestrup, M.W., Jensen, B.C., and Bach, F., "Concrete Plasticity, Beam Shear – Shear in Joints – Punching Shear," *Special Publication*, Danish Society for Structural Science and Engineering, Technical University of Denmark, Lyngby, 1978, 129 pp.

39. Ramirez, J., "A Truss Analysis of the Shear and Torsional Strength of Beams," Ph.D. Thesis, The University of Texas at Austin, 1984.

40. Rodrigues, C.P., and Darwin, D., "Shear Strength of Lighly Reinforced T-Beams in Negative Bending," *ACI Structural Journal*, Jan./Feb. 1987, pp. 77-85.

41. Rogowsky, D.M., and MacGregor, J.G., "Design of Reinforced Concrete Deep Beams," *Concrete International*, Aug. 1986, pp. 49-58.

42. Schlaich, J., Schafer, K., and Jennewein, M., "Special Report: Toward a Consistent Design of Structural Concrete," *PCI Journal*, May/June 1978, pp. 74-150.

43. Sozen, M.A., and Hawkins, N.M., "Discussion of: ACI-ASCE Committee 326, 'Shear and Diagonal Tension,'" *Proceedings*, American Concrete Institute, Vol. 59, Jan., Feb., and Mar., 1962, pp. 1-30, 277-334, and 353-396, *Proceedings*, American Concrete Institute, Vol. 59, Sept. 1962, pp. 1341-1347.

44. Sozen, M.A., Zoyer, E.M., and Siess, C.P., "Investigation of Prestressed Concrete for Highway Bridges, Part I: Strength in Shear of Beams without Web Reinforcement," Bulletin No. 452, University of Illinois Engineering Experiment Station, Urbana, IL, April 1959.

45. Taub, J., and Neville, A.M., "Resistance to Shear of Reinforced Concrete Beams, Part I: Beams without Web Reinforcement," *Proceedings*, American Concrete Institute, Vol. 57, Aug. 1970, pp. 193-220.

46. Thurlimann, B., "Shear Strength of Reinforced and Prestressed Concrete Beams – CEB Approach," Presented at ACI Symposium 1976, Philadelphia, PA, 33 pp.

47. Vecchio, F.J., and Collins, M.P., "Predicting the Response of Reinforced Concrete Beams Subjected to Shear Using Modified Compression Field Theory," *ACI Structural Journal*, May/June 1988, pp. 258-268.